MIXED METAL OXIDE CATALYSTS PREPARED USING SUPERCRITICAL CARBON DIOXIDE

Thesis submitted in accordance with the requirement of Cardiff University for the degree of Doctor of Philosophy

Jonathan Ferguson

December 2009

ProQuest LLC
789 East Eisenhower Parkway
P.O. Box 1346
Ann Arbor, MI 48106-1346

DECLARATION

This work has not previously been accepted in substance for any degree and is not concurrently submitted in candidature for any degree.

Signed ..... (candidate) Date 15/12/09.

STATEMENT 1

This thesis is being submitted in partial fulfillment of the requirements for the degree of PhD

Signed ..... (candidate) Date 15/12/09.

STATEMENT 2

This thesis is the result of my own independent work/investigation, except where otherwise stated. Other sources are acknowledged by explicit references.

Signed ..... (candidate) Date 15/12/09

STATEMENT 3

I hereby give consent for my thesis, if accepted, to be available for photocopying and for inter-library loan, and for the title and summary to be made available to outside organisations.

Signed ..... (candidate) Date 15/12/09.

Abstract

The use of nitrate precursors for the production of mixed oxide catalysts such as iron molybdates and copper manganese oxides has been well documented in the literature. Nitrates have been used because of their high solubility and the ease of removal of the nitrate anion during calcination. In the case of copper manganese oxides, the use of chlorides and sulphates leads to the retention of the anion on the surface of the catalyst, using nitrates leaves no residue on the catalyst. The use of nitrates, however, is unfavourable due to the environmental issues associated with them.

The main aim of this project was to provide a nitrate free route for the production of iron molybdate and copper manganese oxide catalysts. Using supercritical antisolvent precipitation (SAS) provided an alternative preparative route for the production of these catalysts. The catalysts produced exhibited activity when tested in their respective reactions. Some catalysts produced were comparable to those currently prepared using the conventional preparation methods i.e the use of nitrate precursors.

The research performed focussed on the production of theses mixed metal oxides using supercritical carbon dioxide. Optimisation of the supercritical process by varying operational parameters was also investigated to determine their effect on the activity of the catalyst obtained.

By utilising operating parameters and understanding the supercritical antisolvent process, the results obtained showed that it was possible to produce mixed metal oxides, and to tune their catalytic activity.

Acknowledgements

There have been a number of people who have contributed and advised me throughout the course of this research. I would like to thank Prof. Graham Hutchings for his advice and support with this project. I would also like to thank Dr. Sean Axon (Johnson Matthey) for providing ideas and giving an industrial view over the research performed. Also, Dr. Albert Carley for his advice throughout. I would especially like to thank Dr. Stuart Taylor for his support and motivation; even when things were not going right.

Dr. Jonathan Bartley and Dr. Thomas Davies were extremely helpful in the laboratory, and without their help constructing the supercritical reactor and the test facility would have been much more difficult. Both provided key constructive criticism, as did Dr. Stuart Taylor, when writing this thesis and for that I am very grateful.

There were a few key member of the research group, past and present, that made the mundane day to day stuff in the lab a bit more bearable. These include Pete, Neil, Laura, Nick, Nishlan, Edouard, Jo and Jen to name but a few. A special thanks to Matt and Kieran for being there through the good times and the bad!

I would like to thank my family. Mam and Dad, I would not be where I am today had it not been for your love and support (both financially and emotionally) for that I am deeply grateful. Finally, I would like to thank my fiancée Sam, who I love dearly. Thank you for giving me a family and for being a part of yours, Charlie-Ann, Jamie-Bo and Sophie, I love you all.

Contents

Page

1 Introduction

1.1 Green Chemistry

Green chemistry is the design, development, and implementation of chemical products that reduce or eliminate the use and generation of substances hazardous to human health and the environment [1]. Green chemistry is an innovative, non-regulatory, economically driven approach toward sustainability. Green chemistry considers the entire life cycle of chemical processes as an opportunity for design innovation. Green chemistry challenges innovators to design and utilise matter and energy in a way that increases performance and value while protecting human health and the environment [2].

In the past environmental problems have been dealt with using the "command and control" approach, where waste management, treatment and clean up were governed by mandatory regulations; green chemistry looks at preventing pollution at its source. Rather than accepting waste generation and disposal as unavoidable, green chemistry seeks new technologies that are cleaner and economically competitive.

Economic benefits are the main drivers for the implementation of green chemistry into industrial processes. Adopting green chemistry methodologies decreases a wide array of operating costs; the generation of less waste causes the cost of environmental compliance to go down; treatment and disposal become unnecessary when waste is eliminated; the use of less solvent and fewer processing steps lessen the material and energy costs of manufacturing and increase material efficiency. The environmental, human health and the economic advantages are strong incentives to industry to adopt greener technologies.

Green chemistry is guided by a set of principles that are focussed on the reduction, elimination and the generation of hazardous substances in the design, manufacture, and application of chemical products. The 12 principles of Green chemistry developed by Anastas and Warner [3] cover concepts such as minimise the use of raw materials, the design of safe and environmental-benign processes, the improvement of energy efficiency and the better disposal of waste products. These 12 principles are the backbone of Green Chemistry and have been used as guidelines and criteria by chemical scientists. The 12 principles of Green Chemistry are given below:

1. **Prevention** - It is better to prevent waste than to treat or clean up after it is formed.
2. **Atom economy** – Synthetic methods should be designed to maximise the incorporation of all materials used in the process into the final product.

3. **Less Hazardous chemical Synthesis** – Wherever practicable, synthetic methodologies should be designed to use and generate substances that possess little or no toxicity to human health and the environment.
4. **Designing Safer Chemicals** – Chemical products should be designed to preserve efficiency of function while reducing toxicity.
5. **Safer Solvents and Auxiliaries** – The use of auxiliary substances (e.g.) should be made unnecessary wherever possible and innocuous when used
6. **Design for Energy Efficiency** – Energy requirements should be recognised for their environmental economic impacts and should be minimised. Synthetic methods should be conducted at ambient temperature and pressure.
7. **Use of Renewable Feedstocks** – A raw material of feedstock should be renewable rather than depleting wherever technically and economically practicable.
8. **Reduce Derivatives** – Unnecessary derivatisation (blocking group, protection/deprotection, temporary modification of physical/chemical processes) should be avoided whenever possible
9. **Catalysis** – Catalytic reagents (as selective as possible) are superior to stoichiometric reagents.
10. **Design for Degradation** – Chemical products should be designed so at the end of their function they do not persist in the environment, but break down into innocuous degradation products.
11. **Real-time Analysis for Pollution Prevention** – Analytical methodologies need to be further developed to allow for real-time in-process monitoring and control prior to the formation of hazardous substances.

12. **Inherently Safer Chemistry for Accident Prevention** – Substances and the form of a substance used in a chemical process should be chosen so as to minimise the potential for chemical accidents, including releases, explosions and fires.

The emergence of Green chemistry has resulted in many research groups and programs focussing efforts around the 12 principles of green chemistry. Research utilising these principles can be seen in polymer chemistry, catalysis, analytical method development and synthetic methodology development. The types of products and processes that can be seen among those adopting Green chemistry principles include medicine, food production, energy production, packaging, household and commercial cleaning products, electronics, automotive, and a wider range of consumer goods. Green chemistry is dealing with matter and energy at the fundamental level and is affecting all aspects of our economy and our daily life. The breadth of impact across different industries and technologies is essential to Green Chemistry's effectiveness as a tool for progressing and advancing sustainability.

1.2 Green Catalysis

1.2.1 Catalysis and Heterogeneous Catalysis

Catalysis is the acceleration (increase in rate) of a chemical reaction by means of a substance, which itself is not consumed by the overall reaction. A catalyst provides an alternative route of reaction where the activation energy is lower than that of the

original chemical reaction. Catalysts participate in reactions, and are neither reactants nor products of the reactions that they catalyse.

Catalysts work by providing an alternative mechanism involving a different transition state and lower activation energy. The effect of this is that more molecular collisions have the energy needed to reach the transition state. Hence catalysts allow reactions that, albeit thermodynamically feasible, would not take place in their absence. A catalyst can cause the reaction to occur at a much faster rate, more specific, or at lower temperatures.

There are three types of catalysts; these are Heterogeneous, Homogeneous and Biocatalysts. Heterogeneous catalysts are present in different phases from the reactants, for example, a solid catalyst in a gaseous reaction mixture. Homogeneous catalysts are in the same phase, for example, a dissolved catalyst in a liquid reaction mixture. Biocatalysis involves the chemical transformation of organic compounds using enzymes.

Heterogeneous catalysis involves the catalyst providing a surface on which the reactants (or substrates) temporarily become adsorbed. Bonds in the substrate become weakened, and new bonds are created between the adsorbed species on the surface of the catalyst. The bonds between the products and the catalysts are weaker, which results in the release of the products.

Heterogeneous catalysis has several advantages compared to homogeneous processes. These advantages are:

1. **Avoids the formation of inorganic salts;**
2. **Catalysts easy to handle**
3. **Catalysts safe to store and has long life time**
4. **Ease of removal from reaction.**

Heterogeneous catalysts are used in many industrial catalytic processes, such as the Haber process for ammonia synthesis using an iron catalyst. Heterogeneous catalysts offer alternative routes to products that include such financial rewards in industrial processes as lower operating costs, long life time and reduction in separation costs.

1.2.2 Green Catalysis

Developing Green chemistry methodologies is a challenge that may be viewed through the framework of the "Twelve Principles of Green Chemistry" [3] These principles identify catalysis as one of the most important tools in implementing green chemistry. Catalysis offers numerous green chemistry benefits including lower energy requirements, catalytic versus stoichiometric amounts of materials, increased selectivity, and decreased use of processing and separation agents, and allows for the use of less toxic materials.

Heterogeneous catalysis, in particular, addresses the goals of green chemistry by providing ease of separation of product and catalyst, which eliminates the need for

separation through distillation or extraction. Environmentally benign catalysts such as clays and zeolites could possibly replace more hazardous catalysts currently in use. Thus, there is an increasing interest on the topic of green catalysis recently.

Traditional procedures for the commercial preparation of catalysts often involve the use of metal nitrates as reactants or intermediates in the reaction. This results in the generation of nitrate waste, which is problematic in disposal. Therefore, there is increasing interest in the area of green catalysis to develop catalysts that provide alternative reaction routes to conventional nitrate based processes with comparative catalytic performance and product yields.

Various research groups have focused on the idea of using supercritical fluids in catalysis. Baiker and Noyori *et al* have reviewed the works on heterogeneous and homogeneous catalysis in supercritical fluids respectively [4-6]. Supercritical fluids have shown potential in catalytic reactions but can also be used in the preparation of catalysts and catalyst support material [7-9]. The most widely used supercritical fluids in the preparation of catalysts are supercritical water (hydrothermal synthesis) and supercritical CO_2 (antisolvent precipitation).

1.3 Supercritical Fluids

1.3.1 Definition

A supercritical fluid is defined as a substance above its critical temperature (T_c) and pressure (T_p). The critical point represents the highest temperature and pressure that the substance can exist as a vapour and liquid in equilibrium. Supercritical fluids have the unique ability to diffuse through solids like a gas, and dissolve materials like a liquid. Additionally, they can readily change in density upon minor changes in temperature or pressure.

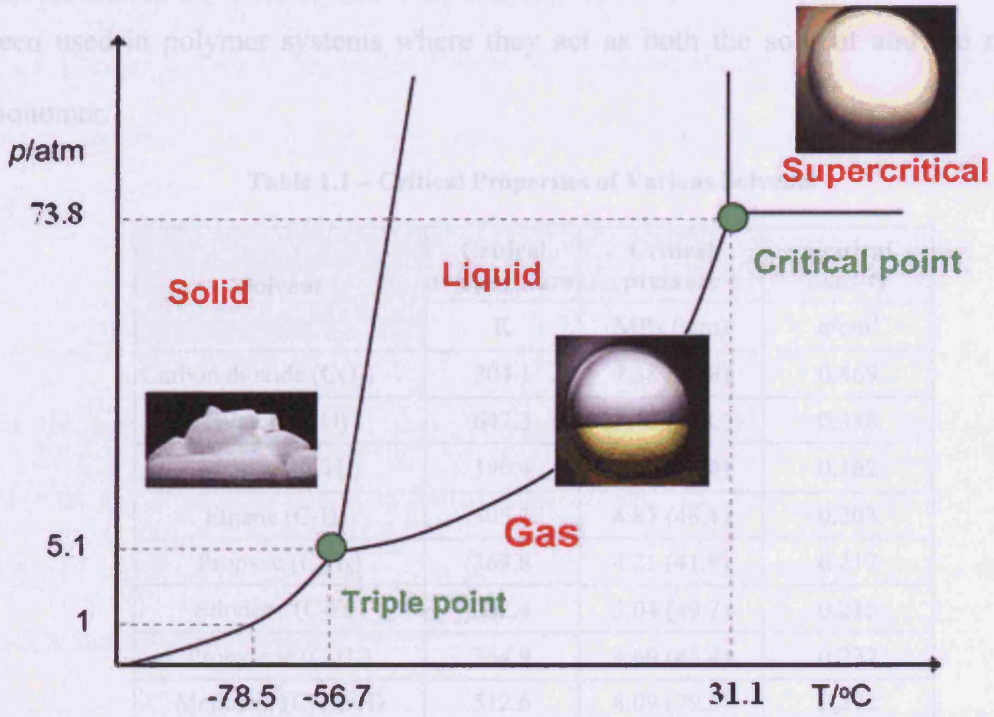

Figure 1.1 – Phase diagram of Carbon Dioxide

Consider the phase diagram for CO_2 shown in Figure 1.1. The boiling curve separates the vapour and liquid region. As the pressure and temperature are increased along the boiling curve, the vapour becomes denser and the liquid becomes less dense. At the

critical point, the densities of the equilibrium liquid phase and the saturated vapour phases become equal resulting in the formation of a single supercritical phase. For carbon dioxide the critical point occurs at 31.1 °C and 73.8 bar.

The critical properties of some substances, which are commonly used as supercritical fluids are shown in Table 1.1. Carbon dioxide and water are most commonly used supercritical fluids. Both are relatively cheap, non-toxic and have easily reached critical states. These supercritical fluids have been used in such applications as extractions, dry cleaning and chemical waste disposal. Ethylene and propylene have been used in polymer systems where they act as both the solvent and the reacting monomer.

Table 1.1 – Critical Properties of Various Solvents

Solvent	Critical temperature	Critical pressure	Critical density
	K	MPa (atm)	g/cm^3
Carbon dioxide (CO_2)	304.1	7.38 (72.8)	0.469
Water (H_2O)	647.3	22.12 (218.3)	0.348
Methane (CH_4)	190.4	4.60 (45.4)	0.162
Ethane (C_2H_6)	305.3	4.87 (48.1)	0.203
Propane (C_3H_8)	369.8	4.25 (41.9)	0.217
Ethylene (C_2H_4)	282.4	5.04 (49.7)	0.215
Propylene (C_3H_6)	364.9	4.60 (45.4)	0.232
Methanol (CH_3OH)	512.6	8.09 (79.8)	0.272
Ethanol (C_2H_5OH)	513.9	6.14 (60.6)	0.276
Acetone (C_3H_6O)	508.1	4.70 (46.4)	0.278

1.3.2. Properties of Supercritical Fluids

Supercritical fluids exhibit properties of both a liquid and a gas, which causes these fluids to be deemed "a hybrid of a gas and a liquid" [10]. These properties include the ability to dissolve solids, miscibility with permanent gases, high diffusivity and low viscosity. It is the exploitation of these properties which give real advantages in coordination, organometallic, inorganic and materials chemistry.

SCFs (Supercritical Fluids) have densities that are greater than those of gases but comparable to those of liquids which enable them to function as solvents. The low viscosities of SCFs and high diffusivities of solutes combined with very high buoyant forces may result in superior mass transfer characteristics compared to conventional solvents.

Since SCF's are highly compressible, it is possible to tune their properties from gas-like through to liquid-like [11]. It is this tunability that renders SCF's highly unusual solvents for a wide range of common compounds; the density of the SCF can be changed continuously by controlling the pressure and temperature. CO_2 is the most widely used fluid because of its easily accessible critical parameters. However, $scCO_2$ (Supercritical carbon dioxide) is not a particularly powerful solvent; the solvent power has been likened to that of n-hexane. But the addition of a polar co-solvent; such as methanol, greatly enhances the solubility of polar compounds in $scCO_2$.

Using supercritical fluids generally involves the application of elevated pressures and temperatures. Therefore, there is always an additional energy cost associated with the

use of supercritical fluids, compared to the use of more conventional solvents. However, it is the beneficial properties associated with the use of SCF's, such as high diffusivities and low viscosities compared with that of conventional solvents that outweigh the cost of using them. Also the use of non-toxic SCF's such as CO_2 and H_2O, prevent the need for solvents which can be potentially be toxic, expensive, difficult to handle and problematic in their disposal

1.3.2 Applications of Supercritical fluids

Over recent years, the environmental impact of long established chemical processes has long been documented, and has lead to increased pressure on the scientific community to find alternative methods for such processes. It is this increased pressure that has catalysed the development of alternative, greener chemical processes; the use of supercritical fluids being one of these.

The tunability of the properties associated with SCF's, allow them to be considered as potential alternatives to conventional solvents for many chemical reactions and processes [11]. SCF's have already been utilised in several chemical processes. These are summarised below:

1. *Catalytic Reactions in Supercritical Fluids* - The cost and associated efficiencies of continuous processes have long been a contributing factor in the design and efficient running of many large-scale industrial plants. When successfully combined with a versatile and environmentally benign solvent system such as supercritical fluids continuous processing can be seen to be

suitable for a wide variety of reactions (hydrogenation, hydroformylation, alkylation etc) which can be conducted efficiently in an environmentally sensitive way [11].

2. *Supercritical extraction* – Typically supercritical extraction has been used for the preparation of food ingredients and in the production of pharmaceutical compounds. However, supercritical processing has also been utilised in a variety of different fields including the production of polymers and superconductors. There are many large scale applications on supercritical extraction such as coffee decaffeination and hop resin extraction.
3. *Particle formation* - Traditional micronization processes can be improved by taking advantage of the unique characteristics of the supercritical antisolvent that include large diffusivities when compared with those liquids and the one step complete elimination of the solvent from the precipitates. Recently, extensive research has gone into the production of micro- and nano-particles utilising supercritical fluids. The production of these particles has mainly been from hydrothermal synthesis using supercritical water and antisolvent precipitation using supercritical CO_2. The environmentally benign properties of CO_2 make it the most widely used supercritical medium in particle formation. The production of such nano-particles as titanium oxide and cerium oxide (used as gold supports) have been major recent developments in the field of supercritical antisolvent precipitation.

1.4 Supercritical Antisolvent Precipitation

1.4.1 Principles of the Supercritical Antisolvent (SAS) Process

A supercritical fluid, as mentioned previously, is defined as a substance above its critical temperature (T_c) and pressure (T_p). Supercritical CO_2 is the most widely used supercritical fluid, largely owing to its mild operating conditions, gaseous standard state under ambient conditions, its non-toxicity and its relatively low cost compared with organic solvents. The favourable physical and chemical properties of CO_2 are some of the reasons why so many applications that use supercritical CO_2 focus on the production of pharmaceutical compounds that decompose under thermal treatment and can degrade in organic solvents [12-14].

In the supercritical antisolvent (SAS) process, supercritical CO_2 is used as an antisolvent that reduces the solubility of a solute dissolved in a solvent. Typically, that substance of interest is dissolved in an organic solvent and supercritical CO_2 enters the vessel [12]. The supercritical fluid should be completely miscible with the liquid solvent, whereas the solute should be insoluble in the supercritical fluid. Due to the phase behaviour of CO_2 with many solvents, the solution expands and its viscosity is greatly reduced. These property changes cause the solubility of the solute to decrease in the solvent. The expanded solution becomes supersaturated, thus forcing the solute to deposit as micro- or nano-sized particles.

The SAS method has been improved and developed by many researchers for the last decade to produce nano-sized particles with a narrow particle size distribution. In PCA (precipitation with compressed antisolvent) [15-17], the organic solvent is

sprayed through a nozzle into a precipitation chamber filled with supercritical CO_2. Mass transfer between the solvent and supercritical CO_2 is enhanced and fine particles are obtained. In SEDS (solution enhanced dispersion by supercritical fluids) process [18], after two streams involving the active substance and supercritical CO_2 are mixed with a co-axial double nozzle, the mixed solution is sprayed into a vessel that is maintained at ambient temperature and pressure. The SEDS allows both effective mixing and expansion of the supercritical CO_2 and enables finer particles to form. In the SAS-EM (supercritical antisolvent with enhanced mass transfer) process [18], a special device is used for forming nano-sized droplets. The jet of the organic solution involving the active substance through the nozzle is deflected by a surface vibrating at ultrasonic frequencies (20 kHz) to atomise the jet into much smaller droplets. In addition, the vibration is effective for preventing particle agglomeration in the solution nozzle resulting in reliable operation.

There are many variations and improvements to the supercritical antisolvent precipitation process as mentioned above. However the focus and main aims of the research that follows is largely based on the PCA (precipitation with a compressed antisolvent) process.

1.4.2 Experimental Apparatus

The use of supercritical antisolvent processes has been proposed as an alternative to liquid antisolvent processes. As mentioned previously there are several advantages to using these processes such as pressure reduction can completely remove the antisolvent to the gas phase. Liquid antisolvent processes require complex post-processing treatments to completely remove any residual liquid from the solute. The high diffusivities of supercritical antisolvent allow much faster diffusion into the liquid solvent, which causes supersaturation of the solute. The resulting precipitate is then composed of micro- or nano-particles, which are not possible to obtain using liquid antisolvents [19].

Supercritical antisolvent micronization has been performed using modified techniques and operating conditions. The results obtained can be influenced by the slight modifications made between various processes. However the majority of systems follow one of two operating methods; these are Batch and Continuous operation.

Batch Operation

Figure 1.2 below gives an overview of the batch apparatus. In this mode of operation, the precipitation vessel is loaded with the liquid solution, containing the solute. The supercritical fluid is then added until the final pressure is reached. The rate of addition of the supercritical antisolvent can have a major influence on the morphology and particle size of the solid particles. This mode of operation can be referred to as liquid batch operation.

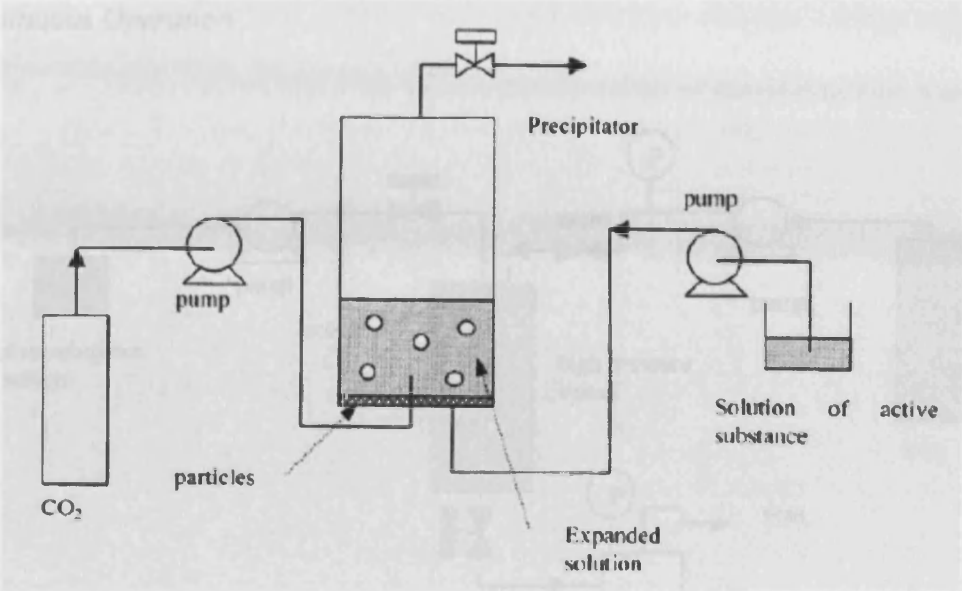

Figure 1.22 – Schematic diagram of SAS batch apparatus [19]

The precipitation chamber can also be charged with the antisolvent and the solvent injected into it. This mode of operation is termed gas batch operation.

The main difference between the two operational modes is that in the first case precipitation occurs in a liquid rich phase, whereas, in the second case it occurs in a supercritical fluid rich phase.

At the end of the precipitation process, the SCF remains to flow through the vessel. This is to remove any residual liquid solvent that may resolubilze the solute upon depressurisation [19].

Continuous Operation

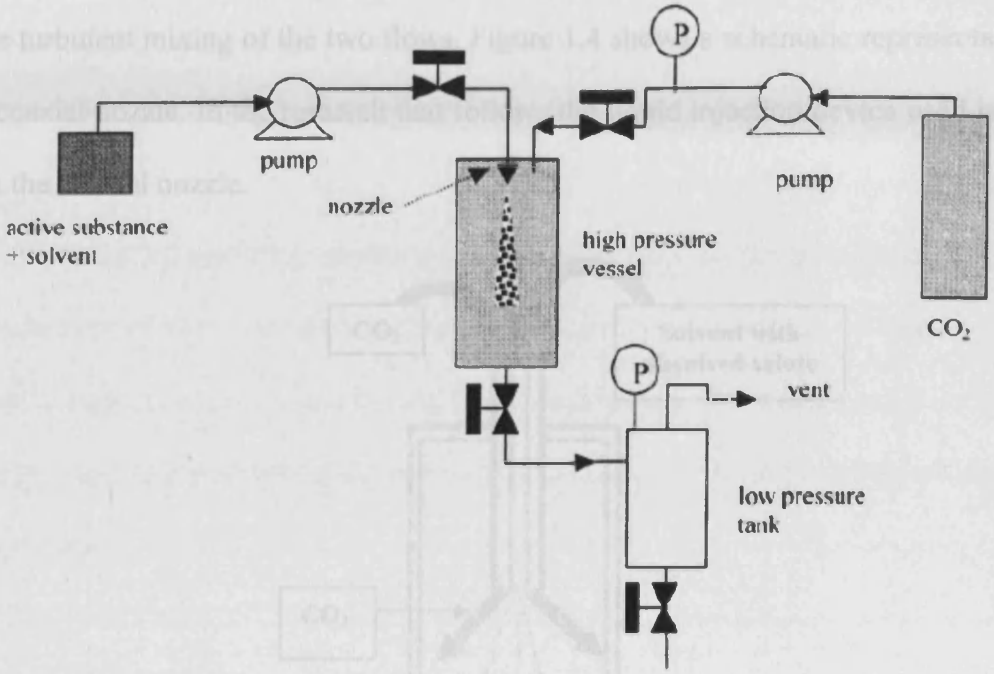

Figure 1.3 – Schematic diagram of SAS continuous apparatus [19]

Figure 1.3 shows a schematic representation of continuous flow apparatus. In this mode of operation both the liquid solution and the supercritical fluid are continuously delivered to the precipitation vessel. The flow rates and their ratio can be an important factor in the precipitation process. The pressure of operation can also be an important factor in this process.

The liquid injection device in this mode of operation is designed to produce liquid jet break-up and the formation of small droplets that expand in the precipitator. Precipitation from the droplet occurs when the local concentration exceeds the supersaturation limit. Various injection devices have been proposed such as capillaries [20, 21], vibrating orifices [20], coaxial devices [22, 23]. A coaxial nozzle is one in

which two capillary tubes deliver the liquid solution and the supercritical fluid simultaneously to the precipitation vessel, the formation of small droplets depends on the turbulent mixing of the two flows. Figure 1.4 shows a schematic representation of a coaxial nozzle. In the research that follows the liquid injection device used is based on the coaxial nozzle.

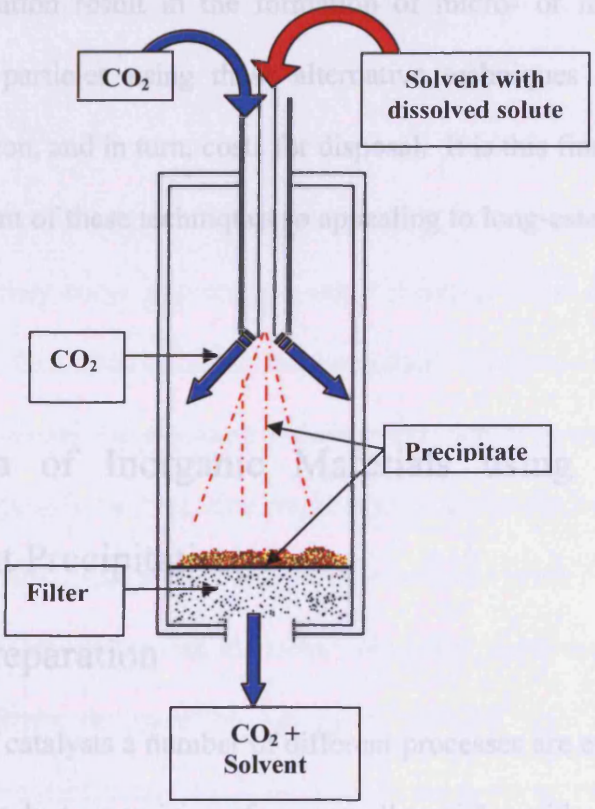

Figure 1.4 – Schematic of a coaxial nozzle as used in SAS apparatus

Various parameters can control the precipitation process, such as the pressure, and concentration of solute in the liquid solvent. The kind of injection device can also affect the precipitation process; the size of the droplets, their coalescence. The mixing of different fluids has to be considered.

The washing step that follows the precipitation process is essential in continuous operation. At the end of the precipitation process the solute is washed with pure antisolvent for a given period of time. This is to prevent condensation of the liquid phase that could resolubilze the solute or modify its characteristics.

Both modes of operation result in the formation of micro- or nanoparticles. The production of these particles using these alternative techniques could potentially reduce waste production, and in turn, costs for disposal. It is this financial benefit that makes the development of these techniques so appealing to long-established industrial processes.

1.5 Preparation of Inorganic Materials using Supercritical Antisolvent Precipitation

1.5.1 Catalyst Preparation

In the manufacture of catalysts a number of different processes are employed with the aim of producing a catalyst comprising of very small particles with very large surface areas. Typically to produce such particles it is necessary to use extreme operating conditions [9].

Supercritical antisolvent (SAS) precipitation has been recently proposed as a new technique for the production of nanoparticles of various materials including explosives [25, 26], proteins [27] and polymers [22, 23]. Supercritical CO_2 is of particular importance as it is cheap, non-toxic and has a relatively low critical state.

Among other materials, zinc oxide has been employed as both a catalyst, and catalyst support for metal and metal oxide catalysts [28]. Reverchon *et al* [9] have studied the SAS process to produce zinc acetate nanoparticles as a model compound for catalyst precursors. The operating parameters of the process, such as the pressure, temperature and solute concentration were varied to determine the effect on the production of nanoparticles.

The effectiveness of the SAS process relies on the very fast expansion process of the liquid droplets when they come into contact with the supercritical antisolvent. Rapid diffusion of the antisolvent into the liquid droplets causes expansion of the droplets, in the form of balloons, until the resulting balloons explode to produce the required nanoparticles. Reverchon found that zinc acetate balloons produced at 95 bar had a diameter of some microns, whereas the zinc acetate balloons produced at 150 bar had exploded producing zinc acetate nanoparticles. However, with increasing pressure there was only a slight decrease in the mean particle size of the produced nanoparticles. It was suggested that this is because in the pressure range of 110 to150 bar, DMSO is completely expanded in supercritical CO_2 and no further decrease of particle size can be obtained.

The concentration of the liquid solution was found to govern the diameter and the polydispersity of the zinc acetate nanoparticles. Using SEM, Reverchon confirmed that with increasing solute concentration there was an increase in particle size and polydispersity.

Changing the solvent had very little effect on the production of zinc acetate nanoparticles. However, Reverchon and co-workers observed one main difference; the zinc acetate nanoparticles produced *via* precipitation from NMP (n-methyl pyrrolidone) showed a partial coalescence. Using SEM, it was shown that the spherical nanoparticles had partly collapsed together. This effect was attributed to an interaction between the precipitated particles and the solution formed by NMP and supercritical CO_2. Also, NMP can have a mild co-solvent effect towards the zinc acetate nanoparticles when solubilised in supercritical CO_2.

Reverchon concluded that the process parameters that mainly control morphology, particle size and distribution of zinc acetate SAS precipitates were the concentration of the starting liquid solution and the liquid solvent used in the precipitation process.

Samarium oxide nanoparticles were also produced by Reverchon *et al* [8]. The thermal decomposition of samarium acetate prepared by supercritical antisolvent precipitate produces the samarium oxide catalyst. The activity of the catalyst for the oxidative dehydrogenation of ethane was compared to that of the conventionally prepared catalyst; the decomposition of the commercial acetate.

Reverchon studied the influence of the concentration on the mean particle size. As the concentration of the samarium acetate in DMSO was increased, an increase in the mean particle size was observed. This coincided with a larger increase in the particle

size distribution. Reverchon stated that the increase in solute concentration in the liquid carrier largely influences the polydispersity of particles.

The conversion of ethane on supercritically prepared samarium oxide increases with the temperature reaching 22 % at 680 °C as shown in Figure 1.5. The selectivity to ethylene increases with increasing the reaction temperature, reaching 12 % at 680 °C. Reverchon stated that this was due to progressive reduction of conversion to CO_2 and, at the higher temperature values to CO [8]. The comparison with the performances obtained with conventionally prepared samarium oxide shows that the consumption rate of ethane on the latter sample was three times higher than on the supercritically prepared samarium oxide when referred to the unit mass of catalyst, but three times lower with reference to the surface area.

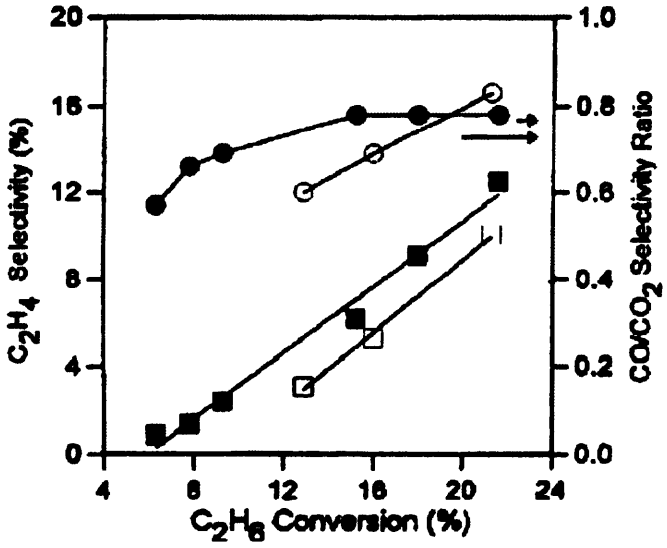

Figure 1.5 – Ethylene yield (■, □) and CO/CO_2 selectivity ratio (●, ○) versus ethane conversion on OxSm (SAS) (solid symbols) and on OxSm (open symbols) catalysts [8].

A further comparison in terms of ethylene yield was obtained. It was observed that the ethylene yield obtained with supercritically prepared samarium oxide was higher than with conventionally prepared samarium oxide at a given value of ethane conversion

Vanadium phosphate compounds are used commercially for the synthesis of maleic anhydride by the partial oxidation of *n*-butane. Therefore vanadium phosphate catalysts have been studied extensively. The current commercial catalysts are prepared from *in situ* activation of $VOHPO_4.0.5H_2O$. The resulting catalysts comprises a complex mixture of $(VO)_2P_2O_7$ in combination with α_{II}- and δ- $VOPO_4$ phases. Hutchings *et al* [23] have shown that rapid precipitation of a vanadium phosphate from an alcohol solution using supercritical CO_2 results in the preparation of an amorphous vanadium phosphate.

Hutchings found that both the alcohol and the method of solvent removal were important for the amorphous material to retain its amorphous character under reaction conditions. It was found that when isopropanol was used as the solvent and supercritical CO_2 as the antisolvent, the VPO material produced remained amorphous under reaction conditions. However, changing the solvent to isobutanol, resulted in the production of microcrystalline domains of $(VO)_2P_2O_7$ during catalyst testing. It was noted that this material was less active for the formation of maleic anhydride.

Liquid CO_2 was used instead of supercritical CO_2, this resulted in the production of an amorphous material. The material produced was found to partially crystallise during catalytic testing, to $(VO)_2P_2O_7$ and $VOPO_4$. Hutchings suggested that using

supercritical CO_2 affords the most rapid precipitation and the nature of the alcohol solvent can influence the precipitation process.

Hutchings *et al* [23] found a number of differences between the VPO material prepared by precipitation with supercritical CO_2 as the antisolvent and the crystalline VPO material prepared from $VOHPO_4.0.5H_2O$. The VPO material prepared using supercritical CO_2 did not require extensive pretreatment in the reactor; when the required operating temperature was attained the catalyst maintained stable catalytic performance for 100 h. However, the crystalline VPO material requires 24-72 h in the microreactor at reaction conditions to maintain a stable catalytic performance [24-27]. This period was required to establish the catalyst structure; $VOHPO_4.0.5H_2O$ transforms to $(VO)_2P_2O_7$. Hutchings and co-workers found that the amorphous VPO catalyst prepared using supercritical CO_2 was more active than the crystalline catalyst. This was because the supercritical derived material remains amorphous during the reaction period and maintains this enhanced activity.

Hutchings *et al* have shown there is an alternative preparation route for vanadium phosphate catalyst where supercritical CO_2 is used as the antisolvent. The resulting VPO catalyst retains its amorphous nature during the reaction period. The amorphous VPO catalyst has shown to be more active than the crystalline VPO catalysts for the selective oxidation of n-butane to maleic anhydride, and do not require pretreatment to establish maximum catalytic activity.

Recently, gold dispersed on metal oxide have been found to exhibit high catalytic activity in a number of reactions including CO oxidation [29]. The nature of the metal oxide support for the gold nanoparticles influences the catalytic activity of the gold catalysts; nanocrystalline oxide supports such as ceria, CeO_2 greatly increase the activity of gold catalysts for CO oxidation. This enhancement in catalytic activity prompted Hutchings *et al* to study the synthesis of nanocrystalline CeO_2 using the supercritical antisolvent process.

Samples of CeO_2 were prepared as a catalyst support in two ways. A standard sample was prepared by calcination of $Ce(acac)_3$ at 400 °C. The second way involved precipitation of a solution of $Ce(acac)_3$ in methanol using supercritical CO_2 as an antisolvent. The precursors obtained appeared amorphous and upon calcination at 400 °C gave the corresponding oxides. Gold was deposited on the surface of these oxides using the deposition precipitation method; 3.5 wt % gold was deposited on the surface of these catalysts.

Hutchings *et al* then assessed the catalytic activity of these catalysts for the oxidation of CO. The catalysts obtained from the supercritical antisolvent process exhibited enhanced catalytic activity by a factor of at least two compared with conventionally prepared Au/CeO_2 material, and the Au/CeO_2 standard material.

The support that produced the most catalytically active sample was found to consist of disordered, amorphous spheroid structures prior to calcination. Upon calcination each sphere crystallises to form a pseudo-spherical agglomerate of CeO_2 nanoparticles.

TEM images obtained by Hutchings and co-workers of the catalysts after Au deposition and calcination presented a clear difference in the support morphology for the standard Au/CeO_2 and the supercritically prepared Au/CeO_2. The $scCeO_2$ displayed polycrystalline pseudo-spherical agglomerates of particles, compared to the standard CeO_2 that consisted of more irregular dense agglomerates of crystallites.

The distribution of the Au particles over the surface was found to differ for the standard Au/CeO_2 compared with the supercritically prepared Au/CeO_2. The standard Au/CeO_2, which was found to be the poorest catalyst for CO oxidation, contained large Au particles in the range 35-80 nm. Compared with the $Au/scCeO_2$, which was the best CO oxidation catalyst, contained no discrete Au particles. Instead the gold was found to be uniformly distributed over the surface; possibly atomically dispersed over the entire surface of the CeO_2 support. Hutchings concluded that highly dispersed Au species on CeO_2 are significantly more active than discrete CeO_2 nanoparticles on CeO_2, and that the high dispersion is enhanced by the $scCO_2$ treatment of the support

Hutchings *et al* have prepared CeO_2 as a support for Au nanoparticles using the supercritical antisolvent process. The catalytic data obtained on the supercritical catalysts showed enhanced activity and stability for CO oxidation compared with the conventionally derived CeO_2. The Au catalysts obtained were amongst the most active catalysts reported for CO oxidation. Hutchings has shown that supercritical antisolvent precipitation has significant potential to produce supports that can be employed to prepare highly active oxidation catalysts. Therefore, using supercritical

CO_2 could potentially offer a nitrate free route to produce catalytic materials in an environmentally positive manner.

1.5.2 Other Reactions

High-temperature superconductors have large potential applications in the electro-technical industry. There are still problems to overcome before their industrial development. One problem is maintaining the superconducting characteristics in the presence of magnetic fields generated during normal operation. To avoid this pinning centres are generated by the precipitation of a secondary phase inducing fine non-conducting defects [30]. It has been suggested that micron or submicron inclusions of yttrium, europium, gadolinium, samarium or neodymium can improve the characteristics of the superconductor. Various microionisation techniques have been used but it has been suggested that supercritical fluids are an alternative to traditional processes [31]

Reverchon *et al* have studied the effect of different preparation parameters on a set of superconductor precursors including EuAc, GdAc, LaAc, YAc and SmAc. The parameters examined included the volumetric expansion of solvent, temperature, pressure, concentration, the feed ratio and different solvents.

Reverchon showed that the volumetric expansion of DMSO controlled the morphology of YAc particles produced by the supercritical antisolvent process. It was suggested that the solute concentration mainly controls the particle size and particle size distribution of the precipitated materials. The increase of diameter and

particle size distribution was found to correlate well with the reduced concentration of the tested solutes. It was found that when using the same reduced concentration for other solvents a similar trend was observed in the particle size and particle size distribution.

Reverchon *et al* have shown that it is possible to control the particle size, particle size distribution and morphology of the obtained particles which is essential for the preparation of nanoparticles and nanoscaled catalysts.

Recently, Alonso *et al* [32] have reported synthesis of titanium oxide from the SAS process without a calcination procedure. The precipitation was performed at a pressure of 10-20 MPa and the temperature of 200-300 °C. The temperature and pressure are both much higher than reported in previous work. Their process can be considered as a combination of precipitation and decomposition of as-prepared particles.

Alonso used the organometallic diisopropoxtitanium bis(acetylacetonate) (DIPBAT) as a precursor for the synthesis of TiO_2. Anatase titanium oxide with a mean diameter of 200 nm was obtained at 20 MPa and 300 °C using ethanol as a solvent. The surface area of the as-prepared anatase TiO_2 was up to 150 m^2g^{-1} using these supercritical conditions. Alonso investigated the effect of temperature, pressure and residence time on the precipitation and these are summarised in the table 1.2 below.

Table 1.2 – Summary of product characteristics at selected operational conditions for the production of TiO2

P (MPa)	T (°C)	Residence time (s)	TiO_2 anatase	Yield (%)	Average size (nm)	Product pollution (% C)	Crystallinity	BET area (m^2/g)
Batch process[a]								
10.0	300		Yes	74	200	7.1	Very good	108
20.0	300		Yes	88	450	1.2	Very good	113
20.0	250		Yes	75	300	2.0	Good	160
20.0	200		¿?	-	-	12.0	Poor	350
Semi-continuous process[b]								
20.0	300	120	Yes	85	250	<1	Very good	159
20.0	300	90	Yes	82	125	<1	Very good	152
20.0	300	60	Yes	80	100	<1	Very good	140
20.0	300	30	¿?	-	-	-	Poor	-
20.0	300	20	¿?	-	-	-	Poor	-

[a] Initial concentration = 0.05 g DIPBAT/g reaction medium. Hydrolysis reactant: ethanol. Molar ratio EtOH/DIPBAT = 28.
[b] Hydrolysis reactant: ethanol. Molar ratio EtOH/DIPBAT = 28.

Alonso attributed the formation of TiO_2 as the hydrolysis of DIPBAT, followed by the decomposition of the hydroxide. The reaction mechanism of the hydrolysis and decomposition process is described as follows:

$$Ti(OR)_2(OR')_2 + H_2O \leftrightarrow Ti(OR)(OR')_2(OH) + ROH$$

$$Ti(OR)(OR')_2(OH) + H_2O \leftrightarrow Ti(OR')_2(OH)_2 + ROH$$

$$Ti(OR')_2(OH)_2 + H_2O \leftrightarrow Ti(OR')(OH)_3 + R'OH$$

$$Ti(OR')(OH)_3 + H_2O \leftrightarrow Ti(OH)_4 + R'OH$$

$$Ti(OH)_4 \leftrightarrow TiO_2 + 2H_2O$$

In this process, water for hydrolysis is generated by decomposition of ethanol in the supercritical process. A molar ratio of at least 28 mol EtOH/ mol DIPBAT is required for the complete reaction to form anatase TiO_2. At the same time, a high temperature of 300 °C is essential to complete the decomposition of titanium hydroxides.

Alonso *et al* have shown that it is possible to produce metal oxides without the need for a post reaction calcination step. This work also shows that it is possible to retain the high surface area of the as-prepared catalyst which is essential for the preparation of nanoscaled oxide catalysts in the future.

1.6 Target Materials

1.6.1 Iron Molybdates

Formaldehyde is an irreplaceable C_1 building block for higher-valued products. The main use of formaldehyde and its polymers is in the synthetic resins industry where it serves principally in the production of thermosetting resins, oil soluble resins and adhesives. Remaining formaldehyde is consumed in the manufacture of textiles, paper fertilizers, miscellaneous resinous products and other chemicals [33].

All the worlds' production of formaldehyde is based on heterogeneous catalytic processes using methanol as feedstock. There are several industrial processes that are used to convert methanol to formaldehyde these include silver based catalysts and iron molybdate catalysts. In the silver process, formaldehyde is produced by methanol oxidation and methanol dehydrogenation [34]. Over iron molybdate catalysts formaldehyde is produced by methanol oxidation only.

Excess air is used in the iron molybdate process to ensure near complete conversion and to avoid the explosion limits of methanol (6.7-36.5 vol% in air). The reaction temperature is maintained below 400 °C to ensure the stability of the catalyst and to limit side reactions. For iron molybdate catalysts the conversion and selectivity can be

as high as 99% respectively. There are two stoichiometric iron-molybdates, ferric $Fe_2(MoO_4)_3$, and ferrous $FeMo_4$, but only the first can be used to catalyse the selective oxidation of methanol to formaldehyde.

A number of techniques have been reported for the production of iron molybdate catalysts based around the coprecipitation method. Adjusting the variables in the coprecipitation technique leads to a change in the physical-chemical characteristics of the prepared iron molybdate, and therefore the catalytic behaviour. The factors of significant importance are the Mo and Fe precursors, concentration of the initial solutions, and order of addition of such solutions, temperature and pH during precipitation, stirring, and aging of the precipitate and calcination conditions.

Kerr *et al* [35] prepared iron molybdates from coprecipitation of sodium molybdate and iron chloride. On the laboratory scale, iron molybdates are prepared from the coprecipitation of iron nitrate and ammonium heptamolybdate which avoids the contamination of sodium and chlorine; which are detrimental to the catalytic activity [36, 37]. The precipitation is carried out under vigorous stirring with a pH between 1.5 and 2. The pH of the solution is maintained throughout by the addition of nitric acid. The temperature of the reaction can vary from room temperature to the boiling point of the parent solutions. The precipitate is filtered, dried and calcined between 300 and 600 ^{o}C for 1-10 hours [36].

Kolovertnov *et al* [38] found that the catalytic activity of iron molybdates depends on the Fe/Mo atomic ratio of the catalyst, and found an optimal activity for Fe/Mo atomic

ratio of 1.7. Industrial iron molybdate catalysts have and Mo/Fe ratio between 2.3 and 5. However, Soares *et al* [39] found that the activity per unit surface area is independent of the Mo/Fe atomic ratio of the catalyst. Sun-Kuo [40] investigated the influence of several variables of the precipitation technique on the catalytic behaviour of iron molybdate catalysts. The authors found that the optimal Mo/Fe atomic ratio was 1.7.

Iron molybdate catalysts can be calcined under varying conditions. Arruano and Wanke [41] investigated the effect of calcination temperature on the catalytic activity. The authors found that catalysts calcined under an air flow at temperatures in the range 530-820 K for 18 h resulted in an increase in specific activity of 30 %. In contradiction to this, extended thermal treatments (572 h) resulted in a decrease in specific activity of the catalyst. Trifirò *et al* [42] found three different transformations in the catalysts with increasing calcination temperatures. The first transformation being observed at 350 °C, attributed to the start of bulk diffusion, an increase in the electric conductivity and high CO selectivity. The second being observed between 450 and 500 °C, and was characterised by the total oxidation of Fe^{2+} to Fe^{3+} with water elimination and the formation of CO_2 during methanol oxidation. The final transformation occurring at 600 °C and was characterised by a decrease in surface area and a severe decrease in catalytic activity.

Iron molybdenum catalysts typically have a large excess of molybdenum. Some authors have attributed the catalytic activity to the $Fe_2(MoO_4)_3$ while others consider the active phase to be the mixed oxide with a slight Mo excess.

Sun-Kuo *et al* [40] suggest that the active phase is the Mo rich iron molybdate as a consequence of the excess Mo to change the coordination from tetrahedral to octahedral. Soares *et al* [39] found that the catalyst activities per unit surface area of the stoichiometric and Mo rich iron molybdate (atomic ratio Mo/Fe = 3) are identical. This indicated that under reaction conditions the surface of the Mo rich iron molybdate is stoichiometric molybdate due to sublimation of Mo excess. Therefore Soares *et al* suggested that the active phase could be assigned to the stoichiometric Mo-Fe-Mo mixed oxide.

Bowker *et al* [43] studied the oxidation of methanol over iron molybdenum catalysts and over each metal oxide. They found that when iron oxide was used, formaldehyde was not detected. Molybdenum oxide displayed high selectivity towards formaldehyde and the mixed Mo-Fe oxides were found to be more active than MoO_3. These authors attributed the difference in behaviour between molybdenum and iron samples to the binding energy of oxygen and the higher concentration of cation sites of iron samples. They postulated that over Fe_2O_3 only bidentate formate species are formed whereas MoO_3 samples mainly lead to methoxy adsorbed species.

From the work above it can be concluded that the active phase is the stoichiometric iron molybdate, but an excess of molybdenum is required to prevent the formation of iron rich phases on the catalyst surface during reaction due to loss of MoO_3.

Farneth *et al* [44] studied the kinetics of methanol to formaldehyde over MoO_3. It was suggested that the reaction mechanism is a Mars-van Krevelen mechanism, which was previously suggested as the mechanism for methanol oxidation over iron molybdate catalysts. From the results obtained Farneth concluded that the oxygen from the catalyst lattice participates in the reaction. TPD tests with deuterated methanol allowed the confirmation that the controlling step is the abstraction of hydrogen from the methyl group. Figure 1.6 shows the proposed scheme for the catalytic cycle for methanol oxidation over MoO_3.

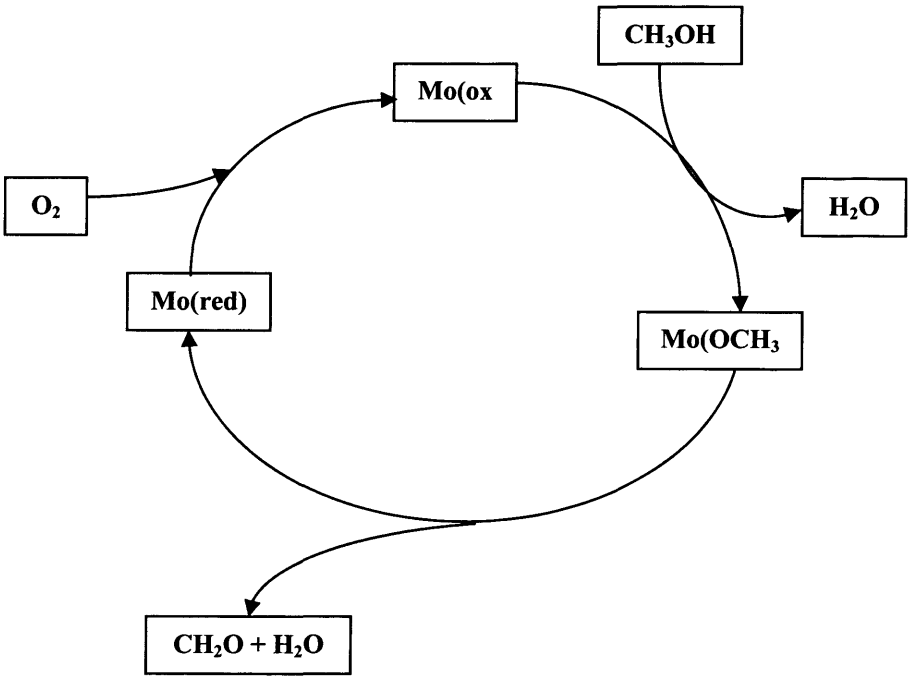

Figure 1.6 - Proposed catalytic cycle for methanol oxidation over MoO_3 [44].

McCarron *et al* [45] have attempted to synthesise methanol molybdenum model compounds that are supposed to participate in the redox cycle during methanol oxidation over molybdate catalysts. These authors prepared and characterised $Mo_2O_5(OCH_3)_2$ and $Mo_2O_5(OCH_3)_2.2CH_3OH$ and found that decomposition of these oxy-methoxides, results in formaldehyde formation as in the proposed catalytic cycle.

Figure 1.7 shows the model catalytic cycle and the reaction chemistry observed by the authors.

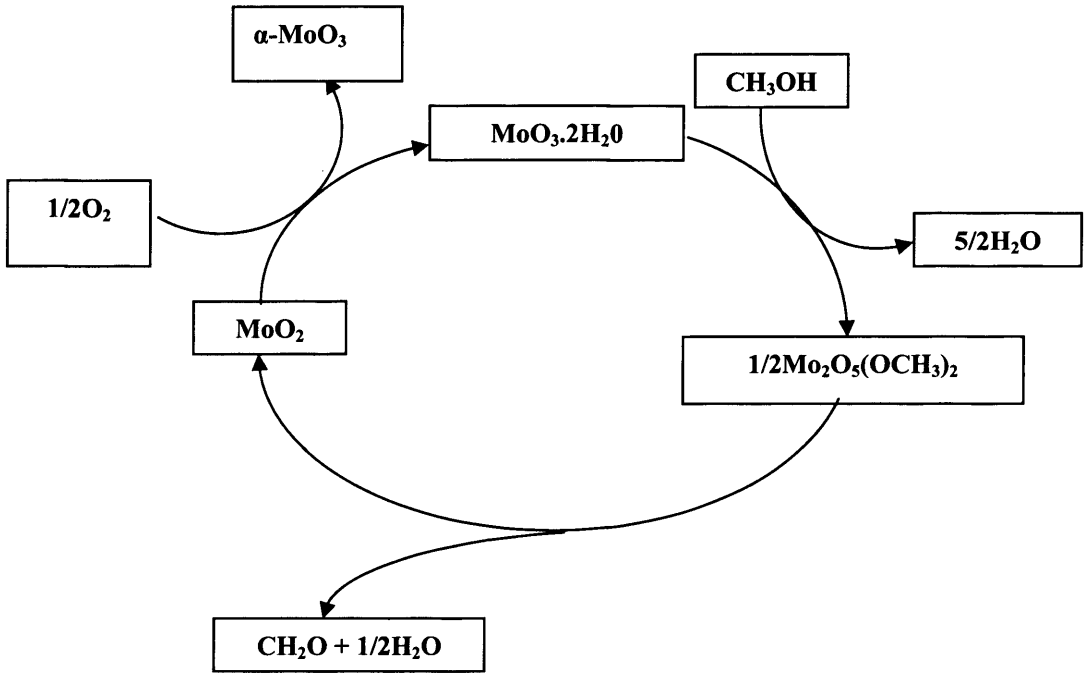

Figure 1.7 – The model catalytic system for formaldehyde production [45].

From the catalytic cycles described above it can be concluded that the oxidation of methanol over iron molybdate catalysts occurs through a Mars-van Krevelen mechanism for which the hydrogen abstraction from methoxy species, adsorbed on the catalyst surface is the controlling step.

Iron molybdate catalysts have high selectivity towards formaldehyde when catalysing the oxidation of methanol. However, other products are formed depending on the catalyst type and reaction conditions. Typically, dimethylether, methylformiate, dimethoxymethane, carbon monoxide and carbon dioxide are produced in side

reactions during the oxidation of methanol. Figure 1.8 shows the reaction scheme proposed by Tatibouët *et al* [46].

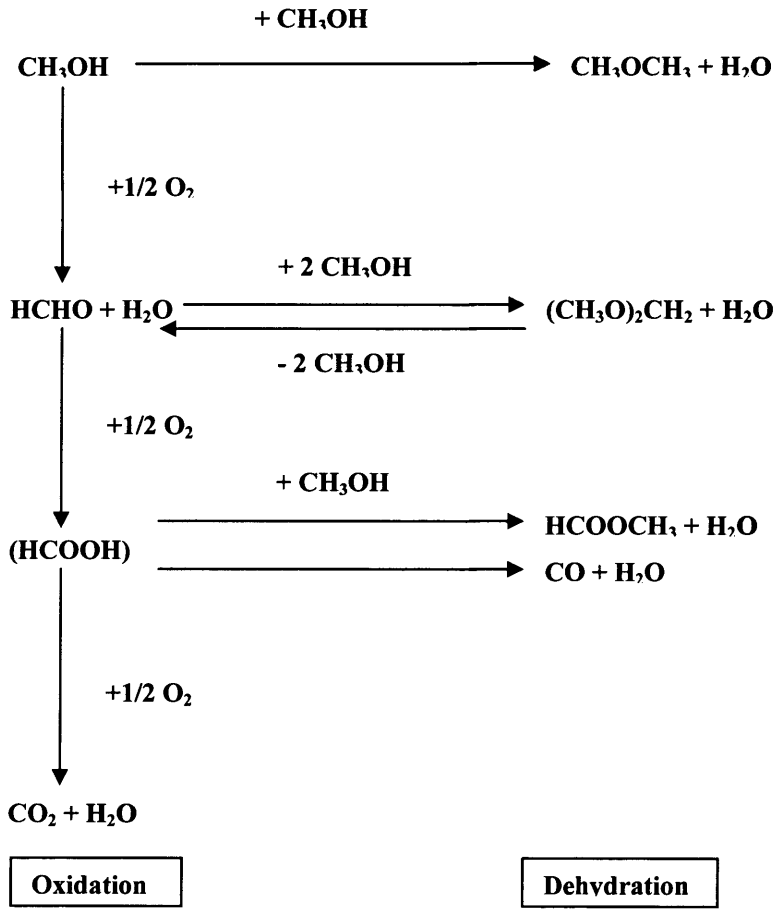

Figure 1.8 – Reactions for oxidation and dehydration of methanol [44].

According to this scheme, the formation of all products requires at least one oxidation step. The formaldehyde formation requires a redox dehydrogenation site, whereas the selective formation of dimethoxymethane involves a dual site including a redox dehydrogenation site and a Lewis acid site. A change in the Lewis acidity of the catalyst in turn causes a change in the dimethoxymethane to formaldehyde selectivity ratio. The formation of dimethyl ether is assigned to the presence of strong acid sites.

Generally, dimethyl ether, methylformiate, dimethoxymethane and carbon monoxide are referred to as by-products of the reaction. CO is considered as the major by-product. The selectivity towards formaldehyde increases with methanol conversion except for high levels of conversion where the formation of CO starts to be important.

Iron molybdates deactivate during methanol oxidation to formaldehyde. Popov *et al* [47] suggested that this deactivation is due to the loss of Mo from the catalysts surface as volatile compounds of Mo and methanol. Aruano and Wanke [41] attributed this loss in activity to the decrease in surface area of the catalyst. The decrease in activity of the catalysts submitted to high temperatures was attributed to the segregation of the catalysts into two different phases, MoO_3 and $Fe_2(MoO_4)_3$.

Pernicone *et al* [48] studied the deactivation of iron molybdates on the laboratory scale to simulate the deactivation process occurring in industrial plants. Pernicone suggested that the deactivation of iron molybdate catalysts in industrial plants is due to loss of Mo by volatilisation, which results in the formation of α-Fe_2O_3. It was found that the catalyst samples from the hot-spots had a red-brown colour instead of the characteristic yellow-green colour of the fresh iron-molybdates. XPS revealed that the deactivated catalyst had at the surface a Mo/Fe atomic ratio of 1, that evidenced the presence of $Fe_2(MoO_4)_3$-$1/2Fe_2O_3$. Pernicone suggested that the reduction of the catalyst in some reactor zones for high methanol concentrations proceeds *via* the reaction shown below:

$$\mathbf{Fe_2(MoO_4)_3 + CH_3OH = 2FeMoO_4 + MoO_3 + HCHO + H_2O}$$

The MoO_3 and $FeMoO_4$ formed in such reactions are less active than $Fe_2(MoO_4)_3$ and the reoxidation of $FeMoO_4$ produces Fe_2O_3. The deactivation of iron molybdate catalysts, during methanol oxidation to formaldehyde, is attributed to the loss of MoO_3 by volitisation. Volatile MoO_3 is formed by the oxidation of $FeMoO_4$ formed in the redox process:

$$\mathbf{2FeMoO_4 + \tfrac{1}{2}O_2 = Fe_2O_3 + 2MoO_3}$$

This process produces the unselective Fe_2O_3 responsible for the reddish-brown colour of waste catalysts.

Therefore there is much scope for the development in the stability of the catalyst to prevent deactivation of the catalyst under reaction conditions; preventing the loss in activity while maintaining the selectivity for formaldehyde.

1.6.2 Copper Manganese Oxides (Hopcalite)

Copper manganese mixed oxides have been used as catalysts for the oxidation of carbon monoxide to carbon dioxide. Copper manganese oxides are powerful oxidation catalysts and can catalyse the oxidation of carbon monoxide at near room temperature. They have been utilised in respiratory protection for mining industries and deep sea diving, where low levels of carbon monoxide are oxidised in personal protective masks and respirators. Catalysts are used in CO_2 lasers for weather monitoring and other remote sensing applications [49, 50]. Recently they have been used in CO sensors, which provide invaluable early warning signals of a potentially lethal build up of CO [51]. Copper manganese mixed oxide catalysts are inexpensive alternatives to precious metal containing catalysts.

Then use of copper manganese mixed oxides for the oxidation of CO has been extensively researched since the beginning of the 20th century. The commercial copper manganese mixed oxide was given the name Hopcalite. The name was derived from the fundamental investigations of carbon monoxide oxidation performed by the Johns Hopkins University ("Hop") and the University of California ("Cal") during the First World War [52]. The development of the Hopcalite catalyst was supported by funding from the U.S. Navy for the manufacture of a carbon monoxide mask for naval use. It was decided that it was necessary to develop a catalyst that would rapidly oxidise carbon monoxide at low temperatures, be robust enough to retain its structure upon rough handling, and be chemically stable.

Spinel-like structured metal oxide and mixed metal oxide systems have considerable electrical and magnetic properties. The nature of the metal ions and their distribution in the crystal lattice greatly influence these properties. The distribution and valence sites of the cations both the tetrahedral (A sites) and octahedral (B sites) sub lattices of the spinel structure continue to be a problem [53].

Zaslavskii and co-workers [53] reported that $CuMn_2O_4$ is an inverse, cubic spinel, but were unable to decide whether the inversion was complete or whether the cation distribution was statistical. Miyahara [54] believed that the absence of distortion could be due to a compensation effect of Cu^{2+} and Mn^{3+}. The presence of Cu^{+} and Mn^{4+} was suggested by Dollimore and Tonge and Sinha and co-workers [55]. The high electric conductivity in $CuMn_2O_4$ [56, 57] requires that the same metal ions should be

present in mixed valence states enabling electron hopping at either the tetrahedral or the octahedral sites; suggesting that it is unlikely that only Mn^{3+} and Cu^{2+} be present. Many investigations have been performed on the structure and oxidation states of the components of $CuMn_2O_4$, however, little is known about the active site of the catalyst, the role of Cu as a promoter, the mechanism of oxidation and the deactivation mechanism of the catalyst.

The activity of the copper manganese oxide is dependent on the structure of the catalyst precursor. The structure of the catalyst precursor is governed by the preparation route. Porta *et al.* [58] reported that the structure of the hydroxyl carbonate phase of copper manganese catalysts is vital in the preparation process. Therefore, it was concluded that preparation conditions can influence the overall catalytic activity for CO oxidation, which caused extensive research to be performed by Hutchings *et al.* [59].

The coprecipitation procedure is typically used for the preparation of copper manganese oxides. In this procedure, suitable metal salts are premixed, usually nitrates, and a precursor is precipitated using sodium carbonate. There are many parameters that can be varied during the preparation that can greatly influence the activity of the final catalyst; one parameter being the ageing process. Hutchings *et al.* studied the influence of the ageing process on the activity of the catalyst [60]. They found that the ageing parameter is one of significant importance in the preparation of copper manganese mixed oxides. The unaged copper manganese oxide precursor was composed of crystalline copper hydroxyl nitrate and manganese carbonate. The

ageing process caused the copper hydroxyl to re-dissolve and the precursors were found to be comprised of poorly crystalline manganese carbonate.

Hutchings and co-workers [61] investigated the effect of preparation conditions on the catalytic performance of copper manganese oxide catalyst for CO oxidation. Several variables were studied including the precipitate ageing time, pH, temperature of precipitation, the Cu/Mn ratio of the precipitation solution and the calcination temperature. The optimum conditions reported for the highest conversion of CO were:

- [Cu]/[Mn] ratio = 1/2
- Precipitation pH = 9.0
- Precipitation temperature = 80 °C
- Ageing time = 12 h
- Calcination = 500 °C for 17 h

The highest CO conversion was found to be the catalyst calcined at 500 °C, which according to powder X-ray diffraction, appeared to be amorphous and composed mainly of the stoichiometric Hopcalite phase $CuMn_2O_4$. Calcination at 300 and 400 °C, resulted in copper manganese oxides comprised of separate $MnCO_3$ and CuO phases which contributed to lower activity (ca 60-80% conversion). At pH 9, the most active catalyst was produced, however the active phase, $CuMn_2O_4$, was prepared at pH 8.3.This was due to the fact that the Cu/Mn bulk ratio was not affected by the solution pH as they were close to the preparation media.

The most active copper manganese oxide catalyst corresponded to a Cu/Mn ratio of a ½. This preparation resulted in the production of the $CuMn_2O_4$ phase. This phase has been identified as the phase with the highest specific activity for CO oxidation [39].

Hutchings *et al.* [62] reported that the presence of residual sodium can lead to catalyst poisoning. Sodium carbonate is used during the co-precipitation procedure to control the pH of the precipitation mixture. The highest activity was recorded for the sample aged for 12 h (ca 80% conversion). The Na/Mn surface ratio was significantly lower with longer ageing time. Analysis of the surface of the catalysts by X-ray photoelectron spectroscopy revealed that the catalysts aged at pH 8.3 showed the lowest concentration of Na^+ cation on the surface.

1.6.2 Continuous Catalytic Reactions in Supercritical Fluids

The increased awareness of the environmental impact associated with a large number of chemical processes has influenced the chemical industry to adopt a cleaner approach to manufacture. When successfully combined with a versatile and environmentally benign solvent system, continuous processing can be achieved for a wide variety of reactions, including hydrogenation, hydroformylation and alkylation, in an environmentally sensitive way.

The main advantage of the continuous reactor over the batch reactor is that no depressurisation step is required to recover the products. The schematic of a continuous reactor is shown in figure 1.9.

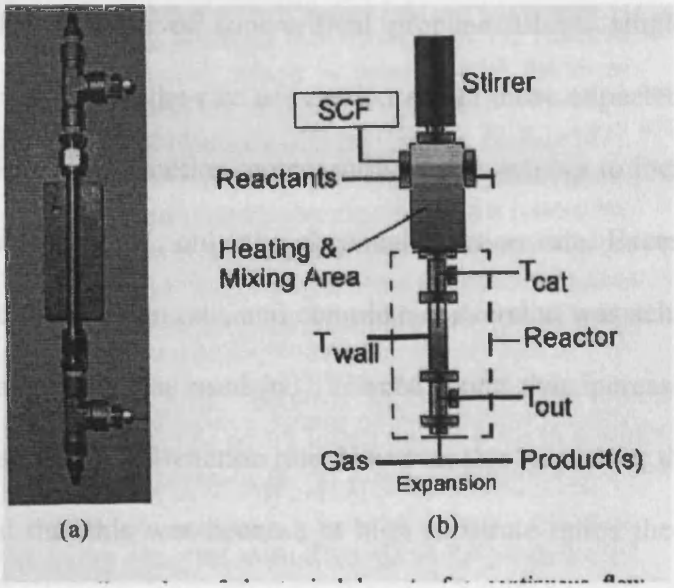

Figure 1.9 – Illustration of a continuous flow supercritical reactor. Actual reactor (a) represents the area within the dotted box in (b) [62].

In a continuous flow system, variables such as temperature, pressure and flow rates can be varied independently of one another. The main benefit of this is that the properties of the fluid can be changed in real-time to optimise the conditions; making continuous reactors more versatile for performing reactions in SCFs.

Hydrogenation reactions have been extensively researched for the application of SCFs in this catalytic process. The main areas of heterogeneously catalysed hydrogenation include the hydrogenation of food compounds, the formation of precursor building blocks for pharmaceutical and fine chemicals and asymmetric hydrogenation.

Härröd *et al* [62] have shown that it is possible to hydrogenate oleochemicals, investigating the effects that both the hydrogen and substrate ratios have on the conversion and the selectivity of the reaction.

Härröd found that the use of supercritical propane allows single-phase reaction conditions which increased the rate of reaction above those expected for multi-phase conditions. Increasing the reaction temperature was shown not to increase the activity of the catalyst above 280°C, only the chemical reaction rate. Excess hydrogen was found to increase the reaction rate, and complete conversion was achieved within 100 ms, when a ratio of 1:64 was used [63]. Härröd found that increasing the substrate ratio resulted in an increased reaction rate. However this was lower than expected and Härröd suggested that this was because at high substrate ratios the viscosity of the reaction mixture increased which in turn lowered the mass transport capabilities of the supercritical fluid and lowered the local concentration of reactants at the catalyst surface. A comparison of $scCO_2/H_2$ and scC_3H_8/H_2 mixtures showed that the $scCO_2$ system allows for a higher conversion but scC_3H_8 permits a higher throughput. Also the scPropane system produced a significant amount of by-products.

The hydrogenation of simple building blocks has also received much interest recently. Hitzler *et al* [64] have utilised the continuous flow reactor for the hydrogenation of cyclohexene. Quantitative conversion at flow rates of up to 20 ml min^{-1} were achieved which were comparable to those reported for hydrogenation of cyclohexene over Pd/C catalyst.

Selective hydrogenation reactions are one of the main drivers for performing larger-scale reactions owing to their tunability properties. The hydrogenation of α,β-

unsaturated aldehydes is an important reaction for high value product synthesis and one of the more studied substrates.

Hydroformylation is the catalytic addition of carbon monoxide and hydrogen to olefinic precursors. The products of this reaction are important precursors and intermediates in both the pharmaceutical and the fine chemical industries. The main problems associated with this reaction are regioselective control, and undesired side reactions.

Sellin *et al* [65] have shown that metal complexes insoluble in $scCO_2$ can catalyse the hydroformylation of hexane, a number of ligand systems were investigated which co-ordinated to Rh in solution leading to an *in situ* generation of the desired heterogeneous catalysts.

Sellin [65] found that all reactions performed resulted in a higher selectivity for the *n*-isomer when reactions were carried out in $scCO_2$. This trend was found to be the complete opposite when compared to reactions carried out in conventional solvents. Also increasing the H_2:CO_2 ratio was found to increase the $\underline{n}$:*i* ratio.

The reductive deposition of rhodium metal onto an activated charcoal support yielded a novel, supported hydroformylation catalyst for the hydroformylation of propene [66]. Aldehyde yields of up to 10% were recorded. Faster reactions were observed with larger pore size supports; this rate enhancement was attributed to the acceleration of the adsorption rate of propene into the larger pores.

Meehan *et al* [67] studied a similar reaction; the hydroformylation of 1-octene. Octene conversions of up to 14.3% were observed with respectable *n:i* ratios. The utilisation of a supported homogeneous catalyst gave rise to a robust catalyst that showed no sign of leaching from the catalytic species, even after prolonged use of the catalysts.

The problems associated with typical Friedel Crafts reactions, both acylation and alkylation are product selectivity and atom inefficiency. Typically these reactions are carried out as batch-type processes involving large amounts of catalysts, which are commonly either Lewis acids or strong mineral acids. Some heterogeneously catalysed Friedel Crafts reactions are beginning to emerge but few are performed in supercritical fluids.

Hitzler *et al* [64] have shown that it is possible to perform Friedel crafts alkylation in supercritical CO_2 using *i*-propanol as an alkylating agent. It was shown that anisole can be efficiently alklylated continuously to produce both the mono- and bis-substituted products.

Shi *et al* [68] have studied the alkylation of benzene by ethylene over a high surface area β-zeolite catalyst. Shi studied the reaction at five different temperatures and pressures near the critical point of the binary system; one was in the supercritical region. The maximum rate of reaction occurred near the critical point, but the presence of a multi-phase mixture may have lead to the degradation of the catalyst. Zeolites have been studied in conventional Friedel crafts reactions, and the decrease in

activity is thought to be due to the formation of carbonaceous coke on the catalyst surface.

1.7 Aims of the Project

The above examples of the reactions performed in supercritical fluids show that they provide an alternative route to a number of target materials in a number of different types of reactions.

The use of nitrate precursors for the production of mixed oxide catalysts such as iron molybdates and copper manganese oxides has been well documented in the literature. Nitrates have been used because of their high solubility and the ease of removal of the nitrate anion during calcination. In the case of copper manganese oxides, the use of chlorides and sulphates leads to the retention of the anion on the surface of the catalyst, using nitrates leaves no residue on the catalyst. The use of nitrates, however, is unfavourable due to the environmental issues associated with them.

The main aim of this project is to provide a nitrate free route for the production of iron molybdate and copper manganese oxide catalysts. Using supercritical antisolvent precipitation to provide an alternative preparative route for the production of these catalysts must result in an activity comparable to those currently prepared using the conventional preparation methods i.e the use of nitrate precursors.

The need for highly active mixed oxide catalyst has also caused the current reactor design to be reviewed to see if it is suitable for the supercritical process. This

investigation has lead to the production of a second reactor which improved design features, and finer parameter control with the aim of improving the activity of the prepared catalysts.

1.8 References

[1] P.T Anastas and L.G Williamson, *Green chemical syntheses and Processes*, American Chemical Society: Washington DC, 200: Chapter 1

[2] S.K. Riter, *Chem. Eng. News*, 2001, **79**, 27

[3] P.T. Anastas, J.C. Warner, *Green Chemistry: Theory and Practice*, Oxford University Press: New York, 1998, p.30

[4] A. Baiker, *Chem.Rev.* 1999, **99**, 453

[5] R. Noyori, *Chem. Com.* 2005, **14**, 1807

[6] P.G. Jessop, T. Ikariya and R. Noyori, *Chem. Rev.* 1999, **99**, 473

[7] E. Reverchon, *J. Supercrit. Fluid*, 1999, **15**, 1

[8] E. Reverchon, G.D. Porta, D. Sannino, L. Lisi and P. Ciambelli, *Stud. Surf. Sci. Catal.* 1998, **118**, 349

[9] E. Reverchon, G.D. Porta, D. Sannino, and P. Ciambelli, *Powder Technol.*, 1999, **102**, 127

[10] J. A. Darr and M. Poliakoff, *Chem. Rev.* 1999, **99** 495

[11] M. Poliakoff, J.R. Hyde, P. Licence, D. Carter, *Appl. Catal. A: Gen* 2001, **222**, 119

[12] H. Hayashi, Y. Hakuta, K. Arai, *Curr. Opin. In Sol. State. and Mat Sci.*, 2003, **7** 341

[13] J.R. Willaims, A.A. Clifford, S.H.R Al-Saidi, *Mol Biotech.* 2002, **22,** 263

[14] H.P. Hentze and M. Antonietti Rev. Mol. Biotecnhol. 2002, **90**, 27

[15] H. Kröber and U. Teipel, J. Supercrit. Fluid, 2002, 22, 239

[16] H. Kröber and U. Teipel, *In: Proc 6th nt. Symp. Supercrit. Fluid,* 2003, **3**, 1641

[17] Y Pérez, F.E. Wubbolts, G.J. Witkamp, *In: Proc 6th nt. Symp. Supercrit. Fluid,* 2003, **3**, 1883

[18]J.C. Hooton, C.S. German, S. Allen, M.C. Davies, C.J. Roberts and P.M. Willaims, *Pharmaceut. Res.* 2003, **20**, 508

[19] E. Reverchon, *J. Supercrit. Fluids*, 1999, **15**, 1

[20] T.W. Randolph, A.D. Randolph, M. Mebes, and S. Yeung, *Biotechnol. Progress*, 1993, **9**, 429

[21] D.J. Dixon, K.P. Johnston and R.A. Bodmeier, *AIChE J.* 1993, **39**, 429

[22] P. York, M. Hanna, *Internat. Patent*, 1994, C07C215/60

[23] S. Jaarmo, M. Rantakyla, O. Aaltonen, *4th Internat. Symp. Supercrit Fluids*, 1997, 263

[25] E. Reverchon, G.D. Porta, S. Pace, A. Di Trolio, *Ind. Eng. Chem. Res*, 1998, **37** 952

[26] E. Reverchon, C. Celano, G.D. Porta, A. Di Trolio, and S. Pace, *Ital. Patent*,1997 No. SA 97A/10

[27] Y. Gao, T.K. Mulenda, Y. –F. Shi, W. –K. Yuan, *4th Internat. Symp. Supercrit Fluids*, 1997, 31

[28] G.A.M. Hussein, *Thermochim. Act*a, 1991, **186**, 187

[29] Z.Tang, J.K. Edwards, J.K. Bartley, S.H. Taylor, A.F. Carley, A.A. Herzing, C.J. Kiely, G.J. Hutchings, *J. Catal.*, 2007, **249**, 208

[30] H. Kamiya, A. Kondo, T. Yokoyama, M. Naito, G. Jimbo, S. Nagaya, M. Miyajima and I. Hirabayashi, *Adv. Powder Technol.* 1994, **5**, 339

[31] E. Reverchon, I. De Marco and G.D. Porta, *J. Supercrit. Fluids*, 2002, **23**, 81

[32] E. Alonso, I. Montequi, S. Lucas and M.J. Cocero, *J. Supercrit. Fluids*, 2007, **39**, 453

[33] H.R. Gerberich, A.L. Stautzenberger and W.C. Hopkins, *Encyclopaedia of Chemical Technology 3rd Edition,* 1983 **11**, 231

[34] J.R. Fair and R.C Kmetz, *Encyclopaedia of Chemical Processing and Design*, 1985, **23**, 350

[35] P.F. Kerr, A.W. Thomas and A.M. Langer, *The Amer. Minerol.*, 1963, **48**, 1

[36] L. Cairati, M. Carbucicchio, O. Ruggeri and F. Trifirò, *Stud. Surf. Sci. Catal.*, 1979, **3**, 279

[37] P. Forzatti, P.L. Villa, N. Ferlazzo and D. Jones, *J. Catal.*, 1982, **76**, 188

[38] G.D. Kolovertnov, G.K. Boreskov, V.A. Dzisko, B.I. Popov, D.V. Tarasova and G.C. Belugina, *Kinet. Catal.* 1965, **6**, 950

[39] A.P.V. Soares, M.F. Portela and A. Kienneman, *Catal. Rev.*, 2005, **47**, 125

[40] M.R. Sun-Kou, S. Mendioroz, J.L.G. Fierro, J.M. Placios and A. Guerrero-Ruiz, *J. Mater. Sci.,* 1995, **30**, 496

[41] J. Arruano and S. Wanke, *J. Chem. Eng.*, 1975, **53**, 301

[42] F. Trifirò, S. Notarbartolo, and I. Pasquon, *J. Catal*, 1971, **22**, 324

[43] M. Bowker, R. Holroyd, A. Elliot, P. Morrall, A. Alouche, C. Entwistle and A. Toerncrona, *Catal. Lett.* 2002, **83**, 165

[44] W.E. Farneth, C.J. Machiels, W.H. Cheng, U. Chowdhry, F. Hong, E.M. Mc Carron and A.W. Sleight, *Appl. Catal.*, 1986, **25**, 249

[45] E. M. McCarron and A. W. Sleight, *Polyhedron*, 1986, **5**, 129

[46] J.M. Tatibouöet, *Appl. Catal. A : Gen*, 1997, **148**, 213

[47] G.D. Kolovertnov, G.K. Boreskov, V.A. Dzisko, B.I. Popov, D.V. Tarasova and G.C. Belugina, *J.. Catal.*, 1996, **6**, 343

[48] N. Pernicone, *Catal. Today*, 1991, **11**, 85

[49] S.D. Gardner, G.B. Hoflund, B.T. Upchurch, D.R. Schryer, E.J. Kielin and J. Schryer, *J. Catal.*, 1991, **129**, 114

[50] S.D. Gardner, G.B. Hoflund, B.T. Upchurch, D.R. Schryer, E.J. Kielin and J. Schryer, *Langmuir*, 1991, **7**, 2135

[51] N. Yamamoto, S. Tonomura and T. Matsuoka, *Jap. J. Appl. Phys*, 1981, **20**, 721

[52] A. Lamb, W.C Bray and C.W. Fraser, *J. Ind & Chem. Eng.*, 1920, **12**, 213

[53] A.I. Zaslavskii, Z.V. Karachentseva and A.I Zharinova, *Kristallografiya*, 1962, **7**, 835

[54] S. Miyahara, *J. Phys. Soc. Japan*, 1962, **17**, 181

[55] D. Dollimore and K.H Tonge, *J. Chem. Soc. A.*, 1970, 1728

[54] G. Blasse, *J. Phys. Chem. Solids*, 1966, **27**, 383

[55] D.B. Ghare, A.B.P. Sinha and L. Singh, *J. Mater. Sci*, 1968, **3**, 389

[56] S. Veprek, D.L Cocke, S. Kehl and H.R. Oswald, *J. Catal.*, 1986, **100**, 250

[57] K. Wahl, W. Klemm and Z. Anorg., *Allg. Chem.*, 1952, **270**, 270

[58] P. Porta, G. Moretti, M. Musicani and A. Nardella, *Catal. Today*, 1991, **9**, 211

[59] G.J. Hutchings, A.A. Mirzaei, R.W. Joyner, M.R.H. Siddiqui and S.H. Taylor, *Catal. Lett.*, 1996, **42**, 21

[60] G.J. Hutchings, A.A. Mirzaei, R.W. Joyner, M.R.H. Siddiqui and S.H. Taylor, *Appl. Catal. A: Gen.*, 1998, **166**, 143

[61] A.A. Mirzaei, H.R. Shaterian, R.W. Joyner, M Stockenhuber, S.H. Taylor and G.J. Hutchings, *Cat. Comm.*, 2003, **4**, 17

[62] M.B. Macher, A. Holmqvist , and M. Härröd *Eur. J. Lipid Sci. Technol.*, 2001, **103**, 81

[63] J.W. Evans, M.S. Wainwright, N.W. Cant, and D.L. Trimm, *J. Catal.*, 1984, **88**, 203

[64] M.G. Hitzler, F.R. Smail, S.K. Ross and M. Poliakoff, *Org. Proc. Res. Develop.*, 1998, **2**, 137

[65] M.F. Sellin and D.J. Cole-Hamilton, *J. Chem. Soc. Dalton Trans.*, 2000, 1681

[66] S. Dharmidhikari and M.A. Abraham, *J. Supercrit. Fluids*, 2000, **18**, 1

[67] N.J. Meehan, A.J. Sandee, J.N.H. Reek, P.C.J. Kamer, P. Van Leeuwen and M. Poliakoff, *Chem. Commun.*, 2000, 1497

[68] Y.F. Shi, Y. Gao, W.K. Yuan and Y.C. Dai, *Chem. Eng. Sci.*, 2001, **56**, 1403

2 Experimental

2.1 Catalyst Preparation

The as-precipitated catalyst precursors are calcined to give final catalysts in static air. Typically calcinations are performed within the region of 300-400 °C for 3h with a ramp rate between 10 °C min^{-1} for iron molybdates and for copper manganese oxides calcinations occur at 300°C for 2h with a ramp rate of 10°C min^{-1}. Detailed preparations can be found in following chapters.

The catalysts are prepared using one of two reactors; either using the Original reactor, or the Second (modified design) reactor. The main difference being the second reactor constructed has several beneficial modifications to the setup. Detailed information on these reactors will follow in the subsequent chapters but below is a summary of their operation.

2.1.1 Preparation of Catalysts Using Original Reactor Setup

Figure 2.1 shows the schematic representation of the experimental setup for the original reactor.

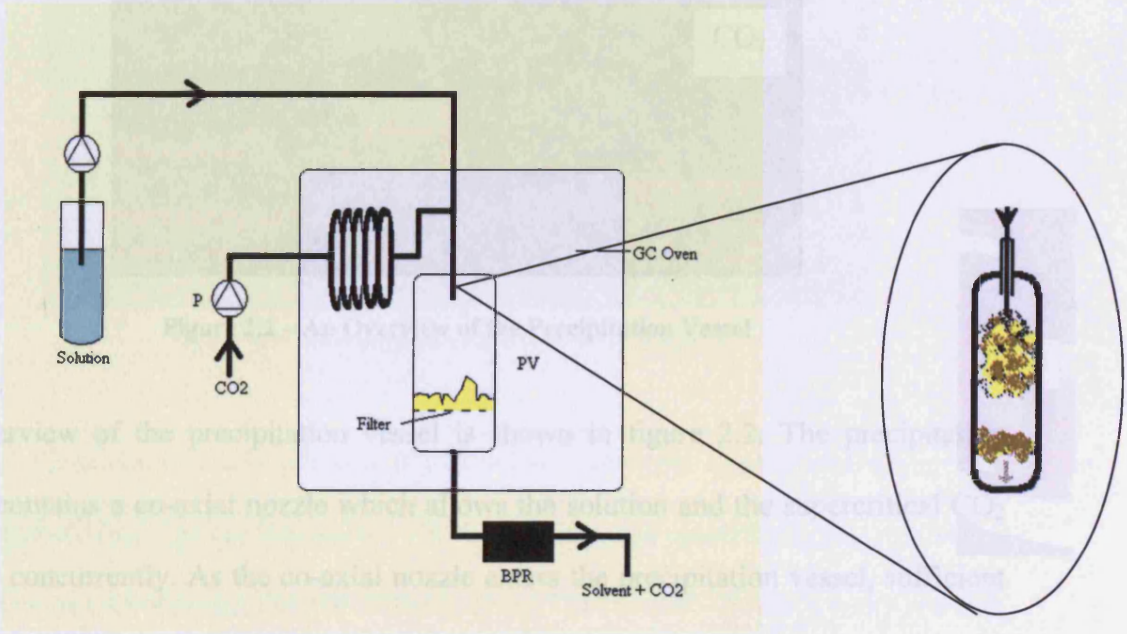

Figure 2.1 – Schematic representation of original reactor; PV is the Precipitation vessel, P is the HPLC pump, BPR is the Back Pressure Regulator

The reactor is controlled by a series of HPLC pumps. The first HPLC pump controlling the CO_2 contains a chiller, which liquefies the gas as it is being pumped. The second HPLC pump controls the flow rate of the solution entering the precipitation vessel. The back pressure regulator maintains a constant pressure throughout the system. The precipitation vessel is enclosed in an oven, which allows the temperature to remain constant through out the precipitation process.

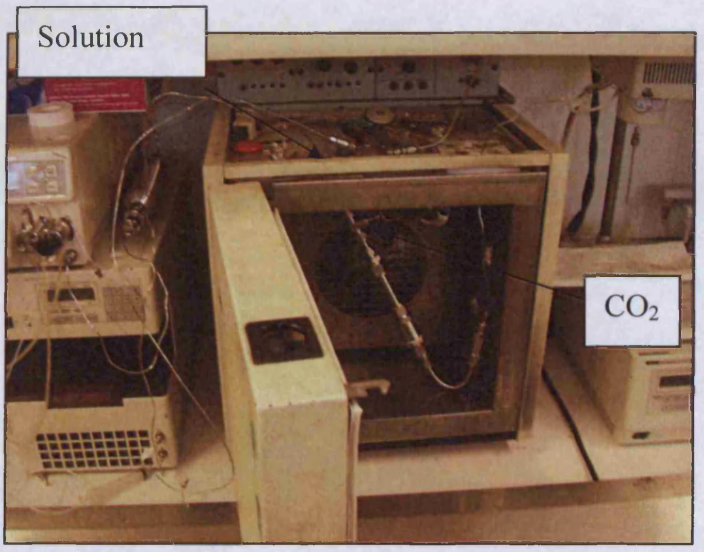

Figure 2.2 – An Overview of the Precipitation Vessel

An overview of the precipitation vessel is shown in figure 2.2. The precipitation vessel contains a co-axial nozzle which allows the solution and the supercritical CO_2 to flow concurrently. As the co-axial nozzle enters the precipitation vessel, sufficient mixing of the supercritical fluid and the solution causes precipitation of the dissolved solute. The resulting precipitate is then collected on a filter at the bottom of the precipitation vessel.

2.2.2 Preparation of Catalysts Using the Second Supercritical Reactor

Figure 2.3 shows a picture of the bottom half of the second supercritical reactor.

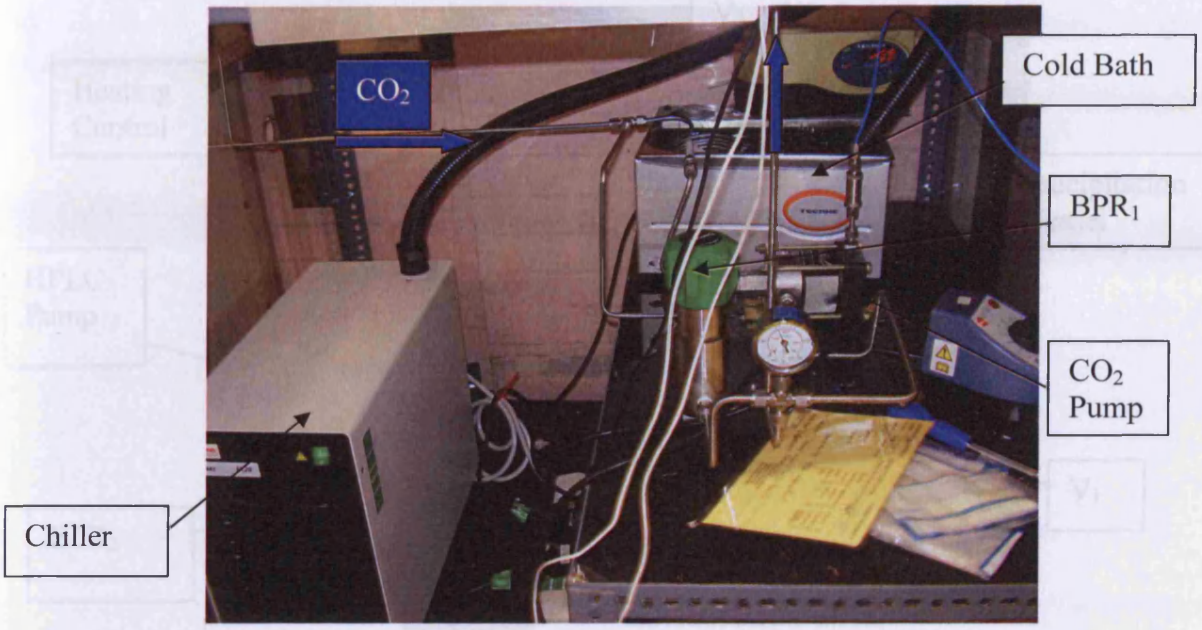

Figure 2.3 – Bottom half of the second SAS Reactor

Initially, all valves and back pressure regulators are left open, apart from the V_3 . CO_2 is then pressurised against this valve. The needle valve is opened slightly to allow a small flow of CO_2 through the rest of the reactor. This is done to remove any residual solvent left from previous reactions performed in the reactor.

Both V_1 and V_3 are then closed. The CO_2 pump is switched on and CO_2 is pumped continuously around the bottom part of the reactor, containing the chiller, which causes the CO_2 gas to liquefy. With liquid CO_2 flowing through this closed loop, the back pressure regulator is then set to the desired pressure. When the pressure is reached on BPR_1, V_1 is opened and the CO_2 flows to the precipitation vessel. The precipitation vessel is heated by the jacket that surrounds it; typically at 50 °C. Therefore, it is at this point that the liquid CO_2 becomes supercritical.

The top part of the reactor, containing the precipitation vessel is shown in figure 2.4.

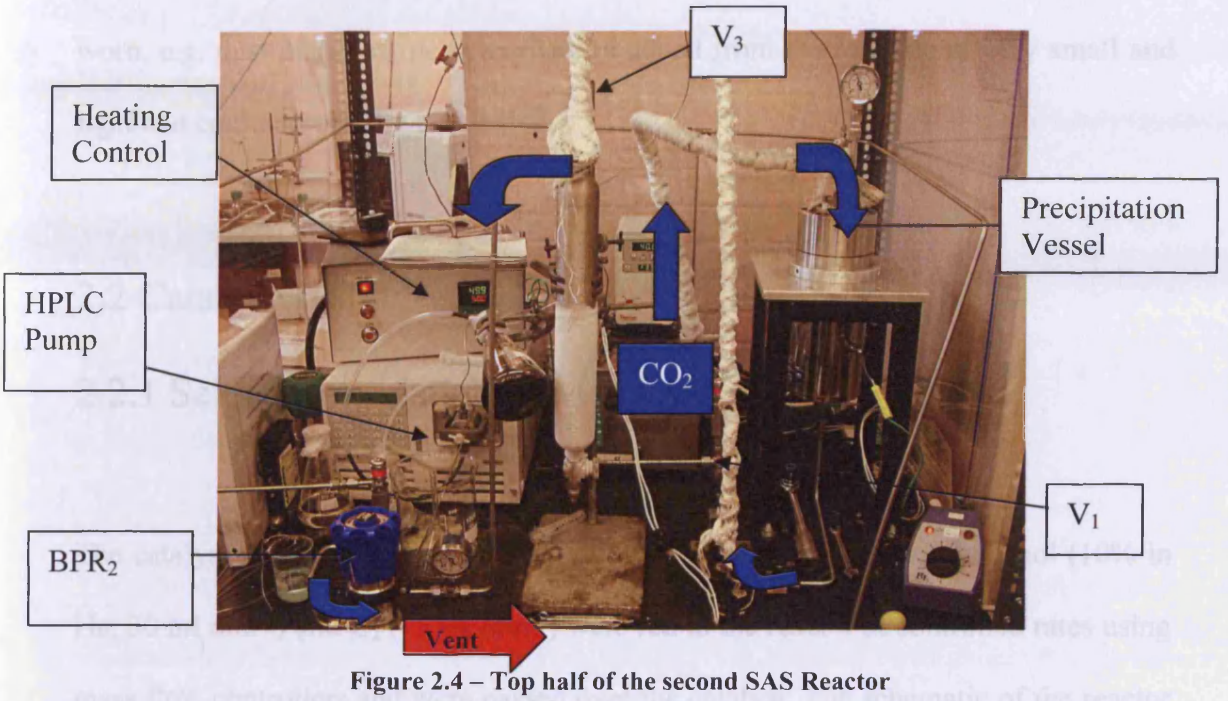

Figure 2.4 – Top half of the second SAS Reactor

When the pressure is stable in the precipitation vessel, V_3 is opened very slightly. At this point a small flow should be displayed on the digital flow meter. BPR_2 is then set to 20 bar. V_3 is adjusted until the flow of CO_2 reaches the desired flow rate for the reaction as indicated by the digital flow meter. CO_2 is allowed to flow for 30 minutes to ensure that all solvent is removed from the lines.

The solvent containing the dissolved solute is the delivered to the precipitation vessel using the HPLC pump. The precipitate from the reaction is collected by Soxhlet thimbles contained within the vessel.

Both the chiller and the heating jacket are continuously switched on to reduce time for heating and cooling between reactions. After completing a reaction in the reactor, the precipitate is collected from the thimble and the thimble is discarded. Care has to be taken when opening the precipitation vessel, and appropriate protective equipment

worn, e.g. dust mask, as the precipitate obtained from the reaction is very small and light and could potentially be inhaled.

2.2 Catalyst Testing

2.2.1 Selective oxidation of Methanol

The catalyst was tested using a fixed-bed laboratory microreactor. Methanol (10% in He, 30 ml min^{-1}) and O_2 (15 ml min^{-1}) were fed to the reactor at controlled rates using mass flow controllers and were passed over the catalyst. The schematic of the reactor is show in figure 2.5. The products were analysed using on-line gas chromatography using a 3m chromosorb column and a 3m carbosieve column in a Varian 3600 CX.

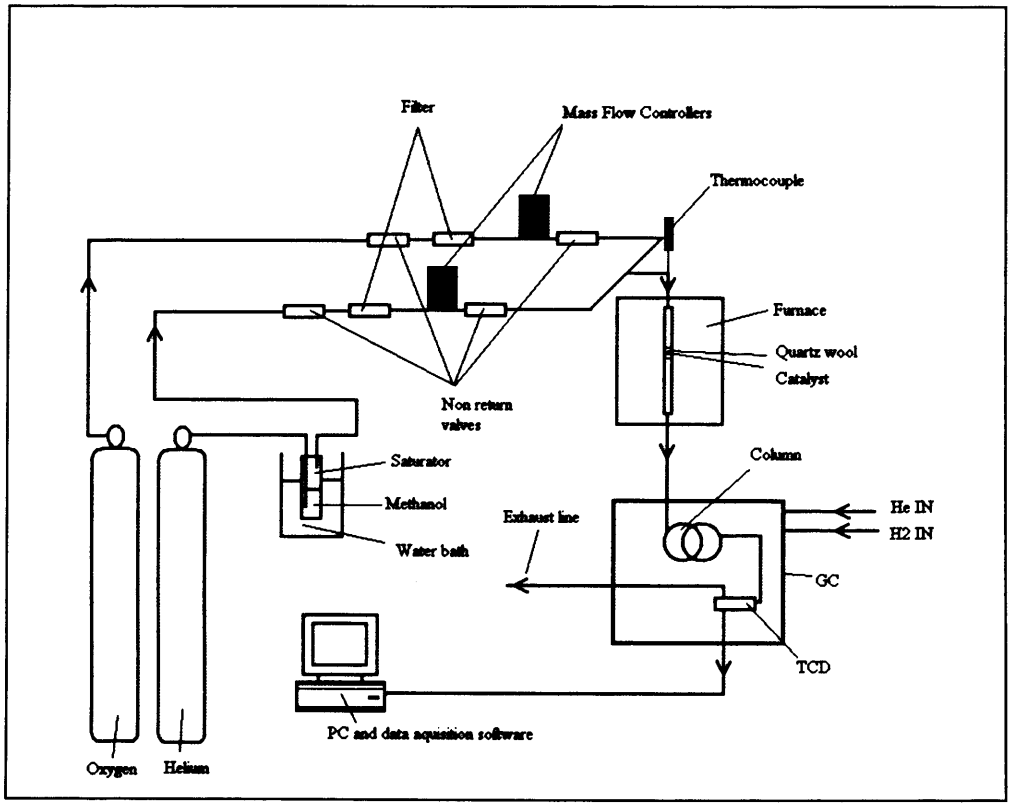

Figure 2.5 – Schematic representation of the methanol oxidation test facility

During the analysis, the GC column was held isothermally at 95 °C. The chromosorb column was suitable for the separation of methanol, formaldehyde and dimethyl ether. The carbosieve column was used for the separation of O_2, CO and CO_2. The method constructed resulted in the methanol, formaldehyde and dimethyl ether being eluted at 1.62, 1.91 and 2.7 minutes respectively, and O_2, CO and CO_2 being eluted at 5.22, 6.26 and 26.60 minutes respectively.

The response factor for methanol was determined by injecting different known concentration mixtures of methanol in helium. The mixture was injected into the sample loop using rotary gas sampling valves and a single injection was made into the GC. Three injections were made for each concentration of methanol and the results were averaged. A graph of concentrations (% methanol) plotted against peak area (number of counts) was constructed; a line of best fit was plotted to allow conversion between the number of counts determined by GC analysis and the % methanol present, the gradient of the graph corresponded to the relative response factor; this is shown in figure 2.6. The calibration for carbon monoxide, carbon dioxide, dimethyl ether and formaldehyde were obtained in a very similar manner.

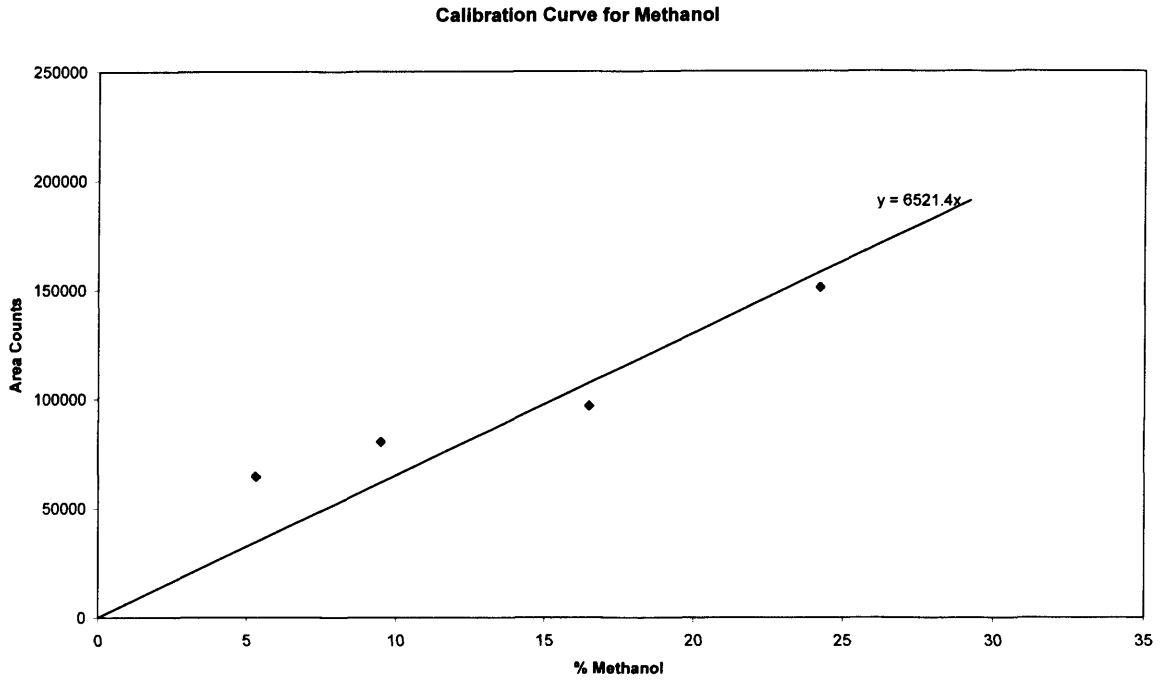

Figure 2.6 – Calibration curve for methanol

By determining the response factor for each component, the conversion of methanol to formaldehyde can be determined, and the selectivity towards the respective products can also be calculated. This was done by using the following equations:

$$Corrected\ Counts = Actual\ Counts / Response\ Factor$$

$$\%\ Methanol\ Conversion = \frac{MaxMethanol\ Corrected\ Counts - MethanolCorrectedCounts}{Max\ Methanol\ Corrected\ Counts} x100\%$$

$$\%\ Selectivity = \frac{Product\ Corrected\ Counts}{Total\ Product\ Corrected\ Counts} x100\%$$

2.2.2 Carbon Monoxide (CO) Oxidation

The catalysts were tested for CO oxidation using a fixed–bed laboratory microreactor. Typically, CO (5000ppm), balance synthetic air, 21.3 ml min^{-1} was fed to the reactor at a controlled rate and passed over the catalyst (12-50mg) at 25 °C. The products were analysed using on-line gas chromatography with a 1.5m packed carbosieve column in a Varian CP-3800 GC. These conditions were equivalent to a total gas hourly space velocity of 12,000 h^{-1}.

During the analysis, the GC column was held isothermally at 195 °C. Helium was used as the carrier gas for analysis. The carbosieve column was used for the separation of O_2, CO and CO_2. Under these conditions, O_2 and CO were eluted at 0.5 minutes as one broad peak; these could not be separated. CO_2 was eluted at 1.5 minutes. Samples were taken every 4 minutes, typically for a period of 2h, using an auto-injector. A tcd detector was used for quantitative analysis of the separated gas mixture.

The GC was calibrated to calculate the conversion of CO to CO_2. A known concentration of CO_2 was used to determine the maximum peak area that would correspond to total conversion (5000ppm CO would produce 5000ppm CO_2). The calculation is shown below.

The GC was calibrated to determine the conversion of CO to CO_2. This was achieved by passing a known concentration of CO_2 through the GC to determine the maximum

peak that would correspond to total conversion (5000ppm CO would produce 5000ppm CO_2). The following equation was used:

$$\text{Conversion} \quad CO\ (\%) = \left(\frac{CO_2 \text{ counts}}{\text{total } CO_2 \text{ counts}} \right) \text{x } 100$$

The total CO_2 counts that corresponded to total conversion were 98000 counts. This was used as a standard value in determining the conversion of CO over all the catalyst tested.

2.3 Characterisation Techniques

2.3.1 Gas chromatography

Gas chromatography (GC) [1-3] is one of the most extensively used separation methods for analytical purposes. It provides a quick and easy way of quantifying the composition of unknown gaseous mixtures. The key parts of a gas chromatograph include:

- Carrier gas – used as the mobile phase
- Injection port – deliver sample to the column
- Column – where separations occur
- Oven – to thermostat the column
- Detector – register presence of chemical in the column effluent
- Data system – to record and display the chromatograph

2.3.1.1 Carrier Gas

The carrier gas ensures that the components of the sample are mobile and can move to the column for separation. In principle any gas which does not interact either with the stationary phase or the components of the sample would be a suitable carrier gas; however the choice of carrier gas is restricted. The choice of carrier gas is limited to nitrogen, argon or helium. The best results are achieved when the carrier gas is of high purity, free of water and oxygen which can reduce the lifetime of some columns.

2.3.1.2 – Injection port

The sample injector is used to introduce the gaseous sample rapidly and in a reproducibly into the column. The efficiency of separation and the accuracy of the results depend on how the sample is introduced into the column. The injector system should allow the sample to reach the column in the shortest time possible and prevent any change in the flow and thermal conditions of the system during the injection. The quantity of the sample and how the sample is injected should be perfectly reproducible.

Rotary gas sampling valves are most commonly used method for the injection of a gas sample. The gas sampling valve ensures reproducibility, and allows for the introduction of the sample to the carrier gas to be done without disruption of the flow. The sample is loaded into the loop, and then with a change in valve position, enters the column under flow of the source gas.

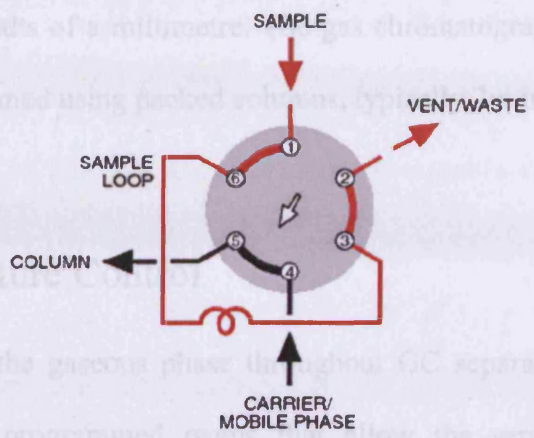

Figure2. 7 – Position A for gas sampling valve

With the valve in position A (figure 2.7), sample flows through the external loop while the carrier gas flows directly through to the detector. When the valve is switched to position B (figure 2.8), the sample contained in the sample loop is injected into the column under the flow of carrier gas to the detector.

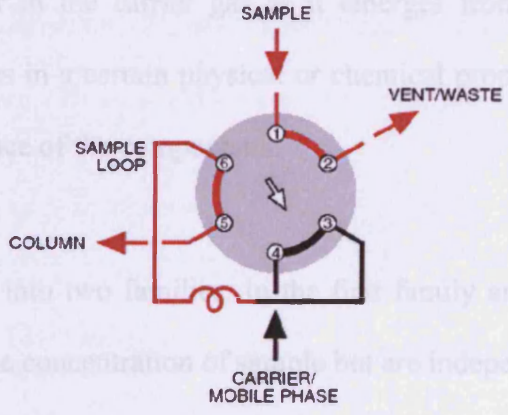

Figure 2.8 –Position B for gas sampling valve

2.3.1.3 Columns

There are two general types of column packed and capillary. Packed columns contain finely divided, inert solid support material. Most packed columns are 1.5 – 10m in length and have an internal diameter of 2-4 mm. Capillary columns have an internal

diameter of a few tenths of a millimetre. The gas chromatography performed in this thesis has been performed using packed columns, typically 3m in length.

2.3.1.4 Temperature Control

Samples must be in the gaseous phase throughout GC separation. Typically, GC's contain temperature programmed ovens that allow the separation of chemicals spanning a range of vapour pressures in a single analysis. The GC ovens are fan assisted and allow an even distribution of heat throughout the oven.

2.3.1.5. Detectors

Detectors have the task to sense continually, rapidly and with high sensitivity the components which appear in the carrier gas as it emerges from the column. The detector senses the changes in a certain physical or chemical property of the effluent gas stream on the appearance of the components.

Detectors can be grouped into two families. In the first family are those that give a response proportional to the concentration of sample but are independent of the rate of flow of the gas, for example, the thermal-conductivity (TCD) detector. The response of the second family of detectors depends upon the rate at which the sample is delivered, but the extent of dilution by carrier gas is irrelevant, for example, the flame-ionisation (FID) detector.

A TCD detector contains a heated resistance element. The resistance of this element is highly temperature dependent. Introduction of the sample causes a change in the temperature and resistance of the heated element. The resistance change is converted to a voltage and measured as such.

Most organic compounds are readily burned when introduced into a hydrogen-oxygen flame producing ions. The FID detector operates on this principle. The ions formed during the combustion of the sample are collected at a charged electrode, and the resulting current measured.

2.3.1.6 Data Systems

With the ongoing development of computers and software, the acquisition of data from GC is a very simple procedure. Signals from the detector amplifier are digitised and stored to disk. Software allows the results to be displayed and standard reports can be generated.

2.3.2 Powder X-ray Diffraction

X-ray diffraction (XRD) [4, 5] is a non-destructive technique that is most commonly used for the identification of crystalline compounds by their diffraction pattern. XRD can be used for phase identification, quantitative analysis, and to determine the degree of crystallinity within the compound.

In XRD, X-rays are generated within a sealed tube under vacuum. A current is applied to the filament within the tube which generates high energy electrons. A high voltage (15-60 kilovolts) is applied within the tube which accelerates the electrons towards the target, typically made of copper. Electrons striking the target results in the production of X-rays. The X-rays produced are directed toward the sample. Interaction of the X-rays with the sample results in the diffraction of the beam, and a diffraction pattern for that substance is obtained.

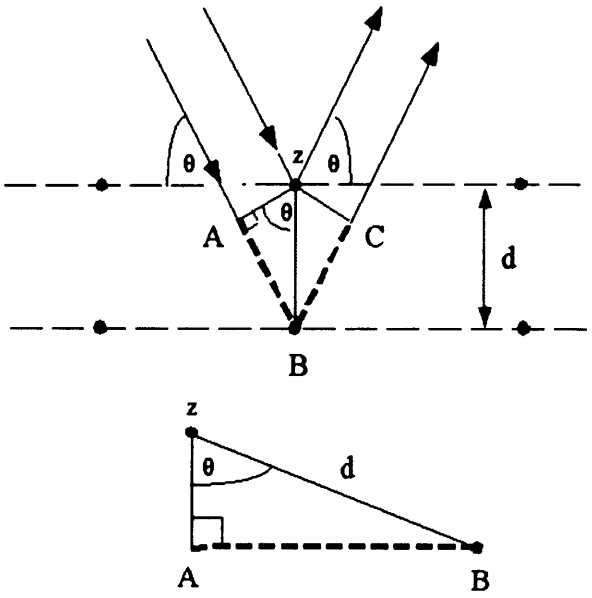

Figure 2.9 – Diagram of Incident Radiation on Surface

The diffraction of the X-ray beam is related to the interplanar spacings in the crystalline powder according to a mathematical relation called Bragg's Law.

Bragg's Law can easily be derived by considering the conditions necessary to make the phases of the beams coincide when the incident angle equals the reflecting angle. The rays of the incident beam are always in phase and parallel up to the point at which

the top beam strikes the top layer at atom z, as shown in figure 2.9. The second beam continues to the next layer where it is scattered by atom B. The second beam must travel the extra distance AB + BC if the two beams are to continue travelling adjacent and parallel. This extra distance must be an integral *n*, and a multiple of the wavelength λ, for the phases of the two beams to be the same:

$$n\lambda = AB + BC$$

Deriving Bragg's Law using the reflection geometry and applying trigonometry, the lower beam must travel the extra distance (AB + BC) to continue travelling parallel and adjacent to the top beam.

Recognizing d as the hypotenuse of the right triangle ABz, we can use trigonometry to relate d and θ to the distance (AB + BC). The distance AB is opposite θ, therefore:

$$AB = d\sin\theta$$

Because AB = BC the equation becomes:

$$n\lambda = 2AB$$

Substituting the equations results in:

$$n\lambda = 2d\sin\theta$$

***n* is an integer**
λ is the wavelength of the X-rays
***d* is the interplanar spacing**
θ is the diffraction angle

The characteristic set of d-spacings obtained in a typical X-ray scan provides a unique fingerprint of that sample, since each crystalline material has a diffraction pattern. X-ray diffraction differs from one material to the next and is dependent on the atoms that

make up the crystal lattice and how these atoms are arranged within the lattice. When properly interpreted, and by comparison with standard reference patterns the XRD diffraction pattern allows for identification of the material being analysed.

The XRD analysis was carried out using an Enraf Nonius PSD120 diffractometer with a monochromatic Cu K1 source operated at 40 keV and 30mA

2.3.3 BET Surface Area Measurements

The adsorption and desorption of gases at the clean surface of a dry solid powder is the most popular method for determining their surface areas. The BET method (Brunauer, Emmet and Teller, proposed in 1938) [6]) has been adopted as the standard procedure for surface area determination. Surface area is an important physical property and can often have a significant contribution to the reactivity of the catalyst.

The BET theory extends the Langmuir model to multilayer adsorption with the following hypotheses: a) gas molecules adsorb on a solid in layers infinitely; b) there is no interaction between each adsorption layer; and c) the Langmuir theory can be applied to each layer.

The Langmuir equation relates the coverage or adsorption of molecules on a solid surface to gas pressure or concentration of a medium above the solid surface at a fixed temperature. The equation was developed by Irving Langmuir in 1916. The equation is stated as follows:

$$\theta = \frac{\alpha \cdot P}{1 + \alpha \cdot P}$$

θ or theta is the fractional coverage of the surface, P is the gas pressure or concentration, α alpha is a constant.

The constant α is the Langmuir adsorption constant and increases with an increase in the binding energy of adsorption and with a decrease in temperature.

By extending the Langmuir model the resulting BET equation can be expressed as

$$\frac{1}{v\left[\left(P_o / P\right) - 1\right]} = \frac{c - 1}{v_m c}\left(\frac{P}{P_o}\right) + \frac{1}{v_m c}$$

P and P_o are the equilibrium and the saturation pressure of adsorbates at the temperature of adsorption, V is the volume adsorbed, V_m is the monolayer adsorbed gas quantity and C is the BET constant that reflects the difference in heat of adsorption between the first and second monolayers and subsequent monolayers.

The BET equation is an adsorption isotherm and can be plotted as a straight line with $1 / v[(P_0 / P) - 1]$ on the y-axis and $\varphi = P / P_0$ on the x-axis according to experimental results. This plot is called a BET plot. The linear relationship of this equation is maintained only in the range of $0.05 < P / P_0 < 0.35$. The value of the slope A and the y-intercept I of the line are used to calculate the monolayer adsorbed gas quantity v_m and the BET constant c. The following equations can be used:

$$v_m = \frac{1}{A + I}$$

$$c = 1 + \frac{A}{I}$$

A total surface S_{total} and a specific surface area can be obtained by using the following equations:

$$S_{total} = \frac{(v_m N s)}{V}$$

$$S = \frac{S_{total}}{a}$$

N is Avogadro's number
s is the adsorption cross section
N_m is the molar volume of adsorbent gas
a is the weight of sample solid

For the BET surface area measurements performed, initially the powdered samples were degassed under a flow of N_2 for approximately 30 minutes. Following the degassing, the sample vessel was connected to a gas inlet, a vacuum pump and an electronic barometer. Liquid N_2 at 77 K was used to cool the vessel. Initially, the chamber of the sample vessel was evacuated to remove any adsorbed molecules from the surface of the sample; N_2 was then allowed into the chamber and the pressure measured.

Analyses of the samples were performed using the Micromeritics Gemini 2360 Analyser, which is a single or multi-point surface area analyser.

2.3.4 Scanning Electron Microscopy

Scanning electron microscopy (SEM) [7] is a type of electron microscope that can produce high- resolution images of a sample surface. An electron microscope uses electrons to illuminate and create an image of a specimen. Compared with optical microscopy; SEM has a much higher magnification and resolving power which produces an image that is a good illustration of a three-dimensional sample.

In a typical SEM (figure 2.10), electrons are thermionically emitted from a tungsten filament situated in the electron gun. The electron beam passes through pairs of scanning coils in the objective lens, which deflect the beam horizontally and vertically so it scans in a raster fashion over a rectangular area of the sample surface. The interaction of the electron beam with the sample results in an energy loss of the electrons via repeated scattering and absorption by the sample. The size of the interaction is dependent on the beam accelerating voltage, the atomic number and the density of the sample. The energy exchange between the electron beam and the sample causes the emission of electrons and electromagnetic radiation which is used to produce an image.

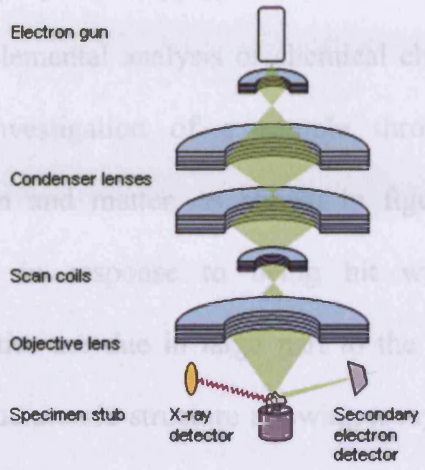

Figure 2.10 – Typical components of an scanning electron microscope

The most common imaging mode monitors low energy (<50 eV) secondary electrons. The electrons are detected and the resulting signal is transferred to a viewing screen, thus forming the SEM image. The brightness of the signal depends on the number of secondary electrons reaching the detector; increasing the angle of incidence of the beam decreases the escape distance of one side of the beam, causing the emission of more secondary electrons. Using this technique, resolutions less than 1 nm are possible.

Backscattered electrons consist of high-energy electrons in the electron beam that are reflected or backscattered from depths well below the surface. Defined as those electrons having energy >50 eV. Backscattered electrons can be used to detect contrast between areas with different chemical compositions, since the backscattered image tends to increase with atomic number. Fewer backscattered electrons are emitted from the sample than secondary electrons, the use of a dedicated backscattered electron detector above the sample allows for detection of more backscattered electrons.

Energy dispersive X-ray spectroscopy (EDS, EDX or EDXRF) is an analytical technique used for the elemental analysis or chemical characterisation of a sample. EDX relies on the investigation of a sample through interactions between electromagnetic radiation and matter, as shown in figure 2.11, analyzing x-rays emitted by the matter in response to being hit with charged particles. Its characterization capabilities are due in large part to the fundamental principle that each element has a unique atomic structure allowing x-rays that are characteristic of an element's atomic structure to be identified uniquely from each other.

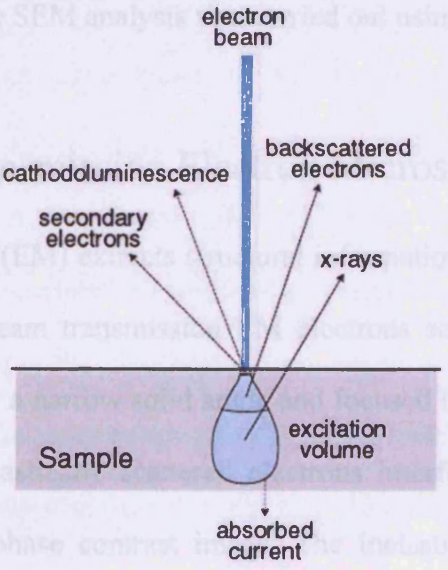

Figure 2.11 – Diagram of Electron beam interacting with sample

A high energy beam of charged particles such as electrons or protons, or a beam of X-rays, is focused into the sample being studied. At rest, an atom within the sample contains ground state (or unexcited) electrons in discrete energy levels or electron shells bound to the nucleus. The incident beam may excite an electron in an inner shell, ejecting it from the shell while creating an electron hole where the electron was. An electron from an outer, higher-energy shell then fills the hole, and the difference in

energy between the higher-energy shell and the lower energy shell may be released in the form of an X-ray. The number and energy of the X-rays emitted from a specimen can be measured by an energy dispersive spectrometer. As the energy of the X-rays are characteristic of the difference in energy between the two shells, and of the atomic structure of the element from which they were emitted, this allows the elemental composition of the specimen to be measured.

The SEM images obtained in this thesis were primarily used to provide information on the surface topography and composition (i.e. the shape and size of the particles that make up the sample). The SEM analysis was carried out using a Carl Zeiss Evo 40.

2.3.5 Scanning Transmission Electron Microscopy, STEM

The electron microscope (EM) extracts structural information carried by the scattered electrons. In the fixed-beam transmission EM electrons scattered by the irradiated sample are collected over a narrow solid angle and focused by the objective lens onto the image plane. The elastically scattered electrons interfere with the unscattered electrons to produce a phase contrast image. The inelastically scattered electrons generate a diffuse background image that is in some EMs eliminated by an energy filter.

In STEM [7] the objective lens focuses the electron beam onto an atomic scale sample volume. All scattered electrons can then be collected by a variety of detectors placed behind the specimen and their information exploited to the fullest extent. An image is generated simply by moving the focused beam step by step over the specimen. Hence

a STEM image may be considered as a collection of individual scattering experiments.

The elastically scattered electron signal, giving rise to a dark-field image, is used for mass determination. The mass of individual particles, the mass-per-length of filamentous assemblies, and the mass-per-area of sheet-like structures can all be determined using this technique.

2.3.6 Raman Spectroscopy

When monochromatic light is scattered by molecules, the frequency of a small proportion of that scattered light differs to the frequency of the incident light; this is known as the Raman effect. The Raman effect [8] occurs when light, incident upon a molecule, interacts with the electron cloud of the bond of that molecule. A molecular polarizability change or amount of deformation of the electron cloud, with respect to the vibrational frequency is required for the molecule to exhibit the Raman effect. The amount of the polarizability change will determine the intensity, whereas the Raman shift is equal to the vibrational level that is involved.

Most collisions of the incident photons are elastic and this is known as Rayleigh scattering. Rayleigh scattering involves the incident photons being scattered in all directions by the interaction of atoms in its path. The inelastic scattering of photons is known as Raman scattering and is used to obtain the Raman spectra.

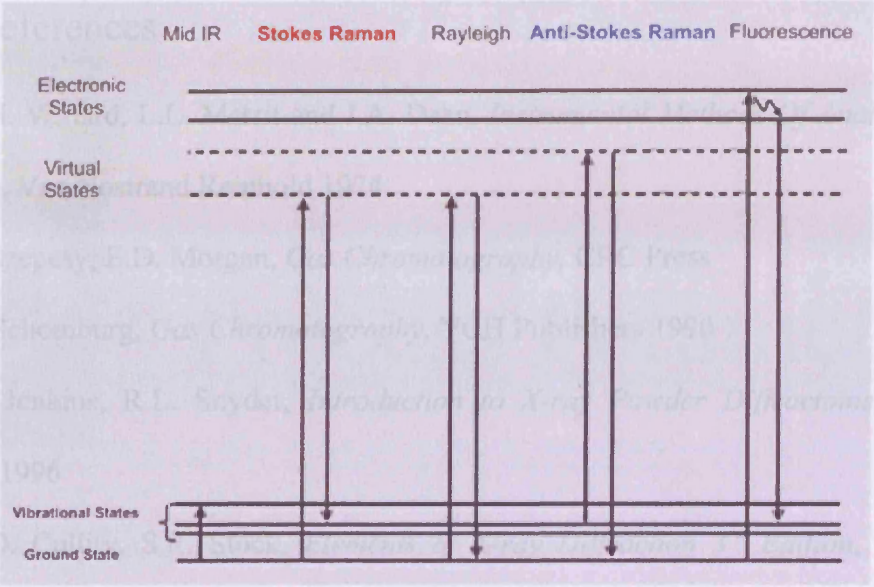

Figure 2.12 – Diagram of different types of scattering effects that can occur upon the absorption of energy

When the incident photon interacts with a molecule in the ground state, the molecule absorbs the energy and is raised momentarily to a higher unstable energy level. The molecule immediately loses energy and relaxes to a lower level; emitting a scattered photon. If the molecule relaxes to the ground sate, the scattered photon will have the same energy as the incident photon (Rayleigh scattering). A small proportion of the molecules fall to the $v = 1$ excited energy level, which results in the emission of a photon with less energy than that of the incident photon; this is known as Stokes scattering. If the molecule is in the initial excited state $v = 1$, it can absorb the photon of energy and return to the ground state, emitting a photon higher in energy than that of the incident photon; this is know as anti-Stokes scattering.

Raman spectra were obtained on a Renishaw Ramascope fitted with a green Argon ion (Ar^+) laser ($\lambda = 514.532$ nm).

2.4 References

[1] H.H. Willard, L.L. Merrit and J.A. Dean, *Instrumental Methods Of Analysis Fifth Edition*, Van Nostrand Reinhold 1974

[2] L. Szepesy, E.D. Morgan, *Gas Chromatography,* CRC Press

[3] G. Schomburg, *Gas Chromatography*, VCH Publishers 1990

[4] R. Jenkins, R.L. Snyder, *Introduction to X-ray Powder Diffractometry*, John Wiley, 1996

[5] B.D. Cullity, S.R. Stock, *Elements of X-ray Diffraction 3rd Edition*, Addison-Wesley, 2001

[6] S. Brubauer, P.H. Emmett, E. Teller, J. Am. Soc. 1938, 60, 309

[7] S.l. Flegler, J.W. Heckman, K.L. Klomparens, *Scanning and Transmission Electron Microscope*, Oxford University Press, 1993

[8] B. Schrader, *Infrared and Raman Spectroscopy*, VCH Publishers 1995

3 Process Parameters

3.1 Supercritical Antisolvent Precipitation

In the supercritical antisolvent (SAS) process, supercritical CO_2 ($scCO_2$) is used as an antisolvent that reduces the solubility of a solute dissolved into a solvent. Typically, the substance of interest is dissolved in an organic solvent and $scCO_2$ enters the vessel [1]. The supercritical fluid should be completely miscible with the liquid solvent, whereas the solute should be insoluble in the supercritical fluid. Due to the phase behaviour of CO_2 with many solvents, the solution expands and its viscosity is greatly reduced. These property changes cause the solubility of the solute to decrease in the solvent. The expanded solution becomes supersaturated, thus forcing the solute to deposit as micro- or nano-sized particles.

The use of supercritical antisolvent processes has been proposed as an alternative to liquid antisolvent processes. As mentioned previously there are several advantages to using these processes. The reduction in pressure can completely remove the antisolvent to the gas phase. Liquid antisolvent processes require complex post-processing treatments to completely remove any residual liquid from the solute. The high diffusivities of supercritical antisolvent allow much faster diffusion into the

liquid solvent, which causes supersaturation of the solute. The resulting precipitate is then composed of micro- or nano-particles, which are not possible to obtain using liquid antisolvents [1].

This process has been utilised to produce both iron molybdates and copper manganese mixed oxides. The apparatus that has been used to produce these compounds will be discussed in detail in this chapter. However, the results obtained during these experiments will be examined at length in the following chapters.

3.2 SAS Experimental Procedure

Two different reactor types have been used to perform the supercritical antisolvent procedure. Both operate as continuous flow reactors. In this mode of operation both the liquid solution and the supercritical fluid are continuously delivered to the precipitation vessel. The liquid injection device in this mode of operation is designed to produce liquid jet break-up and the formation of small droplets that expand in the precipitator. Precipitation from the droplet occurs when the local concentration exceeds the supersaturation limit. In the research that follows the liquid injection device used is based on the coaxial nozzle. Both reactors operate on the same principles but differ in their limitations under reaction conditions.

3.2.1 The Original SAS Reactor

Figure 3.1 shows the schematic representation of the experimental setup for the original SAS reactor.

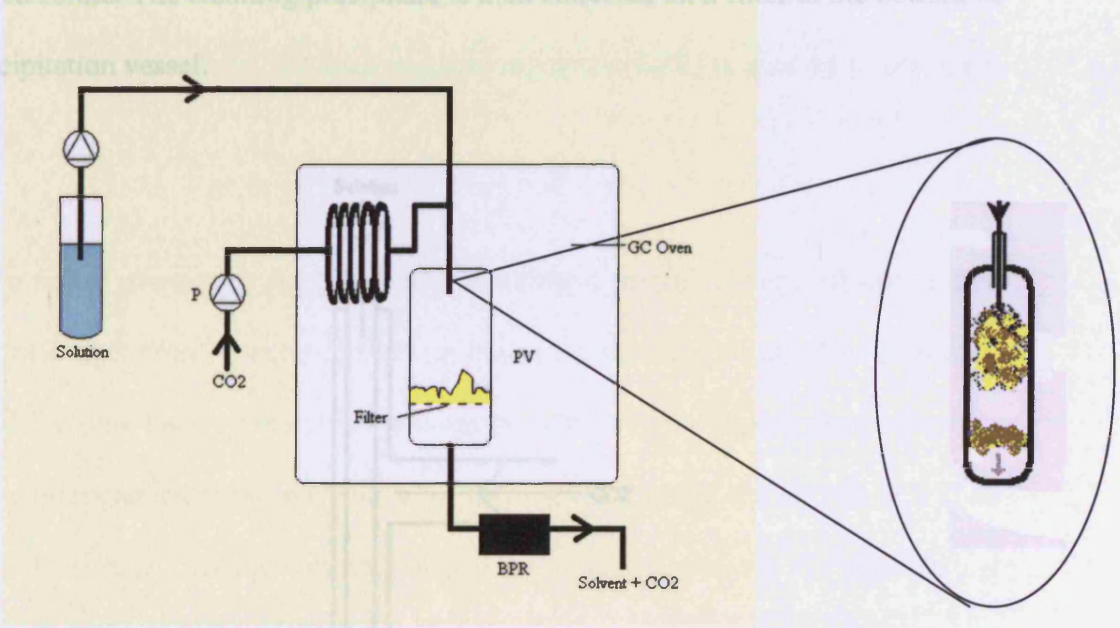

Figure 3.1 – Schematic representation of original reactor; PV is the Precipitation vessel, P is the HPLC pump, BPR is the Back Pressure Regulator

The solution and CO_2 are introduced to the precipitation vessel via HPLC pumps. The HPLC pump controlling the CO_2 contains a chiller, which liquefies the gas as it is being pumped. The second HPLC pump controls the flow rate of the solution entering the precipitation vessel. The back pressure regulator maintains a constant pressure throughout the system. The precipitation vessel is enclosed in an oven, which allows the temperature to remain constant through out the precipitation process.

A schematic of the precipitation vessel is shown in figure 3.1. The precipitation vessel contains a co-axial nozzle which allows the solution and the $scCO_2$ to flow concurrently, as in figure 3.2. As the co-axial nozzle enters the precipitation vessel, sufficient mixing of the supercritical fluid and the solution causes precipitation of the dissolved solute. The resulting precipitate is then collected on a filter at the bottom of the precipitation vessel.

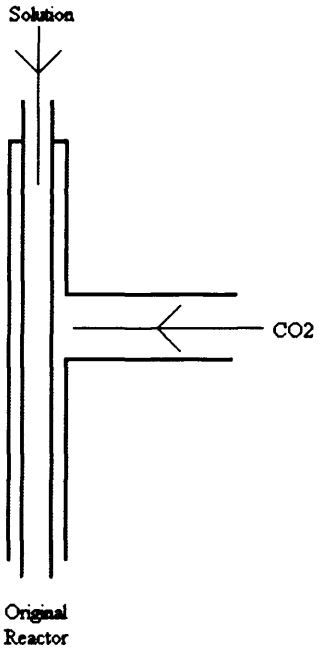

Figure 3.2 – Schematic of Coaxial nozzle used in original reactor

3.2.2 Operation of the Supercritical Reactor

Typically, the solute is dissolved in a solvent that is miscible with supercritical fluid. This is done before the reaction is initiated to guarantee that the solute is completely dissolved. The most commonly used solvents are dimethylsulfoxide (DMSO), ethanol, methanol, and n-methylpyrrolidinone (NMP) [1-15].

Initially, the HPLC pump that is used for delivering the CO_2 is allowed to cool, which allows the CO_2 to liquefy. The CO_2 then flows through the entire reactor at a constant rate, usually 7 ml min^{-1} for half an hour, to remove any residual solvent from any previous reactions that have been performed in the supercritical reactor. With the CO_2 flowing through the reactor, the back pressure regulator (BPR) is then set to the target pressure.

Once the target pressure is reached, 110 bar for most reactions, pure solvent is then passed through the SAS reactor for half an hour to ensure that all previous solvent is removed from the lines. At the target pressure the CO_2 is in the supercritical state. The solvent containing the dissolved solute is then passed through the reactor at a flow rate of 0.1 ml min^{-1}. As the solvent enters the precipitation vessel, the supercritical fluid rapidly supersaturates the solvent, reducing the solvation ability of the solvent, which in turn causes precipitation. The resulting precipitate is collected in a filter at the bottom of the precipitation vessel. Typically, the reaction takes between approximately 10-24 hours to obtain approximately 2g depending on the concentration of the dissolved solute. The $scCO_2$ is allowed to flow for 1 hour after the precipitation process to remove all solvent from the surface of the precipitate.

During the entire precipitation process the oven that houses the precipitation vessel is isothermally heated at 50 °C. The reaction conditions described in the above method have been optimised by previous work performed in the group for the production of single oxide supports. This has not been optimised for the production of the target

materials within this research but is seen as a logical starting place for the investigation.

3.2.3 Problems Associated with the SAS Reactor

The SAS reactor described above has been utilised in the development of active catalyst supports for gold catalysis for carbon monoxide oxidation. The reactor has also been used for the production of mixed metal oxides including both copper manganese oxides and iron molybdates. The production of iron molybdates will be discussed in greater detail in the results section of the thesis.

However, there are several limitations associated with this reactor. The SAS reactor only allows very small amounts of catalyst to be prepared in a single batch; typically ~1g every 10 hours with ~60 % yield. Therefore, to produce a significant amount of catalyst several precipitation processes would have to be performed. Limitations such as flow rates of the pumps, the temperature and pressure restrictions of the Swagelok fittings used restrict the parameters used the in the process.

The reactor has the $scCO_2$ impingent on the solution nozzle, which affects the plume of CO_2 exiting the nozzle. The restriction in the plume hinders the turbulent mixing of the CO_2 plume and the solution which does not allow effective precipitation of the desired product. A diagram of the process is shown below in figure 3.3.

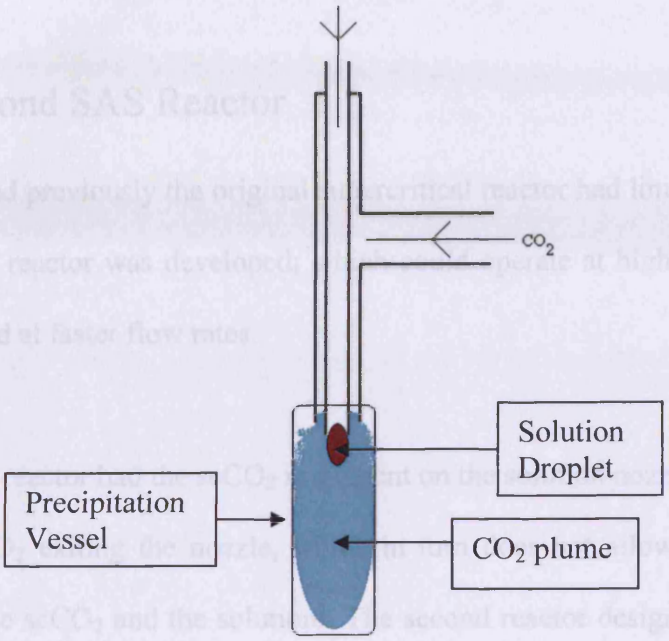

Figure 3.3 – Diagram of Coaxial nozzle showing plume restriction

The HPLC pumps used to deliver both the solvent and the supercritical CO_2 have restricted flow rates. Also the pressure of the system is limited to 150 bar by the fittings used in the filter.

Therefore, if any development of the supercritical antisolvent precipitation process was to proceed the limiting factors need to be removed from the reactor. Limiting factors such as the Swagleok fittings which have a maximum pressure of 150 bar. The oven that houses the precipitation vessel has a maximum temperature of 150°C. Also, to improve the overall efficiency of the process the precipitation vessel will need to be redesigned to allow the full expansion of the plume. The HPLC pumps are limited to 5 ml min^{-1} and 10 ml min^{-1} for the solution and CO_2 pumps respectively. The overall design of the reactor does not provide enough tunability of the process parameters to optimise the process on each specific system.

3.2.4 Second SAS Reactor

As mentioned previously the original supercritical reactor had limitations, so a second supercritical reactor was developed; which could operate at higher temperatures and pressures and at faster flow rates.

The original reactor had the $scCO_2$ impingent on the solution nozzle, which affects the plume of CO_2 exiting the nozzle, which in turn does not allow effective turbulent mixing of the $scCO_2$ and the solution. The second reactor design has a true co-axial nozzle, with the CO_2 being pumped around the outside of the nozzle; this should facilitate CO_2 diffusion into the exiting solvent and cause precipitation; improving the overall yield of the product. The exiting plume of CO_2 is very large and the original reactor has a 0.5 inch diameter precipitation vessel, restricting the plume of CO_2 preventing efficient precipitation. However, the second reactor has a 10cm diameter, 0.5 litre precipitation vessel, which should prevent any restriction of the plume of CO_2.

The HPLC pumps which were originally used to deliver both the solvent and the supercritical CO_2 to the nozzle. The HPLC pump chosen for this allows much faster flow rates up to 50 ml min^{-1}. Pumping of supercritical CO_2 was done by an air driven industrial pump which has the capability of pumping up to 250 ml min^{-1}.

The fittings used in the reactor were capable of much higher pressures. The pressure limiting fittings (the filters) were removed and the precipitate collected using a

Soxhlet filter (single thickness extraction thimble); which are not affected by increasing pressure.

3.2.5 Operation of the Second SAS Reactor

Figure 3.4 shows schematic representation of the second supercritical reactor.

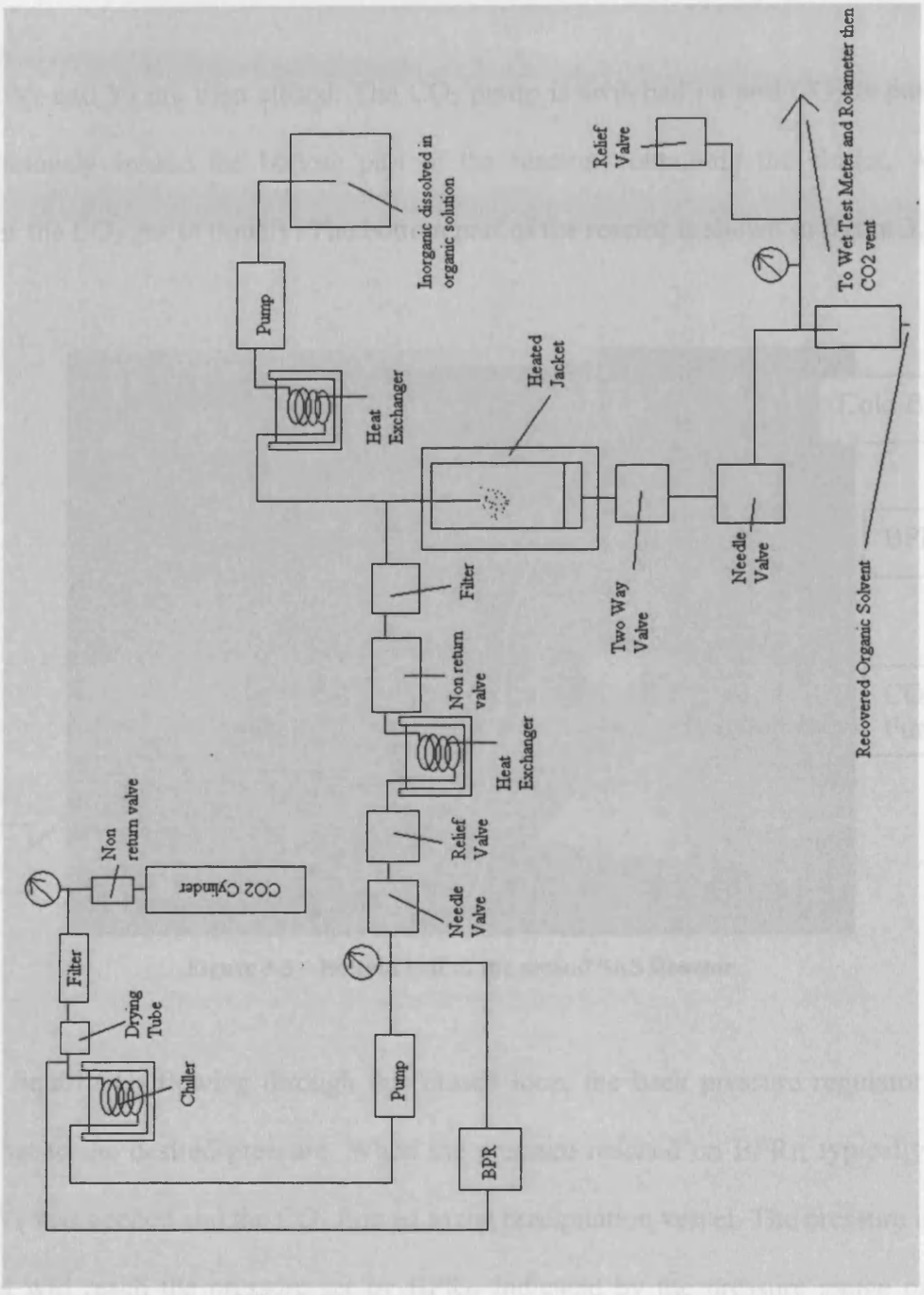

Figure 3.4 – Schematic representation of second SAS reactor setup

Initially, all valves and back pressure regulators are left open, apart from the V_3. CO_2 is then pressurised against this valve. The needle valve is opened slightly to allow a small flow of CO_2 through the rest of the reactor. This is done to remove any residual solvent left from previous reactions performed in the reactor.

Both V_1 and V_3 are then closed. The CO_2 pump is switched on and CO_2 is pumped continuously around the bottom part of the reactor, containing the chiller, which causes the CO_2 gas to liquefy. The bottom part of the reactor is shown in figure 3.5.

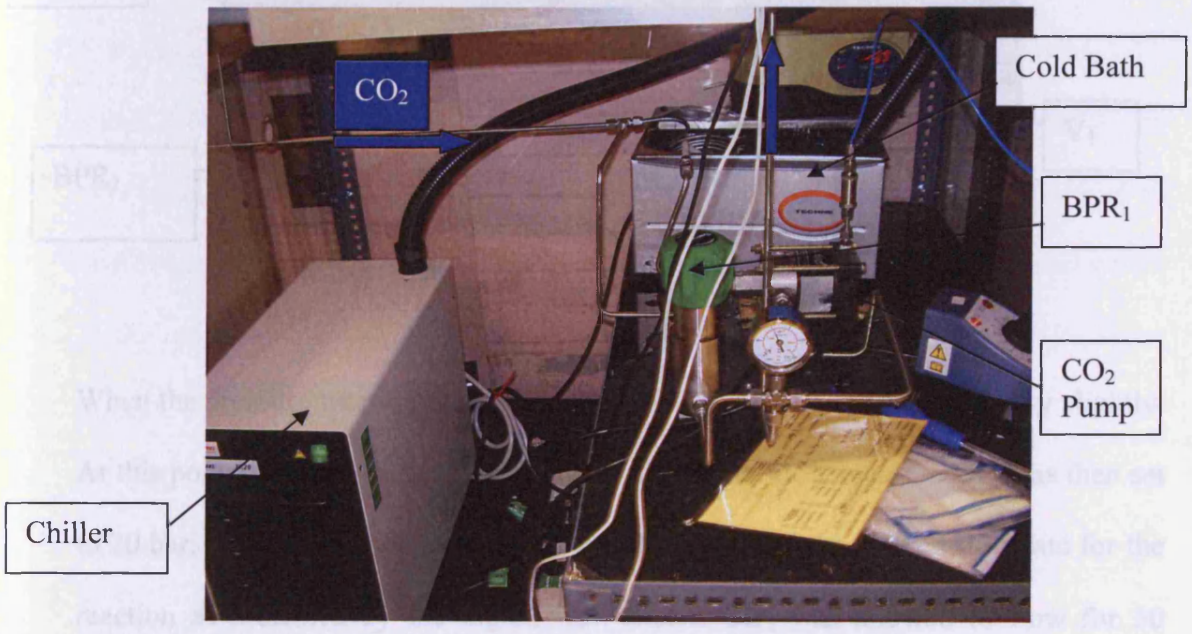

Figure 3.5 – Bottom half of the second SAS Reactor

With liquid CO_2 flowing through this closed loop, the back pressure regulator was then set to the desired pressure. When the pressure reached on BPR_1, typically 110 bar, V_1 was opened and the CO_2 flowed to the precipitation vessel. The pressure in the vessel will reach the pressure set by BPR_1, indicated by the pressure gauge on the precipitation vessel. The precipitation vessel was heated by the jacket that surrounds it; typically at 50 °C. Therefore, it is at this point that the liquid CO_2 becomes supercritical.

The top part of the reactor, containing the precipitation vessel is shown in figure 3.6.

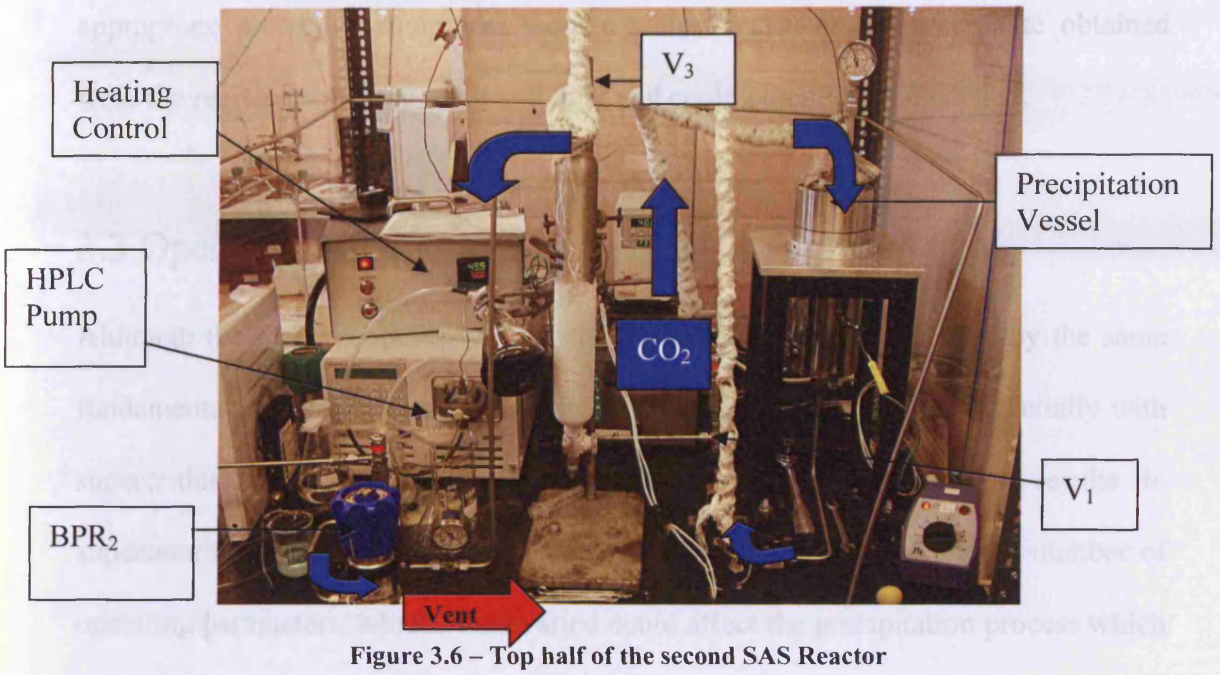

Figure 3.6 – Top half of the second SAS Reactor

When the pressure was stable in the precipitation vessel, V_3 was opened very slightly. At this point a small flow was displayed on the digital flow meter. BPR_2 was then set to 20 bar. V_3 was adjusted until the flow of CO_2 reached the desired flow rate for the reaction as indicated by the digital flow meter. CO_2 was allowed to flow for 30 minutes to ensure that all solvent was removed from the lines.

The solvent containing the dissolved solute was then delivered to the precipitation vessel using the HPLC pump. The precipitate from the reaction was collected by Soxhlet thimbles contained within the vessel.

Both the chiller and the heating jacket were continuously switched on to reduce time for heating and cooling between precipitation processes. After processing in the reactor, the precipitate was collected from the thimble and the thimble was then discarded. Care had to be taken when opening the precipitation vessel, and

appropriate protective equipment worn e.g. dust mask, as the precipitate obtained from the reaction was very small and light and could potentially be inhaled.

3.3 Operating Parameters

Although the reactors operate with a different procedure, both function by the same fundamental principles; dissolved solute in organic solvent is pumped coaxially with supercritical CO_2, this in turn dissolves into the solvent droplet, results in supersaturation of the droplet and precipitation of the solute. There are a number of operating parameters, which when varied could affect the precipitation process which could potentially be beneficial or detrimental to the activity of the catalyst. These parameters are temperature, pressure, concentration of solution, flow rates of both the solution and the $scCO_2$, and the ratio of CO_2 rate to solution rate. Some of the parameters have been investigated by different research groups and the results are discussed below. Within the literature parameters such as the viscosity of the solvent, and comparisons of starting material used have not been investigated in detail.

3.3.1 Pressure

During the liquid batch processing the rate of pressure increase is the most relevant parameter in controlling particles size and morphology [1]. However, for gas batch and continuous operation contradictory results have been obtained by several authors [2-8]; a reduction in pressure resulted in a particle size decrease.

Reverchon *et al* [1] have investigated the effect of pressure on particle size. It was found that for pressures larger than the asymptotic volume expansion, there was no major effect on the particle size for the primary particles or more complex morphologies. However, for the case of PLLA (Poly-L-Lactide) from methylene chloride a slight decrease of particle size with increasing pressure was found [9].

Reverchon *et al.* [10] also studied the effect of pressure on precipitated zinc acetate particle. It was found that increasing the pressure between 110 and 150 bar caused a slight decrease in the mean particle size of the zinc acetate particles. Reverchon concluded that the small change in particle size was dependent on the fact that in the pressure range between 110 and 150 bar, DMSO was completely expanded in supercritical CO_2 and no further decrease in the particle size can be obtained.

Miguel *et al* [11] have studied the precipitation of lycopene from dichloromethane using supercritical CO_2. Maintaining a constant temperature, but varying the pressure from 9 to 15 MPa resulted in an increase in the lycopene particle size. This was the case for all experiments preformed in this pressure range, a more pronounced increase was observed in the pressure range 9-12 MPa than in the pressure range 12-15 MPa. Miguel concluded that this trend is coherent with the variation of the maximum supersaturation, which decreases with pressure in the pressure range 9-15 MPa. Thus, the higher maximum supersaturation achieved at lower pressures lead to smaller particles.

Miguel, however, found that increasing the pressure from 7 to 9 MPa caused a decrease in the particle size. This was attributed to the fact that operating at 7 MPa lies below the mixture critical point, while the other experiments were performed above the critical point.

Martin *et al* [12] studied the effect on pressure on the particle size of β-carotene. The variation of particle size with pressure was found to be complex for this process. It was found that initially, the particle size increased with pressure, going through a maximum at 15 MPa, then decreasing. Martin concluded that with higher pressures, the solubility of β-carotene in CO_2 was higher, but the solubility in the organic solvent was lower. Therefore, at higher pressures, the increase of the supersaturation in the solvent-rich region can balance the decrease in the CO_2-rich region.

Alonso *et al* [13] have investigated the effect of pressure on the synthesis of titanium oxide particles. The effect of pressure was studied in the range 10-20 MPa. At 20 MPA, the product was a white fine powder, whereas, at 10 MPa the product was yellow in colour due to the rest of reactants/or byproducts. Therefore, Alonso concluded that pollution of the product was much higher at lower pressures. This result was explained that the reactants/or byproducts solubility decreases when pressure is decreased, and their elimination is worse. Alonso found that when the pressure was increased particle size increased. Alonso stated that higher pressures create higher medium densities, and the degree of supersaturation decreases, diminishing nucleation rate and particle growth is favoured.

Overall, increasing the pressure of a system causes the densities of the SCF and the solvent to increase, however, the solubility of the solvent decreases with increasing pressure. This causes a decrease in the degree of supersaturation, favouring particle growth, resulting in the formation of larger particles.

There are many aspects of the system that need to be considered, as changing the pressure of the system appears to have different effects on the particle size. The pressure range and solvent system used needs to be considered in detail, as different solvent systems expand in CO_2 over different pressure ranges; if solvent expands in the pressure range, degree of supersaturation increases, favouring nucleation, resulting in smaller particles. The solubility changes in both the solvent and SCF over the pressure range needs consideration; increase in solvent solubility in CO_2, degree of supersaturation increases, smaller particles produced.

3.3.2 Temperature

Reverchon *et al.* [1] have studied the effect of temperature on particle size for yttrium and samarium acetates. It was found that operating at pressures larger than the asymptotic volume expansion, an increase of temperature produces an increase in particle size for yttrium acetate. Reverchon stated that larger particles may be produced by higher growth rates at higher temperatures.

The effect of temperature on particle size was investigated by Miguel *et al.* [11] for the precipitation of lycopene. Maintaining constant pressure and increasing the temperature from 308 to 318 K caused a decrease in the particles size from 15 to 8

μm. The formation of smaller particles on the longer needle like particles was observed for the experiment performed at 318 K. Higher temperatures were not investigated to avoid thermal decomposition of lycopene particles. Miguel stated that at a pressure of 9MPa the solubility of the solute decreases with temperature. Therefore, the decrease of solubility with temperature allows a higher supersaturation to be reached at higher temperatures, which produces smaller particles

Martin *et al* [12] have found similar results when precipitating β-carotene using supercritical CO_2. Martin found that increasing the temperature had a strong effect on the solubility of β-carotene in the supercritical antisolvent at constant pressure. The solubility was found to increase with temperature over the entire concentration range. Therefore, at higher temperatures, supersaturation was reduced, and bigger particles were formed.

The effect of temperature on particle size was investigated by Alonso *et al.* [13] for the production of titanium oxide. Particle size is dependent on operational temperature. Higher temperatures lead to larger particles. Alonso found that particles obtained from high operational temperature, which were well crystallised, presented a lower specific surface area compared to amorphous particles that exhibited large BET surface areas. In terms of particle size, the bigger the particles the smaller the BET specific area. Alonso stated that the specific area represents the external surface are but also the internal one; when particle crystallinity is not good, particle porosity increased. When bigger particles are produced the porosity is increased.

3.3.3 Concentration

The effect of the concentration of the starting solution on particle size of lycopene has been studied by Miguel *et al* [11]. The concentration was varied from 125 to 500 ppm, keeping the other parameters constant. The obtained mean particle size was 20 μm at the lowest concentration of 125 ppm, 7 μm at the intermediate concentration of 250ppm and 10μm at the highest concentration. Although there was no definite trend, the particle size seemed to decrease with an increase in initial concentration of the solution. Miguel concluded that this would be coherent with the increase in the maximum supersaturation due to the increase of concentration of lycopene in the fluid.

A similar study was performed by Reverchon *et al* [14] for the precipitation of GdAc. The concentration of the solute was varied from 20 to 350 mg/ml. A marked influence of liquid solution concentration on the mean particle size distribution of the precipitated powders was observed. It was found that increasing the solute concentration resulted in an increase of the particle size distribution. Reverchon noted that as the concentration approached saturation, large numbers of particles with micron-range diameters were obtained. Reverchon explained the increase in particle size in terms of nucleation and growth processes; injecting dilute solutions causes saturation and precipitation to occur very late during the droplet expansion process. Therefore, nucleation is the prevailing mechanism at these conditions and smaller particles are formed. Injecting more concentrated solutions results in solute precipitation earlier during the expansion process and the mechanism of particle growth intersects with nucleation, producing larger particles.

Reverchon also studied the effect of concentration on ZnAc particles [10]. The concentration was varied from 15 to 90 mg/ml. Increasing the solute concentration resulted in an increase in particle size. The increase in particle size was attributed to higher growth rates when compared to nucleation rates.

Martin *et al.* [12] notice two opposing effects when studying the effect of concentration on particle size of β-carotene. It was found that with higher concentrations, it was possible to achieve higher supersaturations, which diminish particle size. On the other hand, condensation is directly proportional to the concentration of the solute; and the increase of the condensation rate with higher concentrations tends to increase the particle size.

From the literature there appears to be a number of results that contradict with one another. Perhaps where a dilute concentration is used, as mentioned by Reverchon [1] the saturation of the droplet is very late in the expansion process and nucleation is favoured, producing small particles. With increasing concentration, precipitation occurs earlier in the droplet expansion process, favouring particle growth giving rise to large particles; therefore, at a certain concentration there is cross over between both of these processes.

Other parameters could potentially affect the results obtained from concentration; the concentration in relation to the CO_2 flow rate could be important. Increasing the CO_2 flow rate would cause a decrease in the amount of solvent present in the bulk fluid causing a decrease in the solute solubility; small particles formed regardless of

concentration. It appears that it is crucial to consider all aspects of the system to fully understand the processes that take place giving rise to different particle sizes

3.3.4 Flow Rates

Subra *et al.* [15] studied the effect of increasing the solution flow rate on the size and yield for the precipitation of theophylline. A change of flow rate from 0.7 to 0.8 ml min^{-1} had no noticeable effect on the size and yield of the crystals obtained. Subra concluded that the regime was a mixing regime at whatever the solution flow rate was. The mixing zone was found to enlarge with an increase in solution flow rate, but had no major effect on the product characteristics. In terms of droplet formation, the change was noticeable at 333.15 K. At 9.5 MPa and 333.15 K, the range of size was 7-30 μm at 0.8 ml min^{-1}, compared to the 10-50 μm for the crystals obtained at 3 ml min^{-1}.

Both the solution flow rate and CO_2 flow rates have been studied by Martin et al. [12] Increasing the solution flow rate, increases the mixing between the jet and the surroundings due to the stronger turbulence. This leads to higher supersaturation in the jet. However, the effect of this parameter was found to be very small compared to other parameters which affect the phase equilibrium such as pressure and temperature. Martin *et al* concluded that the solution flow rate does not have a significant effect on the yield or the particle size. CO_2 flow rate has a small influence on the mixing; with higher flow rates, turbulence increases, and higher saturations are reached in the border of the jet. Martin stated that the main influence of the CO_2 flow rate on the process is that it determines the composition of the bulk fluid that results of complete

mixing between CO_2 and solvent. Increasing the CO_2 flow rate results in the bulk fluid having a smaller amount of organic solvent, the solubility of the solid in this fluid is smaller, and therefore smaller particles are obtained. The increase in the CO_2 flow rate may increase or decrease the yield, because it is possible that the decrease in solubility does not compensate the increase in the total amount of fluid that is introduced in the precipitation vessel.

For the case of flow rates, from the literature the effect of flow rates on particle size seems to be negligible. Overall, it appears that increasing the flow rates causes an increase in the turbulent mixing between the jet and SCF and does not impact on the solubilities and densities of various media present; improvement in mixing, with a larger mixing zone, no discernible effect on particle size.

In the literature, all research performed has been carried out on single oxide systems. The research that has been performed in this thesis has been carried out on mixed oxide systems. The general concepts have been applied to the mixed oxide system which means considering it as a bulk solution i.e. a one component system. However, the individual components, in terms of their solubility within the solvent and within the SCF needs to be considered as this could influence the formation of potentially, varied mixed oxide systems, single oxides and in turn affect the overall activity of the catalysts obtained.

In the literature there are many conflicting arguments on the effect of changing the process parameters on particle size. The overall concept from the literature is a change

in a parameter that affects a change in the densities of the medias present, causes a change in the solubility of the media. An increase in the solubility of the solvent, causes an increase in the degree of supersaturation, favouring nucleation, which results in production of small particles. However, a decrease in the solubility of the solvent causes a decrease in the degree of supersaturation, favouring particle growth, resulting in the formation of larger particles. During this research a number of parameters, such as temperature, pressure and flow rates have been varied to elucidate their effect on the particle size and in turn the overall catalytic activity; therefore giving a clear indication on the parameters of importance and how they can be tuned to improve catalytic performance.

3.4 References

[1] E. Reverchon, *J. Supercrit. Fluids*, 1999, **15**, 1

[2] P.M. Gallagher, V.J. Krukonis and G.D. Botsaris, *AIChE. Symp. Series*, 1991, **284**, 96

[3] S.-S. Yeo, G.-B. Lim, P.G. Debenedetti and H. Bernstein, *Bioengng*, 1993, **41**, 341

[4] T.W. Randolph, A.D. Randolph, M. Mebes and S. Yeung, *Biotechnol. Progess*, 1993, **9**, 429

[5] D.J. Dixon, K.P. Johnston and R.A. Bodmeier, *AIChE J.*, 1993, **39**, 127

[6] J. Robertson, M.B. King, J.P.K. Seville, D.R. Merrifield and P.C. Buxton, *4th International Symp. Supercrit Fluids*, 1997, 47

[7] W.J. Scmidt, M.C. Salada, G.G. Shook and S.M. Speaker, *AIChe J.*, 1995, **41**, 2476

[8] R. Bodmeier, H. Wang, D.J. Dixon, S. Mawson and K.P. Johnston, *J. Pharm. Res.*, 1995, **13**, 1211

Y. Gao, T.K. Mulenda, Y.-F. Shi and W.-K. Yuan, *J. Supercrit. Fluids*, 1998, **13**, 369

[9] I. De Rosa, *MSc Thesis*, University of Salerno, Italy, 1998

[10] E. Reverchon, G.D. Porta, D. Sannino and P. Ciambelli, *Powder Technol.*, 1999, **102**, 127

[11] F. Miguel, A. Martin, T. Gamse and M.J. Cocero, *J. Supercrit. Fluids*, 2006, **36**, 225

[12] A. Martin and M.J. Cocero, *J. Supercrit. Fluids*, 2004, **32**, 203

[13] E. Alonso, I. Montequi, S. Lucas and M.J. Cocero, *J. Supercrit. Fluids*, 2007, **39**, 453

[14] E. Reverchon, I. De Marco and G.D. Porta, *J. Supercrit. Fluids*, 2002, **23**, 81

[15] P. Subra, C.G. Laudani, A.Vega-Gonzalez and E. Reverchon, *J. Supercrit. Fluids*, 2005, **35**, 95

4 Results and Discussion

Iron Molybdates Prepared Using Supercritical Antisolvent Precipitation

4.1 Introduction

To investigate the influence of various reaction conditions on the structure and activity of the prepared catalysts, various solvents, pressures and temperatures were explored. All of these as-prepared catalysts were characterised by the analysis of XRD, BET, FT-IR and in some cases SEM.

4.2.1 Materials

All of the materials were used as supplied. Table 4.1 lists the details on all these materials including solvents, metal salts and CO_2 gas.

Table 4.1 – Materials used for the production of iron molybdates

Materials	Grade	Company
CO_2	SFC, 99.99%	BOC
Iron (II) acetate	ACS reagent, ≥ 98%	Sigma-Aldrich
Molybdenum (II) acetate	ACS reagent, ≥ 98%	Aldrich
Dimethyl sulfoxide	ACS reagent, ≥ 98%	Aldrich
H_2O_2	30% H_2O_2 in water	Aldrich

4.3 Results and Discussion

4.3.1 Using pure DMSO as solvent

DMSO is a clean, low toxic and dipolar aprotic solvent which widely functions as a reaction solvent in pharmaceutical, agricultural, polymer processes and sugar esters [5]. Many metal salts are soluble in DMSO, and DMSO is completely miscible with supercritical CO_2; owing to these characteristics DMSO has been considered an important solvent in the production of metal oxide precursors in supercritical antisolvent processes. As DMSO has successfully been used by several research groups to produce metal oxides [6,7]. The results showed well-defined nanoparticles of metal oxide precursors, obtained with high yield due to the excellent miscibility between DMSO and supercritical CO_2 as well as the good solubility with regard to metal acetates in DMSO.

In view of the previous work done by other research groups, the initial synthesis of iron molybdates was performed using pure DMSO as a solvent. Experiments were

conducted for about 9 hours, which results in the synthesis of approximately 1.2g of a brown-yellow solid. The yield was calculated to be approximately 55-60% based on the starting materials of iron(II)acetate and molybdenum(II)acetate.

4.3.1.1 Characterisation of the precursor.

The precursor obtained from supercritical antisolvent process was characterised by the analysis of XRD, Raman, BET, SEM and ICP-MS.

The XRD patterns of the as-prepared precursors are shown in Figure 4.1. The iron molybdate precursor produced from the supercritical process exhibits some crystallintiy at low reaction temperatures. This contrasts vastly to the crystalline starting materials of iron acetate and molybdenum acetate. As the temperature of the process was increased the precursors produced became much more crystalline. At 150 ^{o}C the XRD pattern corresponded to a mixture of different oxides; Fe_2O_3, MoO_3 and $Fe_2(MoO_3)_4$. This is possibly due to the fact that the reaction temperature is too high, and because of the process setup, some of the solvent is evaporating before entering the precipitation chamber causing the starting materials to precipitate out of the solution before reaction occurs with supercritical CO_2. Increasing the temperature causes an increase in the densities on the media present, which results in a decrease in the degree of supersaturation. Precipitation occurs later in the droplet expansion process favouring particle growth; this increase in particle growth could cause the production of more crystalline phases.

It could also be due to preferential precipitation of one of the components of the starting solution; this could result in limited production of the active phase, $Fe_2(MoO_3)_4$, and could lead to increased production of oxides upon calcination, causing a decrease in the overall activity of the catalyst.

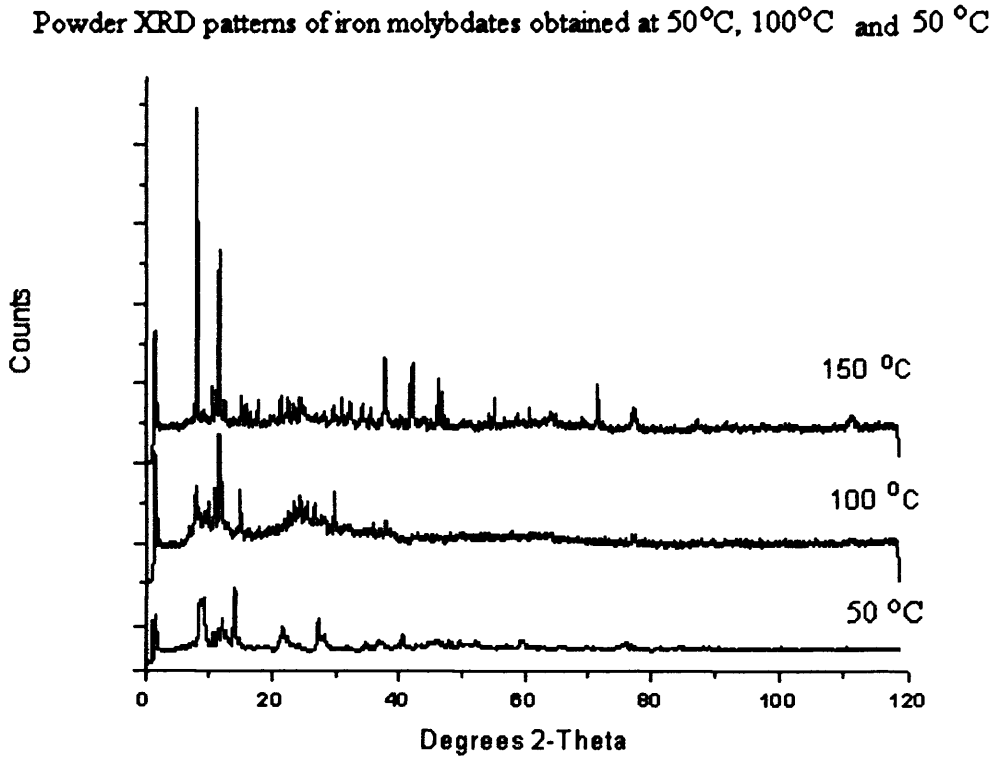

Figure 4.1 – Powder XRD pattern of as-precipitated iron molybdates prepared using different reaction temperatures

Table 4.2 shows the d-spacings obtained for the precursors obtained from the different process temperatures and the phases that they correspond to.

Table 4.2 – Phase assignment of d-spacings

D space			
50 °C	***100 °C***	***150 °C***	***Assignment***
4.348	4.3	4.36	$Fe_2(MoO_3)_4$
4.052	4.058	4.074	$Fe_2(MoO_3)_4$
3.895	3.861	3.885	$Fe_2(MoO_3)_4$
3.59	3.553	3.577	$Fe_2(MoO_3)_4$
	3.462	3.478	MoO_3/ $Fe_2(MoO_3)_4$
3.288	3.26	3.277	MoO_3
	2.661	2.668	MoO_3
2.37	2.305	2.312	MoO_3/ $Fe_2(MoO_3)_4$
	1.978	1.987	MoO_3
1.867		1.851	MoO_3

The Raman spectra of the iron molybdates produced with increasing reaction temperature are shown in Figure 4.2. The bands of importance are shown in table 4.3.

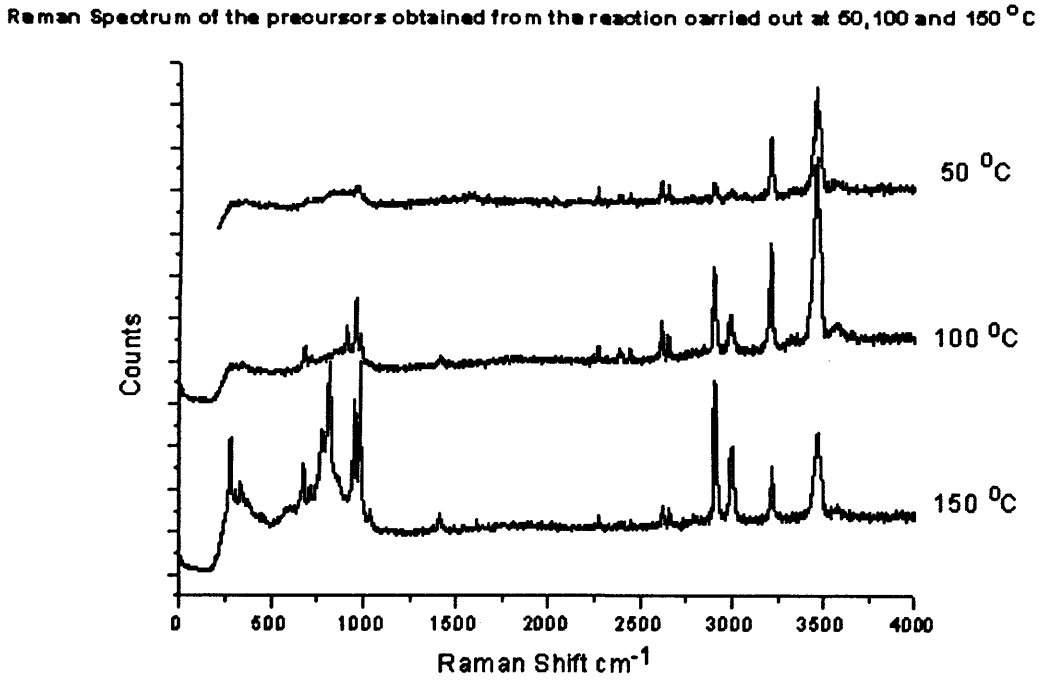

Figure 4.2 – Raman spectrum of the as-precipitated iron molybdates prepared using different reaction temperatures

Table 4.3 – Important Raman bands for Iron molybdates

Band or Band range cm^{-1}	*Assignment*
290	α-Fe_2O_3 / stretching vibration Fe-OOH
335/375	δ bending vibration in MoO_4^{2-}
660	OMo_3 vibrations (MoO_3)
774	Antisymmetric Mo-O-Mo stretching vibrations
813	ν asymmetric stretching vibration Mo=O
990	symmetric stretching vibration Mo=O (MoO_3 crystalline phase)

From the Raman spectra of the as-precipitated precursor at 50 °C the bands correspond to the presence of an iron molybdate and molybdenum oxide [8-12]. As the temperature of the oven was increased to 150 °C, the bands present in the spectra correspond to a mixture of oxides of the starting materials, Fe_2O_3 and MoO_3, and an iron molybdate. As mentioned previously, this could be due to evaporation of the solvent from the solution, or preferential precipitation of one of the components of the starting solution.

The BET measurements are shown in Table 4.4. The surface areas of the as-precipitated precursors are exceptionally low, regardless of the temperature precipitation has been performed at. From the literature iron molybdates typically have low surface areas; however the surface areas of the as-precipitated precursors are negligible. The precursors obtained from the process are light and mobile. The low surface areas could be due to the fact that the precursor is being drawn into the instrument when under vacuum, resulting in a lower or decreased surface area. Therefore, the surface area obtained is not a true indication of the surface area present.

Table 4.4 – Surface area measurements of the as-precipitated catalysts at different reaction temperatures

Sample	*Surface Area / m^2g^{-1}*
Precursor precipitated at 50°C	< 1
Precursor precipitated at 100 °C	< 1
Precursor precipitated at 150 °C	< 1

The structural composition of the iron molybdates was obtained from ICP-MS, the results obtained are shown in Table 4.5.

Table 4.5 – Ratio of iron and molybdenum present in the as-prepared catalysts

Sample	**Ratio of Fe:Mo**
Precursor precipitated at 50°C	1 : 4.5
Precursor precipitated at 100 °C	1 : 5.0
Precursor precipitated at 150 °C	1 : 6.0

Industrial iron molybdates typically have an Fe:Mo ratio of between 2.3 and 5. The as-precipitated iron molybdates were calculated to have a general Fe:Mo ratio of 1:5. The Fe:Mo ratio increased as the reaction temperature was increased. This could be attributed to a preferential precipitation of the molybdenum acetate starting material as the reaction temperature was increased. The total yields, from the starting materials, for both iron and molybdenum have been calculated and are shown in Table 4.6. The yield of Mo was much higher than that of Fe, supporting the idea that Mo is preferentially precipitated during the supercritical process. To investigate this process

further, a solubility study of the metal acetates in supercritical CO_2 would need to be performed on an appropriate test facility; this was not available during this research but could be considered as an area of study for future work

Table 4.6 – Percentage composition of molybdenum and iron present in the as-precipitated precursor

Temperature of Reaction /°C	*% Fe*	*%Mo*
50	5	37
100	4	37
150	6	38

The SEM image of the as-precipitated precursor obtained from the reaction at 50 °C is shown in Figure 4.3. The composition of the precursor comprised largely of small spherical particles, with a diameter of less than 1μm. However, across the surface of the precursor there are a number of large particles with a diameter between 2 and 5 μm. In the literature the general composition of precursors obtained from the supercritical antisolvent process are small spherical particles, as obtained during this process. As the temperature of the reaction was increased the particles appeared to lose their spherical nature, and become more irregularly shaped; the SEM image of the reaction at 100 °C is shown in figure 4.4. The loss in spherical nature could be due to evaporation of solvent during the process or a change in the physical properties of the supercritical fluid; the supercritical fluid becoming more dense with increasing temperature.

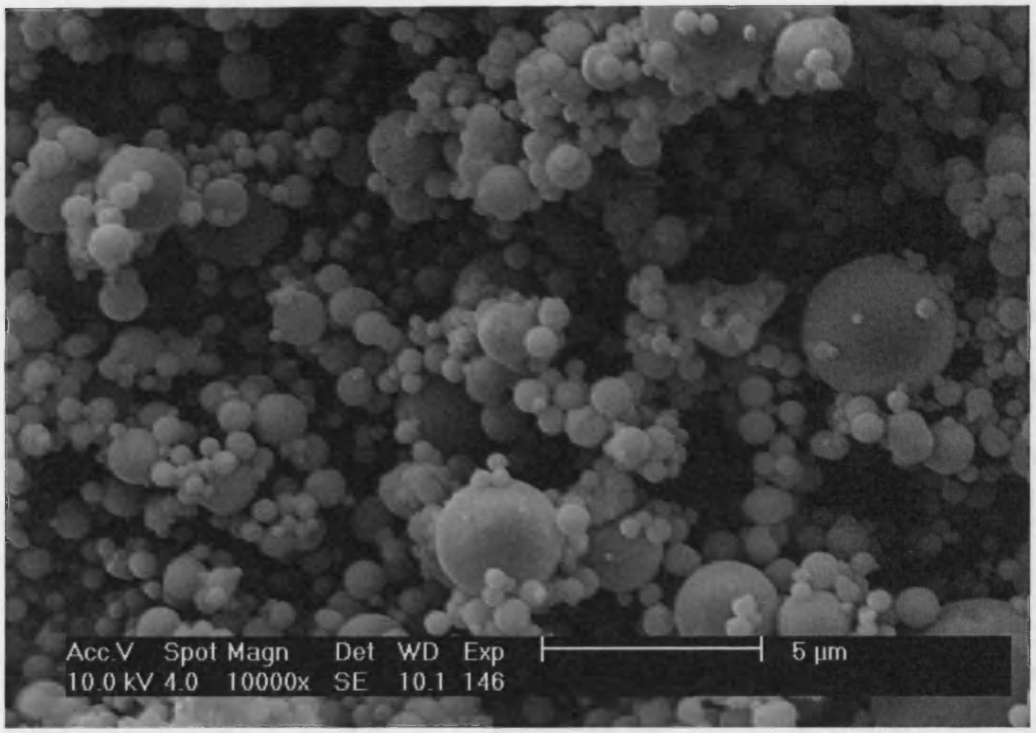

Figure 4.3 – SEM Image of the as-precipitated precursor precipitated at 50 °C

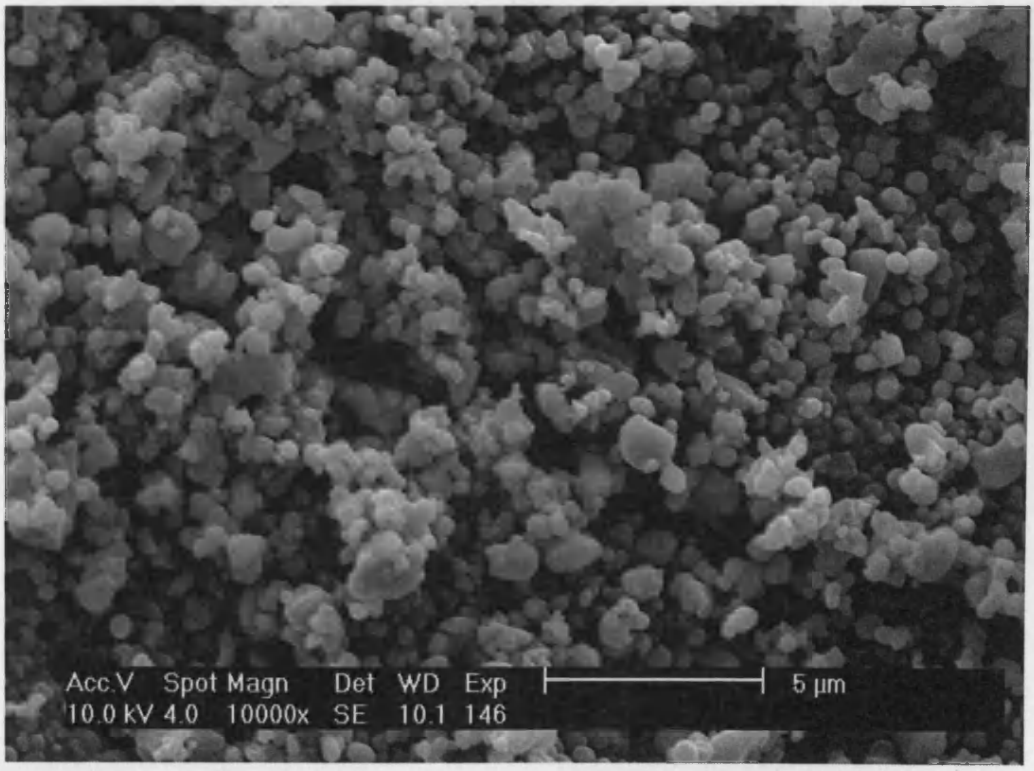

Figure 4.4 – SEM image of the as-precipitated precursor precipitated at 100 °C

4.3.1.2 Characterisation and Catalytic Performance of As-calcined catalysts

The powder XRD patterns of the catalysts obtained after calcination at 400 ^{o}C (at 20 ^{o}C min^{-1}) for 2 hours in air are shown in figure 4.5. Generally, there is a distinct increase in the crystallinty of the catalysts upon calcination; the phases are becoming more ordered upon thermal treatment and correspond to the presence of an iron molybdate and molybdenum oxide.

The iron molybdate catalysts exhibit almost the same crystallinity after calcination, even under different reaction conditions. There are distinct differences in the crystallinity of the precursors prior to calcination, but upon calcination these differences disappear. The calcination temperature is much higher than the reaction temperature, therefore, any residual starting material or single phases present after the reaction would decompose and oxidise, and the iron molybdate precursor would be oxidised to the catalyst. The reflections in the diffraction patterns obtained for the catalysts correspond to an iron molybdate and molybdenum oxide.

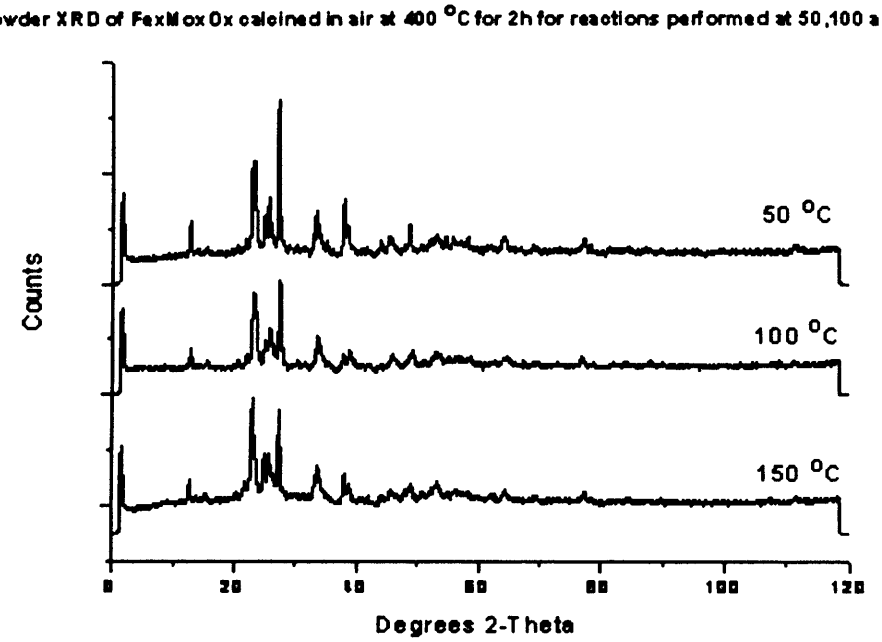

Figure 4.5 – Powder XRD pattern of as-calcined iron molybdates prepared using different reaction temperatures

From the Raman spectra of the catalysts over the different reaction temperatures the bands correspond to the presence of an iron molybdate and molybdenum oxide, the Raman spectra are shown in figure 4.6. The differences in the spectra could be due to subtle differences in the composition of the catalyst; the bands that differ are at 810 and 770 cm^{-1}, which correspond to $Fe_2(MoO_3)_4$ and MoO_3 respectively [10].

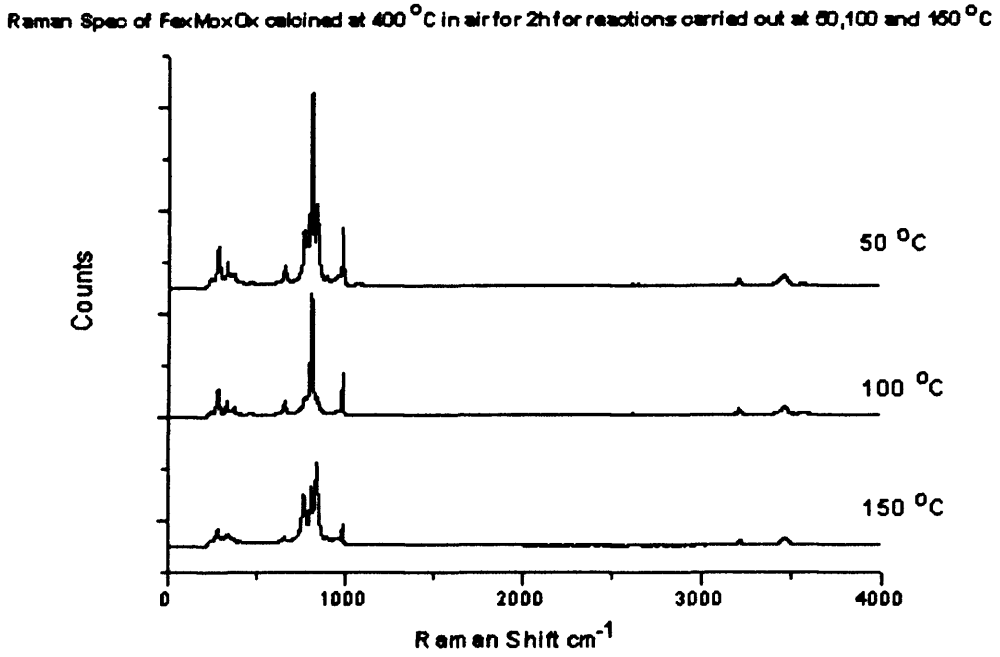

Figure 4.6 – Raman spectrum of the as-calcined iron molybdates prepared using different reaction temperatures

The BET measurements are shown in Table 4.7. Calcination of the precursors resulted in an increase in the surface area of the catalysts compared to that of the precursor. Upon calcination the catalysts became much more agglomerated. The increase in surface area could be attributed to the fact that this is a true measurement, unlike that of the precursor where the material could have been drawn into the machine.

Table 4.7 – Surface area measurements of the as–calcined catalysts obtained at different reaction temperatures

Sample	Surface Area / m^2g^{-1}
$Fe_xMo_xO_x$ at 50 °C calcined at 400 °C	13
$Fe_xMo_xO_x$ at 100 °C calcined at 400 °C	12
$Fe_xMo_xO_x$ at 150 °C calcined at 400 °C	12

The SEM images of the catalyst are shown in figure 4.7. The SEM image of the precursor shows the composition to be mainly comprised of small spherical particles,

based on observation the particle size appeared to be less than 1μm. After calcination, the structure of the catalyst changes; it is mainly composed of "rosette" shaped particles, with a diameter of less than 5 μm. There are also sparsely distributed large irregularly shaped particles of approximately 20 μm across the surface of the catalyst. After calcination, figure 4.8, the precursors obtained from different reaction temperature show very little difference under the microscope. Therefore, increasing the reaction temperature has a negligible effect on the structure and composition of the catalyst after calcination.

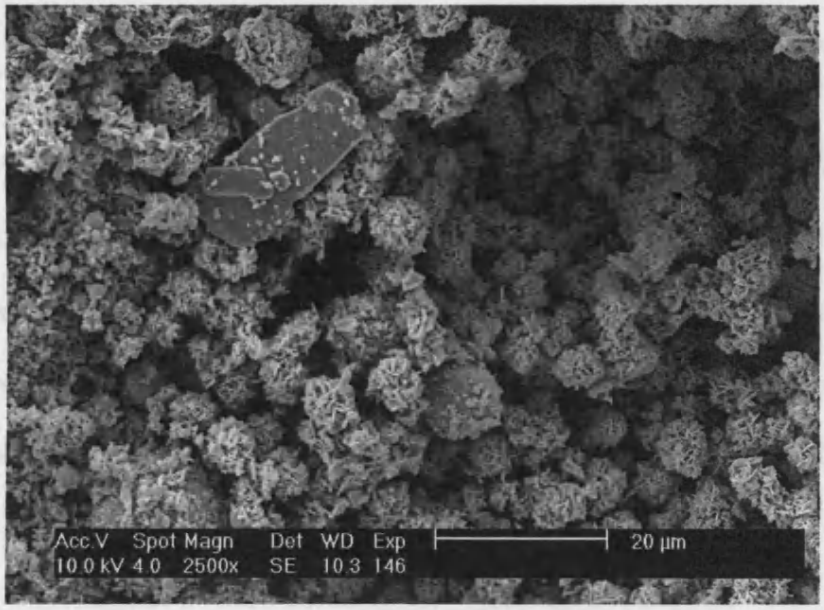

Figure 4.7 – SEM image of the as-calcined iron molybdate calcined at 400 °C prepared at 50°C

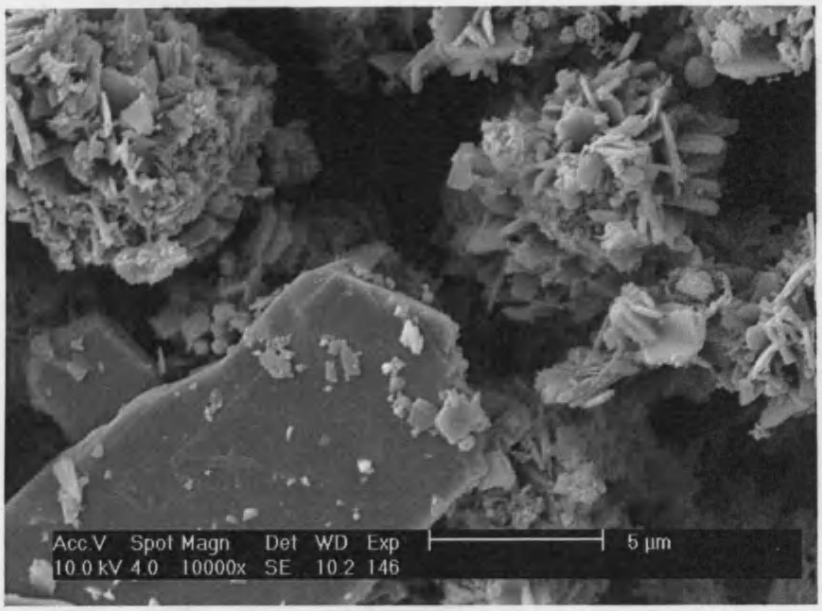

Figure 4.8 – SEM image of the as-calcined iron molybdate calcined at 400 °C, prepared at 50°C, increased magnification

The activity of the catalyst for the selective oxidation of methanol was determined using a continuous flow reactor. Methanol (10% in He, 30 ml min^{-1}) and O_2 (15 ml min^{-1}) were fed to the reactor at controlled rates using the mass flow controllers and were passed over the catalyst at the required reaction temperature. The products were analysed using on-line gas chromatography. The results obtained for the catalyst prepared at 50 °C are shown in figure 4.9.

From the results obtained, the production of an iron molybdate using the SAS process has been a success. Generally, increasing the reaction temperature resulted in an increase in the conversion of methanol; reaching a maximum of 56% conversion at 280°C. The selectivity of the reaction to formaldehyde increased with increasing reaction temperature reaching a maximum of 90% selectivity at 220°C. The activity of the catalyst suggests that the active phase, $Fe_2(MoO_3)_4$, has been produced by the SAS process

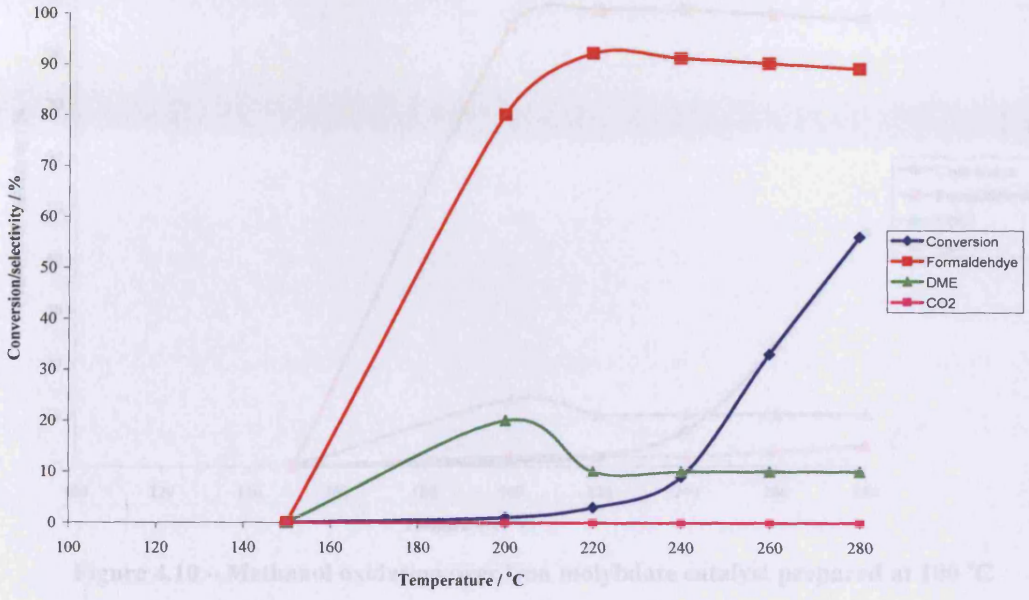

Figure 4.9 – Methanol oxidation over iron molybdate catalyst prepared at 50 °C

Increasing the process temperature further resulted in a decrease in the conversion of methanol as shown in figure 4.10. Increasing the reaction temperature resulted in an increase in the conversion of methanol but only reached a maximum of 45% conversion at 280°C. The selectivity of the reaction to formaldehyde increased with increasing reaction temperature. However, the production of by-products such as CO_2 and dimethyl ether, increased as the reaction temperature increased.

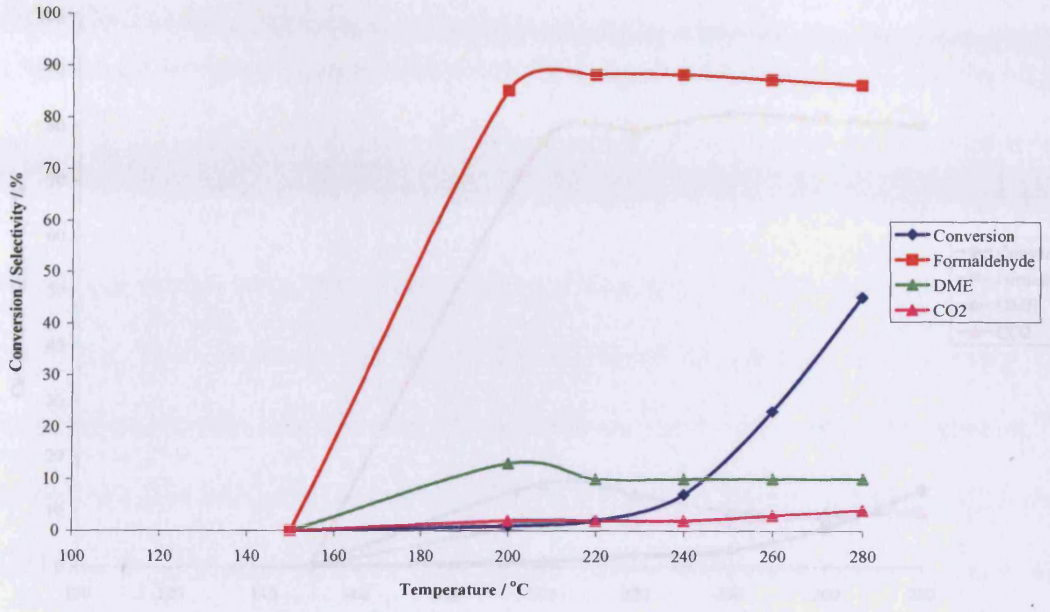

Figure 4.10 – Methanol oxidation over iron molybdate catalyst prepared at 100 °C

Increasing the process temperature further to 150°C proved detrimental to the activity of the catalyst. The conversion of methanol decreased to 23% at 280°C. The production of by-products such as, CO_2 and dimethyl ether, increased further with increasing reaction temperature. This is shown in figure 4.11.

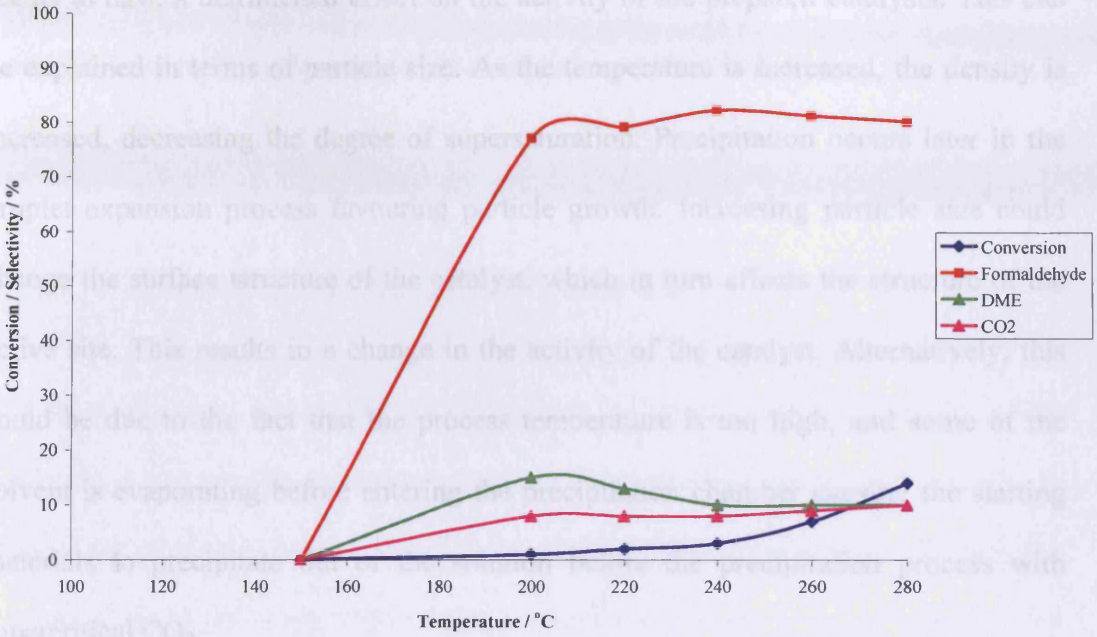

Figure 4.11 – Methanol oxidation over the iron molybdate catalyst prepared at varying process temperature at a reaction temperature of 150°C

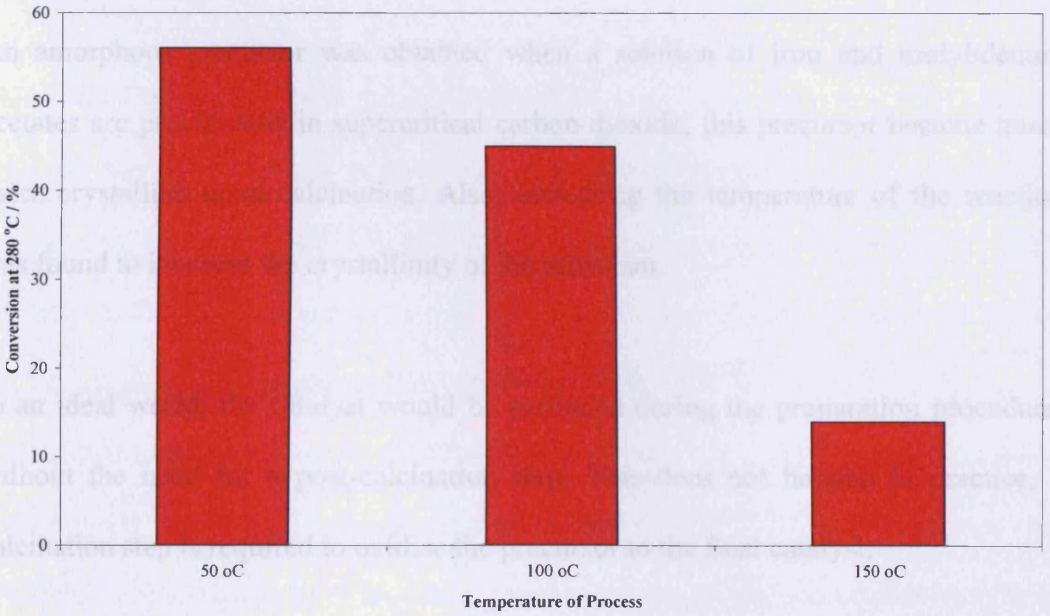

Figure 4.12 – Comparison of the conversion of methanol over the catalysts at 280 °C

The comparison of the methanol conversion over each of the catalyst is shown in figure 4.12. Increasing the process temperature at which the catalysts are prepared at,

seems to have a detrimental effect on the activity of the prepared catalysts. This can be explained in terms of particle size. As the temperature is increased, the density is increased, decreasing the degree of supersaturation. Precipitation occurs later in the droplet expansion process favouring particle growth. Increasing particle size could change the surface structure of the catalyst, which in turn affects the structure of the active site. This results in a change in the activity of the catalyst. Alternatively, this could be due to the fact that the process temperature is too high, and some of the solvent is evaporating before entering the precipitation chamber causing the starting materials to precipitate out of the solution before the precipitation process with supercritical CO_2.

4.3.2 Preoxidation of Starting Solution

An amorphous precursor was obtained when a solution of iron and molybdenum acetates are precipitated in supercritical carbon dioxide; this precursor became much more crystalline upon calcination. Also, increasing the temperature of the reaction was found to increase the crystallinity of the precursor.

In an ideal world, the catalyst would be produced during the preparation procedure, without the need for a post-calcination step. This does not happen in practice, a calcination step is required to oxidise the precursor to the final catalyst.

Preoxidation of the starting material, before processing in the supercritical reactor was investigated, with the overall aim of producing a catalyst that would not require a calcination step. Oxidation of the precursor was performed by the addition of an

oxidant. Initially, hydrogen peroxide was used to oxidise the precursor, "ageing" the solution by bubbling air through it was also tried.

4.3.2.1 Addition of Hydrogen Peroxide to the Starting Solution

4.3.2.1.1 Characterisation of the Precursor.

Hydrogen peroxide was added to the starting solution before processing in the supercritical reactor; this was done in varying concentrations, 0.25 and 0.5 vol %, to observe the effect this has on the precursor obtained from the reaction. The reaction was performed at 50 °C and 110 bar. The solution was pumped at a flow rate of 0.1 ml min^{-1}, and the CO_2 was pumped at 7 ml min^{-1}. These conditions were used for all reactions performed.

Figure 4.13 shows the XRD pattern obtained from the precursors. The XRD pattern obtained for the precursor without the addition of hydrogen peroxide shows the precursor to be amorphous. The addition of hydrogen peroxide had no effect on the structure of the precursor; regardless of the concentration of hydrogen peroxide added to the solution before processing, precipitation yielded an amorphous precursor. Perhaps the addition of hydrogen peroxide did not affect the solubility of the solvent with regards to the SCF, and the saturation and droplet expansion processes that occurred were similar in all three cases; resulting in the production of precursors with similar structures. The addition of hydrogen peroxide in varying concentrations may affect the phases produced from the process but not necessarily the overall structure; amorphous in all three cases.

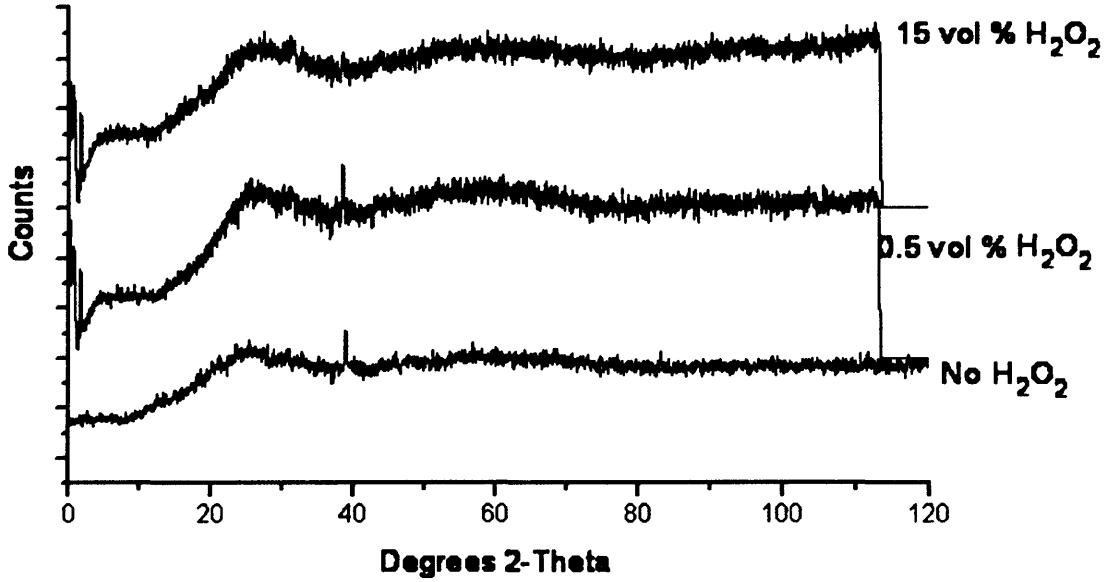

Figure 4.13 – Powder XRD pattern of as-prepared iron molybdates prepared by adding different concentrations of hydrogen peroxide

The Raman spectra obtained on the precursors are shown in figure 4.14. The bands of importance are at 335, 770, and 990 cm^{-1}; these correspond to the δ bending vibration in MoO_4^{2-}, $Fe_2(MoO_3)_4$ and the symmetric stretching vibration in Mo=O from MoO_3. These bands were found in each of the precursors obtained. Therefore, the precursors obtained from the process were mainly comprised of $Fe_2(MoO_3)_4$ and MoO_3. The addition of 0.25 vol % hydrogen peroxide did not appear to change the structure of the precursor obtained. At 0.5 vol % hydrogen peroxide there appears to be a band present at 290 cm^{-1}, which corresponds to the presence of Fe_2O_3. This suggests that the starting material, iron (II) acetate, has been oxidised to Fe_2O_3. Possibly, the addition of 0.25 vol % hydrogen peroxide was not enough to oxidise the starting material or to effect a change in the structure of the precursor obtained. However, 0.5 vol% hydrogen peroxide causes oxidation of the starting material This could prevent sufficient production of the active phase, $Fe_2(MoO_3)_4$, which in turn could be detrimental to the overall activity of the catalyst.

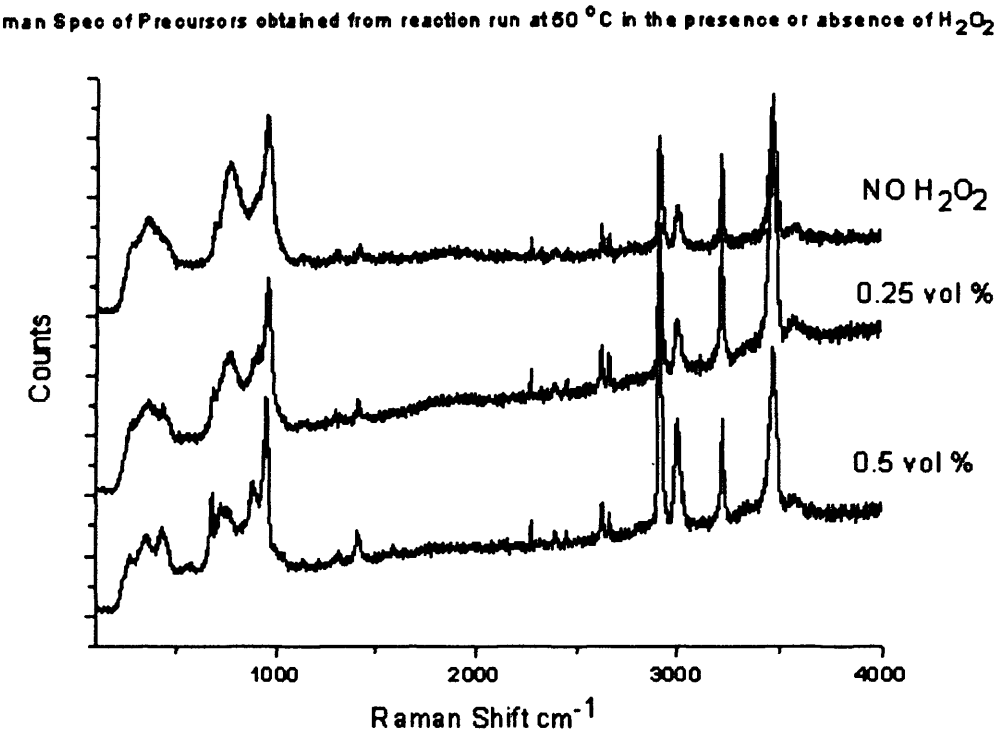

Figure 4.14 – Raman spectrum of the as-prepared iron molybdates prepared by adding different volumes of hydrogen peroxide

The BET surface area measurements of the precursors are shown in table 4.8. The surface area of the as-precipitated precursor, in the absence of H_2O_2, was low. The precursor obtained from this process was found to be light and mobile. The low surface area could be due to the fact that the precursor is being drawn into the instrument when under vacuum, resulting in a lower or decreased surface area. However, the precursors obtained by the addition of the hydrogen peroxide were much more agglomerated and darker in colour. The increase in surface area, compared to that prepared in the absence of H_2O_2, could be attributed to the fact that this is a true measurement, unlike that of the precursor where the material could have been drawn into the machine.

From the results, it appears that adding more hydrogen peroxide to the starting solution is detrimental to the surface area of the obtained precursor. Bands from the Raman spectra were found to correspond to Fe_2O_3, as well as $Fe_2(MoO_3)_4$ and MoO_3. Oxidation of the starting material to the corresponding oxide instead of the required iron molybdate has altered the structural composition of the precursor; this change in structural composition has resulted in a decrease in the surface area of the precursors, and potentially a decrease in the activity of the catalyst.

Table 4.8 – Surface area measurements of as-prepared iron molybdates prepared by adding different concentration of hydrogen peroxide to the starting solution

Reaction	*Surface Area / m^2g^{-1}*
No H_2O_2	<1
0.25 vol% H_2O_2	12
0.5 vol % H_2O_2	2

4.3.2.1.2 Characterisation and Catalytic Performance of the As-calcined Catalysts

The precursors obtained from the reactions performed in the supercritical rig were calcined at 400°C in a Carbolite tube furnace for 2 h in air.

The XRD patterns of the as-calcined catalysts are shown in figure 4.15. The XRD patterns of the catalysts which had been prepared in the presence and absence of hydrogen peroxide were very similar. The reflections in the XRD patterns correspond the presence of $Fe_2(MoO_3)_4$ and MoO_3. The addition of hydrogen peroxide to the starting solution results in the production of a catalyst whose bulk composition

appears to be very similar to the catalysts prepared in the absence of hydrogen peroxide.

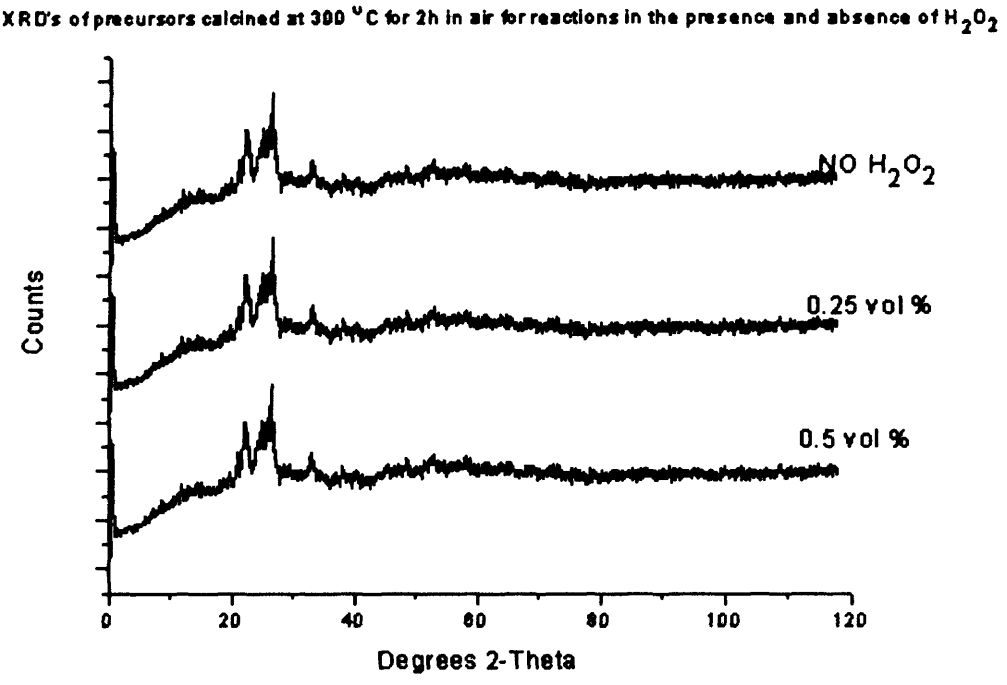

Figure 4.15 – Powder XRD pattern of as-calcined iron molybdates, calcined at 300°C, prepared by adding different concentrations of hydrogen peroxide at a process temperature of 50°C.

The Raman spectra of the as-calcined catalysts are shown in figure 4.16. There appears to be similarities in the spectra obtained for the catalysts with 0 and 0.25 vol %. Both spectra contain bands at 350, 770 and 990 cm^{-1} [8]. These bands correspond to the δ bending vibration in MoO_4^{2-}, $Fe_2(MoO_3)_4$ and the symmetric stretching vibration inj Mo=O from MoO_3; therefore the catalyst is predominantly composed of $Fe_2(MoO_3)_4$ and MoO_3.vol% However, the Raman spectra of the 0.5 vol% catalyst shows some differences compared to that of the lower concentrations. At 0.5 vol% hydrogen peroxide there appears to be a band present at 290 cm^{-1}, which corresponds to the bending vibration in Fe_2O_3. As with the precursor the presence of this band suggests that the starting material, iron (II) acetate, has been oxidised to Fe_2O_3. As mentioned previously the 0.5 vol%, with oxidation of the starting material, could

prevent sufficient production of the active phase, $Fe_2(MoO_3)_4$, and in turn effect the overall activity of the catalyst.

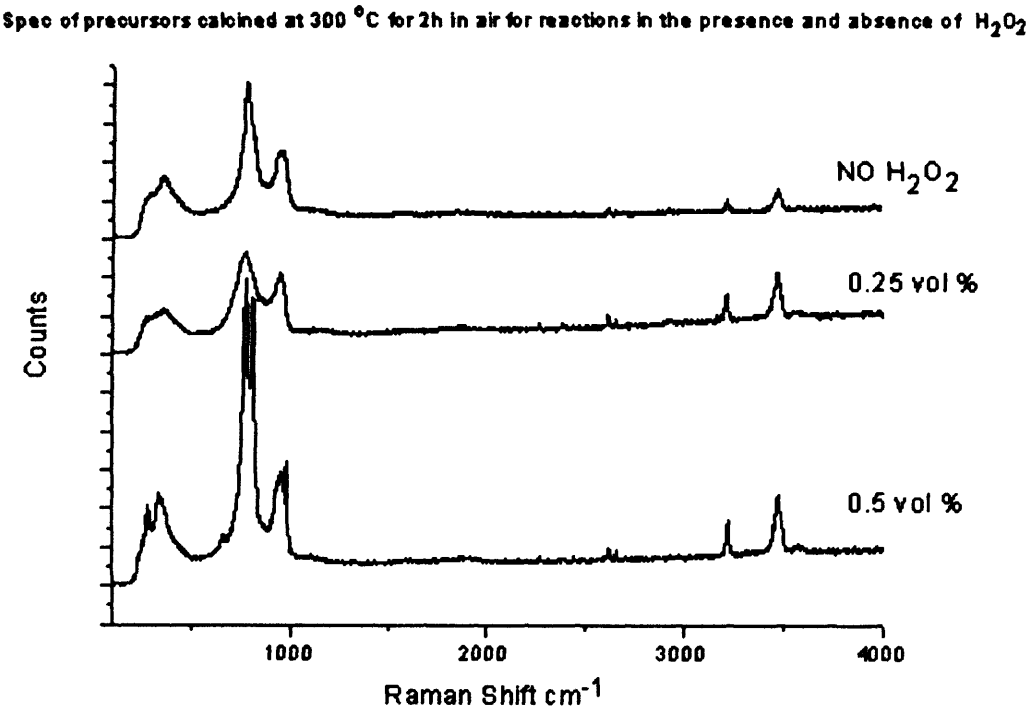

Figure 4.16 – Raman spectrum of the as-calcined iron molybdates prepared by adding different volumes of hydrogen peroxide

The BET surface area measurements of the precursors are shown in table 4.9. Generally, for all the catalysts obtained upon calcination there was a decrease in surface area from that of the precursor. The addition of hydrogen peroxide to the starting material is detrimental to the surface area of the precursor and the as-calcined catalyst. Bands from the Raman spectra of the catalyst prepared with 0.5 vol% H_2O_2, were found to correspond to Fe_2O_3, as well as $Fe_2(MoO_3)_4$ and MoO_3. The presence of Fe_2O_3, as indicated by the Raman spectra, shows that the addition of hydrogen peroxide altered the structural composition of the precursor; which in turn caused a decrease in the surface area of the as-calcined catalysts. The catalyst prepared using 0.25 vol% H_2O_2 exhibited a decrease in surface area, however, according to the characterisation data appeared to be very similar, structurally, to that of the catalyst

prepared in the absence of H_2O_2. Perhaps by adding 0.25 vol% H_2O_2 there isn't sufficient H_2O_2 to oxidise the starting materials, which does not produce Fe_2O_3. This causes a subtle change in the structural composition of the surface of the catalyst causing a decrease in surface area.

Table4. 9 – Surface area measurements of as-calcined iron molybdates, calcined at 300°C for 2h in air, prepared by adding different concentration of hydrogen peroxide to the starting solution

Reaction	*Surface Area / m^2g^{-1}*
No H_2O_2	13
0.25 vol % H_2O_2	5
0.5 vol % H_2O_2	1

The activity of the catalysts for the selective oxidation of methanol was determined using a continuous flow reactor. The result of the catatlyst prepared in the absence of H_2O_2 is shown in Figure 4.17. The selectivity of the reaction to formaldehyde increased with increasing reaction temperature reaching a maximum of 90% selectivity at 220°C.

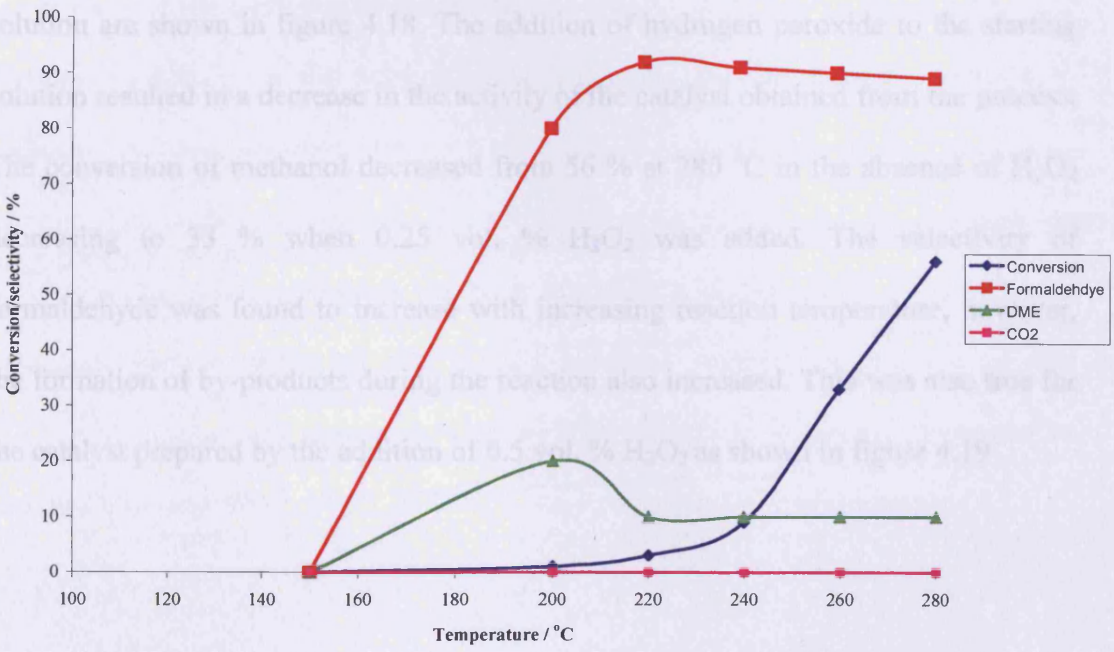

Figure 4.17 – Methanol oxidation over iron molybdate catalyst prepared at 50 °C

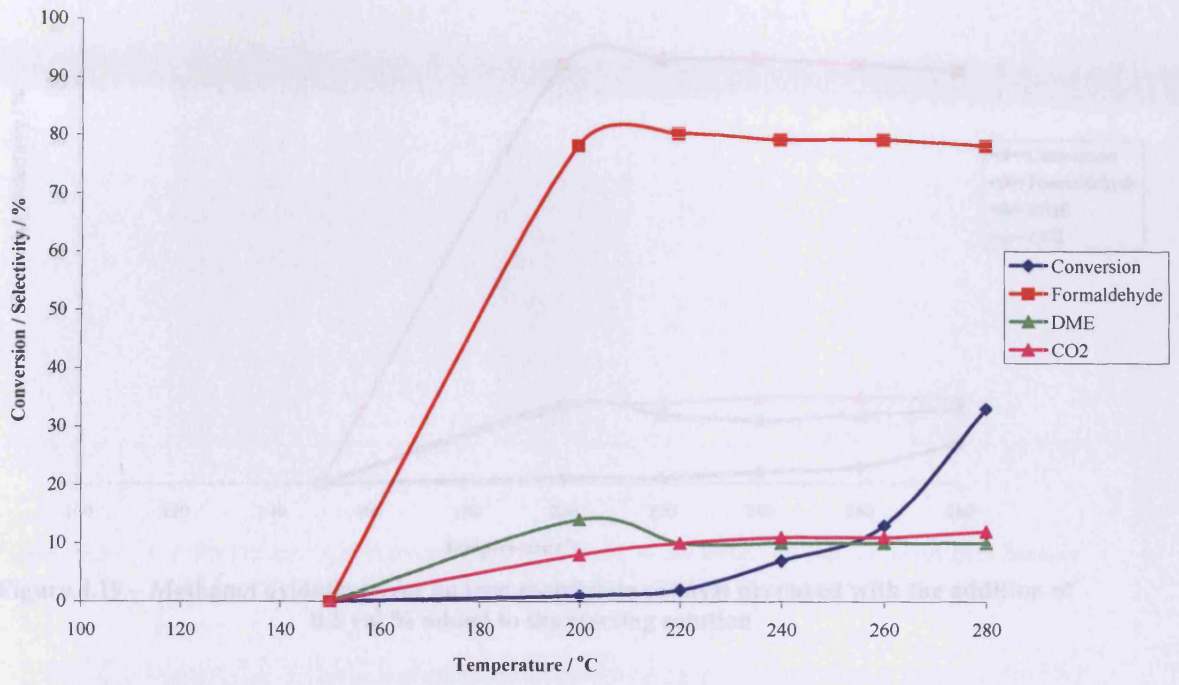

Figure 4.18 – Methanol oxidation over an iron molybdate catalyst prepared with the addition of 0.25 vol % added to the starting solution

The results obtained for the catalyst prepared with 0.25 vol. % added to the starting solution are shown in figure 4.18. The addition of hydrogen peroxide to the starting solution resulted in a decrease in the activity of the catalyst obtained from the process. The conversion of methanol decreased from 56 % at 280 °C in the absence of H_2O_2 decreasing to 33 % when 0.25 vol. % H_2O_2 was added. The selectivity of formaldehyde was found to increase with increasing reaction temperature, however, the formation of by-products during the reaction also increased. This was also true for the catalyst prepared by the addition of 0.5 vol. % H_2O_2 as shown in figure 4.19

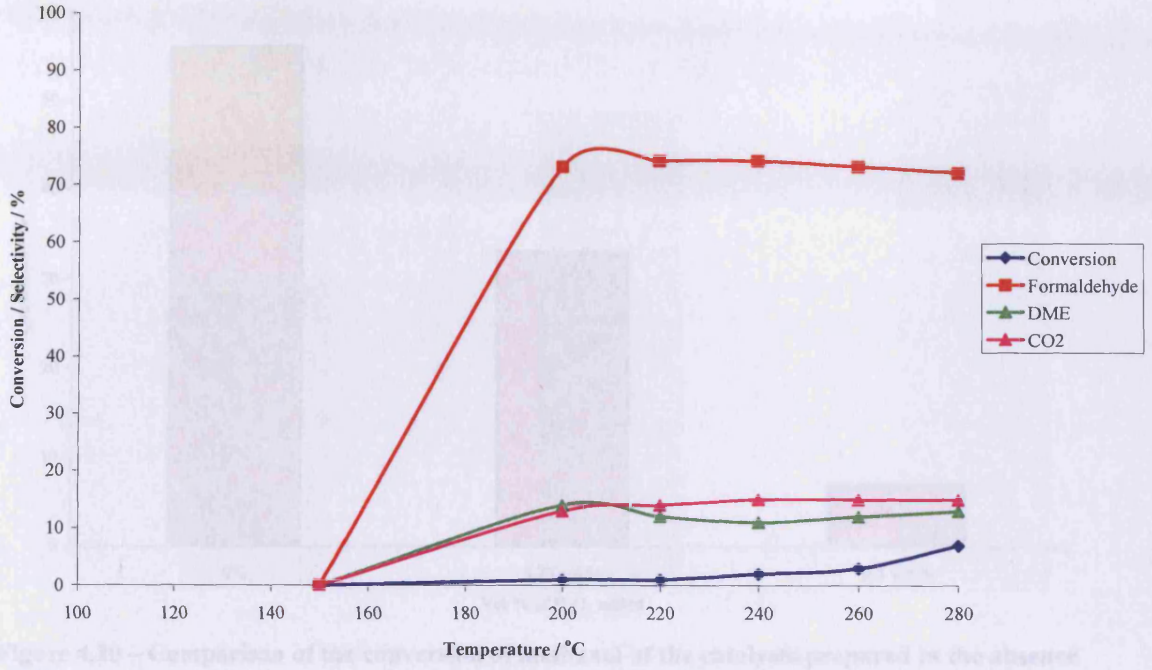

Figure 4.19 – Methanol oxidation over an iron molybdate catalyst prepared with the addition of 0.5 vol % added to the starting solution

By adding more hydrogen peroxide to the starting solution the impact on prepared catalyst was that the conversion of methanol decreased further to 7% at 280 °C. A comparison of the activities of the catalysts at 280 °C is shown in figure 4.20. The decrease in activity in the catalyst could be due to the fact that the addition of hydrogen peroxide oxidises some of the starting material present in the starting solution. The more hydrogen peroxide added the more starting material oxidised. On processing the solution through the SAS reactor, the active phase, $Fe_2(MoO_3)_4$ is produced. The oxidation of the starting material reduces the amount of this $Fe_2(MoO_3)_4$ phase being produced; there is an increase in production of single oxides such as Fe_2O_3 and MoO_3. Fe_2O_3 is detrimental to the selectivity of the catalyst.

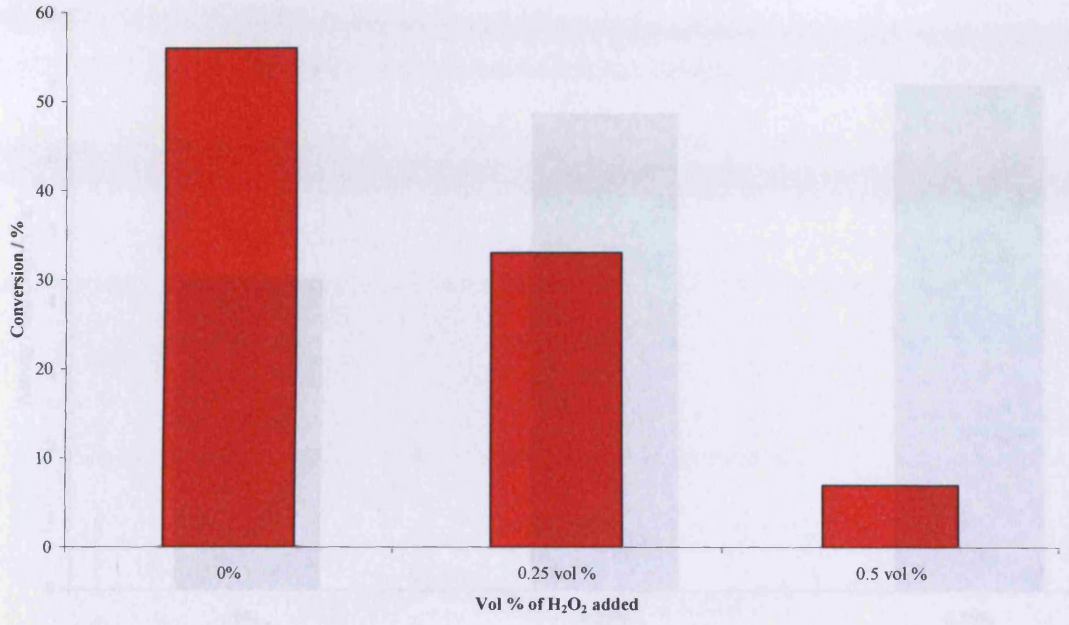

Figure 4.20 – Comparison of the conversion of methanol of the catalysts prepared in the absence and presence of hydrogen peroxide at 280°C reaction temperature

Figure 4.21 shows the conversion of methanol for each of the catalysts normalised by surface area. After normalising for surface area the trend was reversed. The impact on the catalyst produced, increasing the vol % of H_2O_2 added, was that the conversion per unit area increased. The catalyst prepared with 0.5 vol % H_2O_2 had the highest conversion per unit area, but had the lowest conversion of methanol. Therefore, from the results the activity of the catalysts obtained appears to be surface area dependent. This surface area dependency means that it is crucial that the highest surface area is achieved post calcination, which will ensure that the maximum conversion of methanol is attained for that catalyst. As the addition of H_2O_2 was detrimental to the surface area of the final catalyst, preoxidation of the starting solution has to be done using an alternative which enhances or maintains the surface area.

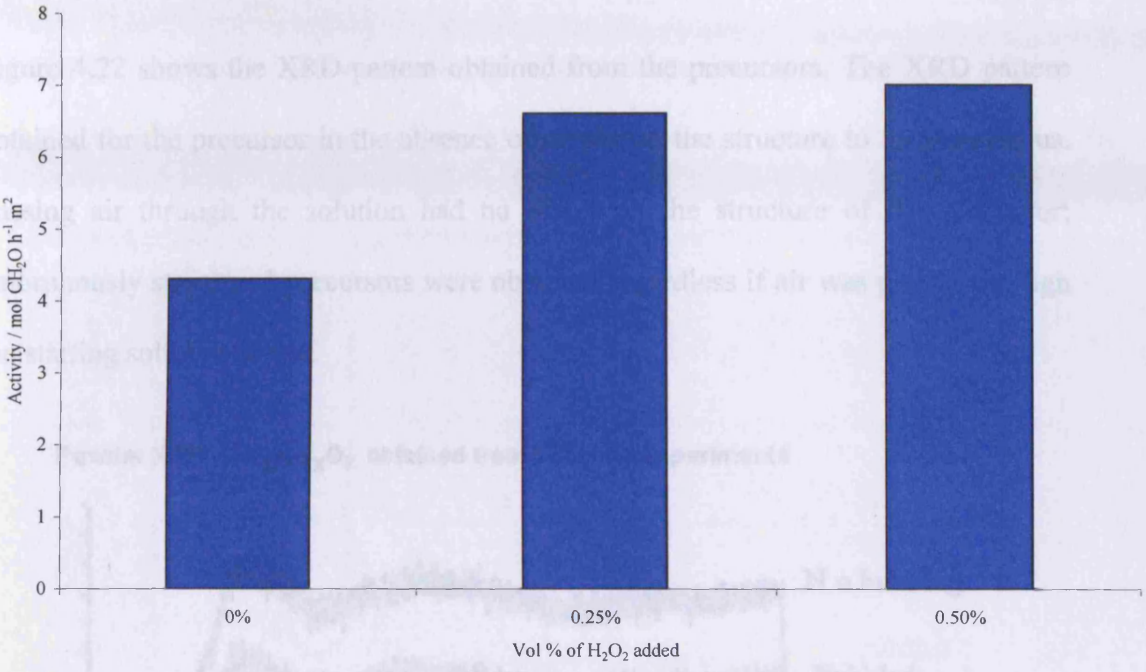

Figure 4.21 – Comparison of the conversion of methanol of the catalysts prepared in the absence and presence of hydrogen peroxide at 280°C reaction temperature normalised per unit area

4.3.2.2 Passing Air through the Starting Solution

4.3.2.2.1 Characterisation of the Precursor

The use of hydrogen peroxide as an oxidant had detrimental effects to the surface area and the overall catalytic activity of the iron molybdate catalysts obtained from the supercritical process. Therefore, an alternative oxidant was tried with the aim of maintaining the surface area post calcination step, and eventually to produce a final catalyst without the need for a calcination step. Air was passed through the starting solution for 4 h at room temperature, prior to processing in the supercritical reactor; air was used as it is much less potent than hydrogen peroxide. The precipitation was performed at 50 °C and 110 bar. The solution was pumped at a flow rate of 0.1 ml min^{-1}, and the CO_2 was pumped at 7 ml min^{-1}. These conditions were used for all reactions performed.

Figure 4.22 shows the XRD pattern obtained from the precursors. The XRD pattern obtained for the precursor in the absence of air shows the structure to be amorphous. Passing air through the solution had no effect on the structure of the precursor; amorphously structured precursors were obtained regardless if air was passed through the starting solution or not.

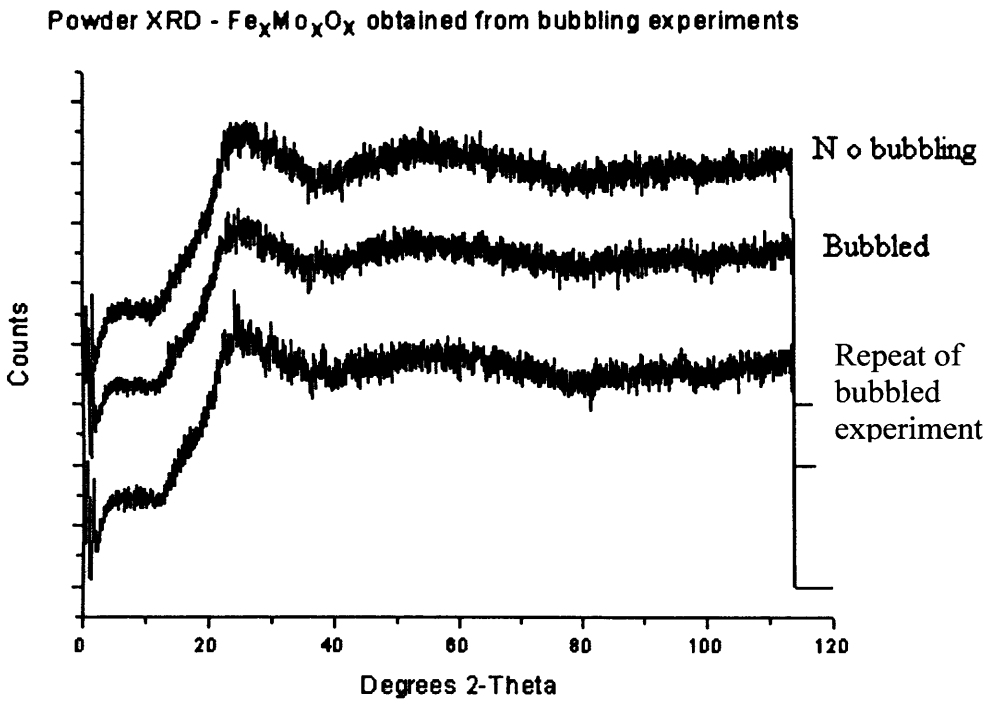

Figure 4.22 – Powder XRD pattern of as-prepared iron molybdates prepared at a process temperature of 50 °C by bubbling air through the starting solution

The Raman spectra obtained on the precursors are shown in figure 4.23. The Raman spectra for both precursors, in the absence and presence of air are very similar. Both contain bands at 335, 770, and 990 cm^{-1} corresponding to the δ bending vibration in MoO_4^{2-}, $Fe_2(MoO_3)_4$ and the symmetric stretching vibration in Mo=O from MoO_3 [8]. The composition of both precursors are $Fe_2(MoO_3)_4$ and MoO_3. In comparison to the precursors obtained when hydrogen peroxide was used, there is no band present at

290 cm^{-1}, corresponding to Fe_2O_3. The absence of this band suggests that passing air through the starting material does not react with individual components of the starting material, which in turn does not yield unfavourable oxides i.e. Fe_2O_3.

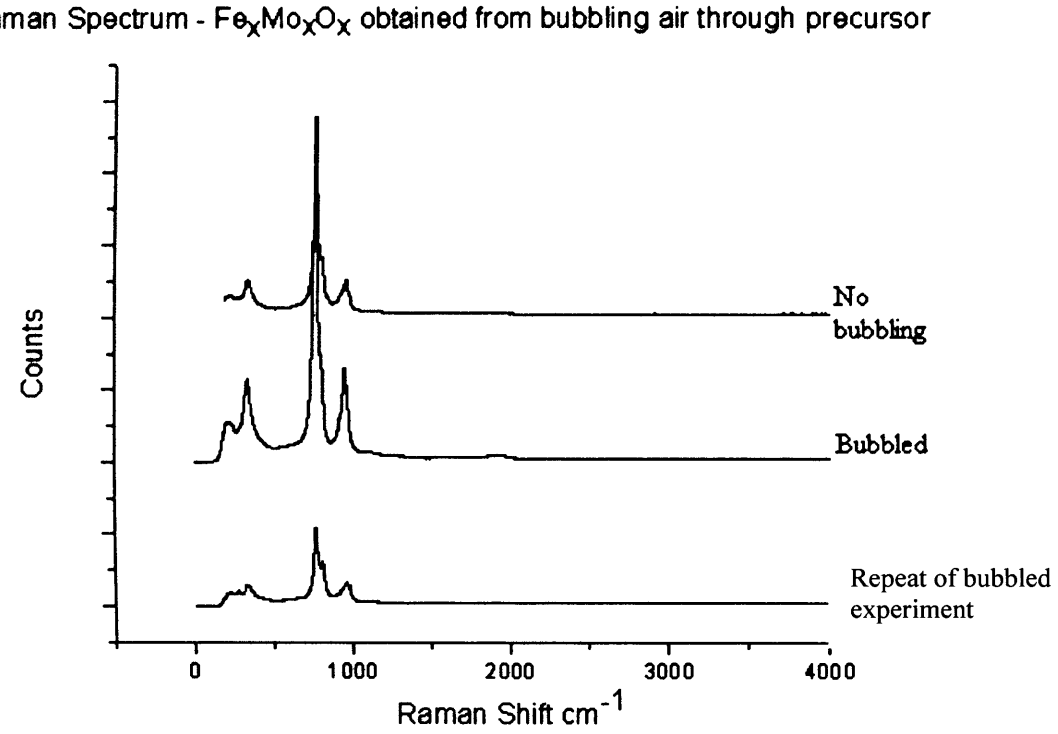

Figure 4.23 – Raman spectrum of the as-prepared iron molybdates prepared by bubbling air through the starting solution

The BET surface area measurements of the precursors are shown in table 4.10. As with the addition of hydrogen peroxide to the starting solution, passing air results in a decrease in the surface area of the precursor compared to the surface area of the precursor obtained in the absence of air.

Table 4.10 – Surface area measurements of as-prepared iron molybdates prepared by bubbling air through the starting solution

Reaction	*Surface Area / m^2g^{-1}*
No bubbling	<1
$Fe_xMo_xO_x$-1 BUBBLED 4 hrs	3
$Fe_xMo_xO_x$-2 BUBB4 hrs	1

4.3.2.1.2 Characterisation and Catalytic Performance of the As-calcined Catalysts

Figure 4.24 shows the XRD pattern obtained from the as-calcined catalysts. The XRD patterns obtained show the structures of the catalysts to be crystalline in both cases. From the reflections in the XRD patterns, the phases present correspond to $Fe_2(MoO_3)_4$ and MoO_3. Passing air through the starting material, according to the XRD patterns obtained, has very little effect on the overall structure of the catalyst.

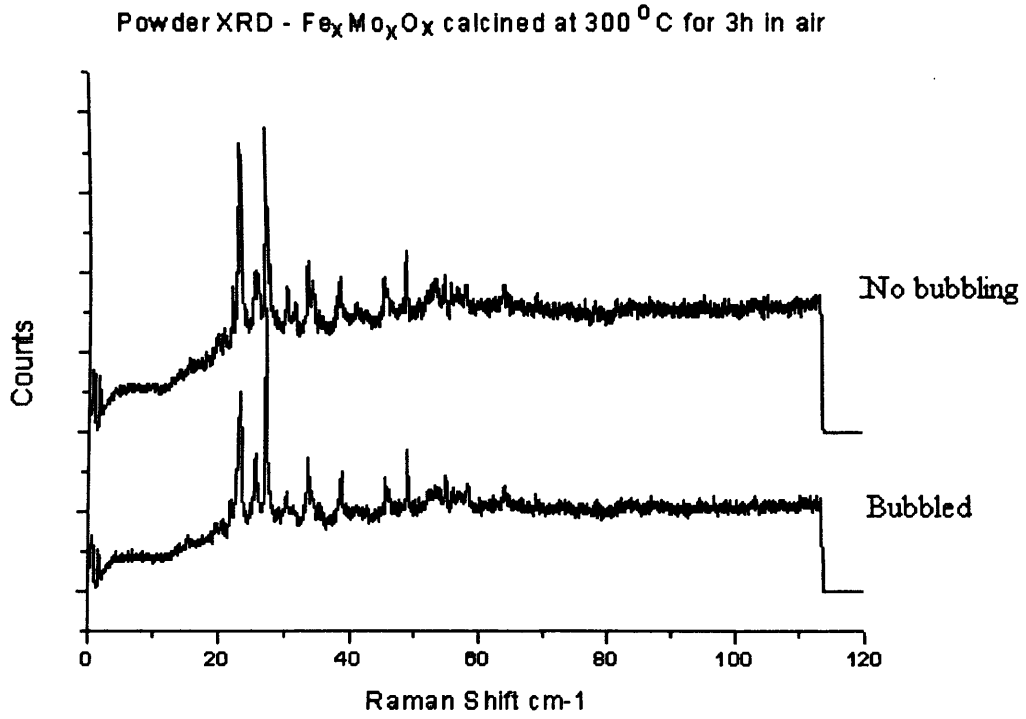

Figure 4.24 – Powder XRD pattern of as-calcined iron molybdates prepared by bubbling air through the starting solution

The Raman spectra of the catalysts are shown in figure 4.25. The Raman spectra obtained on the precursors are shown in figure 4.21. The Raman spectra for both

catalysts, contain bands at 335, 770, and 990 cm^{-1} which corresponds to $Fe_2(MoO_3)_4$ and MoO_3 [8]. The main difference between the catalysts obtained, is that when air is passed through the starting solution, the Raman spectra for both the precursor and catalyst are very similar; therefore successful preoxidation has taken place. The bands in both the precursor and the catalyst correspond to the presence of $Fe_2(MoO_3)_4$ and MoO_3..

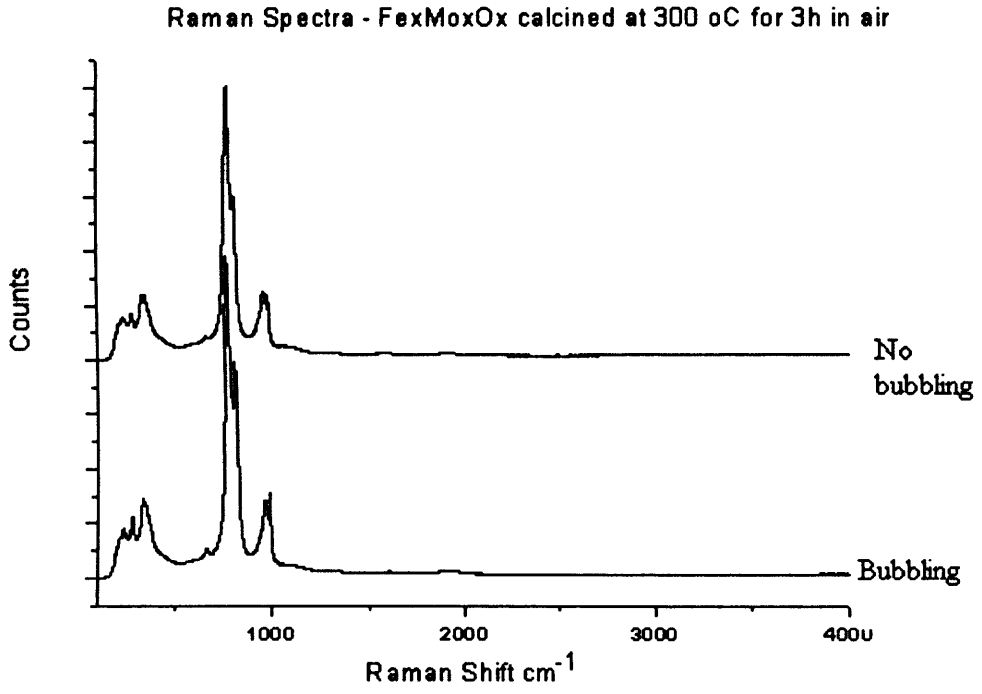

Figure 4.25 – Raman spectrum of the as-calcined iron molybdates prepared by bubbling air through the starting solution

The surface area measurements of the precursor were low. Upon calcination the surface area increased. The BET surface area measurements of the catalysts are in table 4.11. Therefore, passing air through the starting material has enhanced the surface area of the catalyst after calcination. This did not happen to the catalyst

obtained in the absence of air, the opposite occurred; there was a decrease in the surface area of the catalyst upon calcination.

Table 4.11 – Surface area measurements of as-calcined iron molybdates prepared by bubbling air through the starting solution

Reaction	*Surface Area / m^2g^{-1}*
$Fe_xMo_xO_x$ – No bubbling calcined at 300 °C for 3h in air	13
$Fe_xMo_xO_x$ – Bubbled calcined at 300 °C for 3h in air	10

The activity of the catalyst for the selective oxidation of methanol was determined using a continuous flow reactor. The result of the catalyst prepared without bubbling air through the starting solution is shown in Figure 4.26. The selectivity of the reaction to formaldehyde increased with increasing reaction temperature reaching a maximum of 90% selectivity at 220°C.

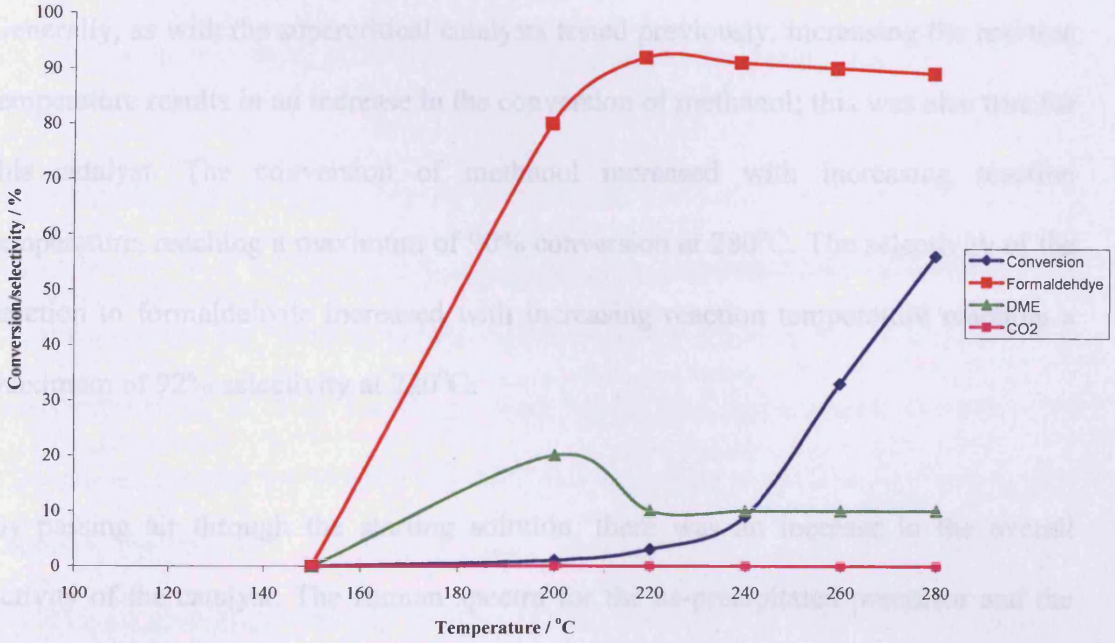

Figure 4.26– Methanol oxidation over iron molybdate catalyst prepared at 50 °C

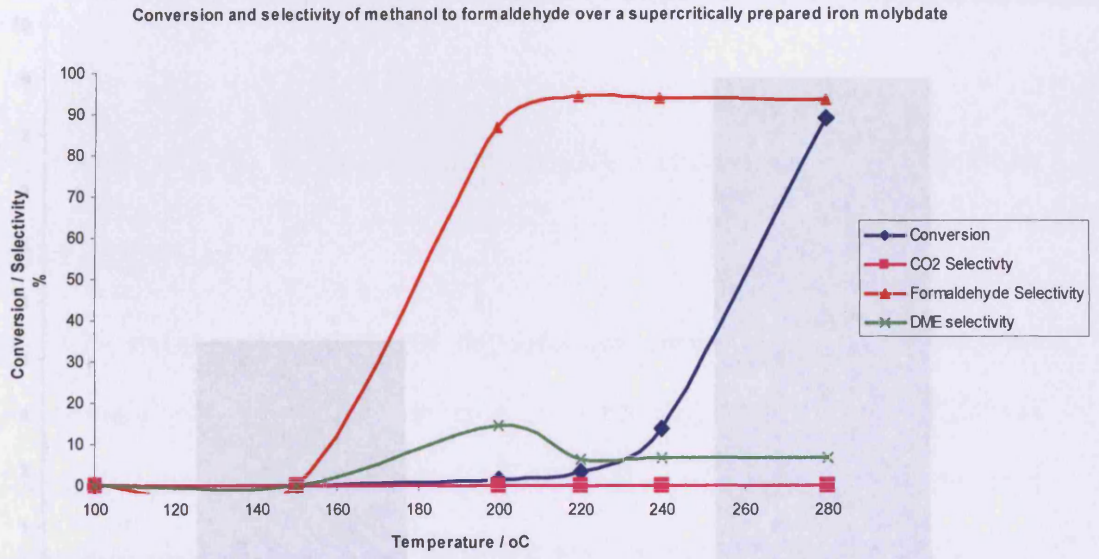

Figure 4.27 – Conversion and selectivity of methanol to formaldehyde over iron molybdate prepared by bubbling air through the starting solution

Generally, as with the supercritical catalysts tested previously, increasing the reaction temperature results in an increase in the conversion of methanol; this was also true for this catalyst. The conversion of methanol increased with increasing reaction temperature, reaching a maximum of 90% conversion at 280°C. The selectivity of the reaction to formaldehyde increased with increasing reaction temperature reaching a maximum of 92% selectivity at 220°C.

By passing air through the starting solution, there was an increase in the overall activity of the catalyst. The Raman spectra for the as-precipitated precursor and the catalyst were very similar. This implies that calcination has not dramatically changed the surface structure of the catalyst. The surface area also increased upon calcination

of the as-precipitated precursor. The increase in catalytic activity could be attributed to the increase in surface area. Figure 4.28 shows the conversion normalised per unit area for both catalysts.

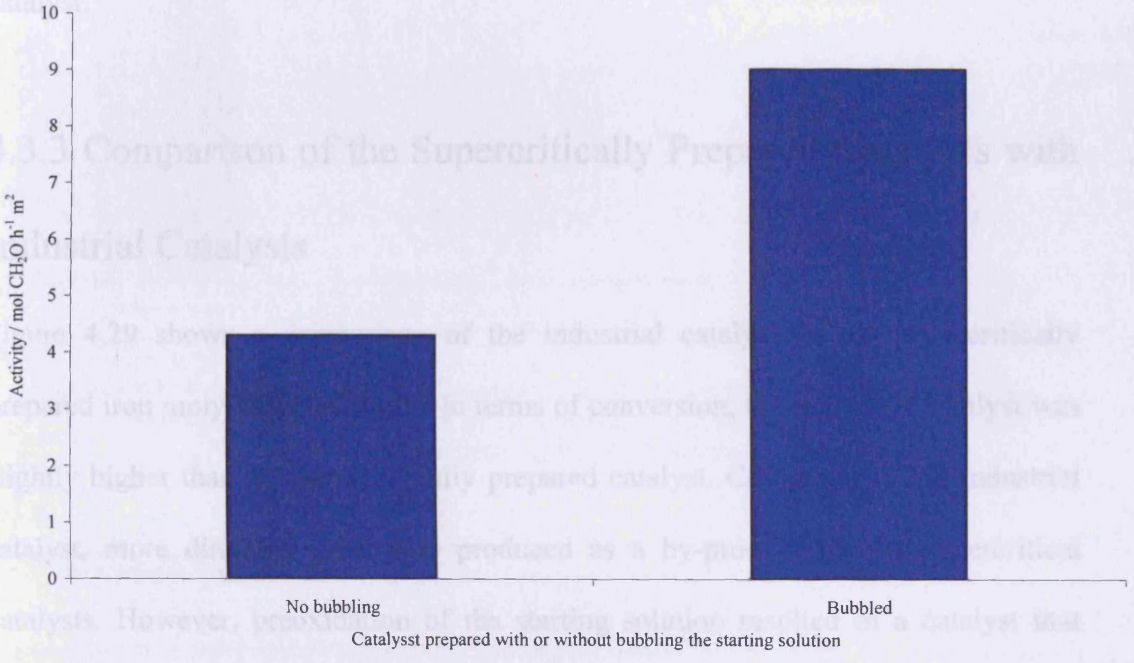

Figure 4.28 – Comparison of the conversion of methanol of the catalysts prepared in the with and without bubbling at 280°C reaction temperature normalised per unit area

On comparing the conversion per unit area of both catalysts it can be clearly seen that the there is a vast difference between them. The conversion per unit area of the catalyst prepared by bubbling air through the starting solution is double that of the catalyst prepared without bubbling, even though the surface area is lower. By bubbling air through the starting solution, and according to the characterisation data obtained, the precursor and catalysts were structurally very similar. It appears that bubbling air through the starting solution has increased the conversion per unit area as well as increased the conversion of methanol, unlike H_2O_2 which was detrimental to the surface area. Perhaps the increased conversion is due to subtle structural changes

on the surface of the catalyst which have enhanced the catalytic activity of the catalyst. Further research and characterisation data are required to determine the effect bubbling air through the starting material has on the surface composition of the catalyst.

4.3.3 Comparison of the Supercritically Prepared Catalysts with Industrial Catalysts

Figure 4.29 shows a comparison of the industrial catalyst to the supercritically prepared iron molybdates at 280°C. In terms of conversion, the industrial catalyst was slightly higher than the supercritically prepared catalyst. Compared to the industrial catalyst, more dimethyl ether was produced as a by-product by the supercritical catalysts. However, preoxidation of the starting solution resulted in a catalyst that with comparable selectivity to formaldehyde as that of the industrial catalyst. Therefore, an iron molybdate was successfully prepared using supercritical CO_2, using metal acetates, which resulted in a catalyst with activity comparable to that of the industrial catalyst.

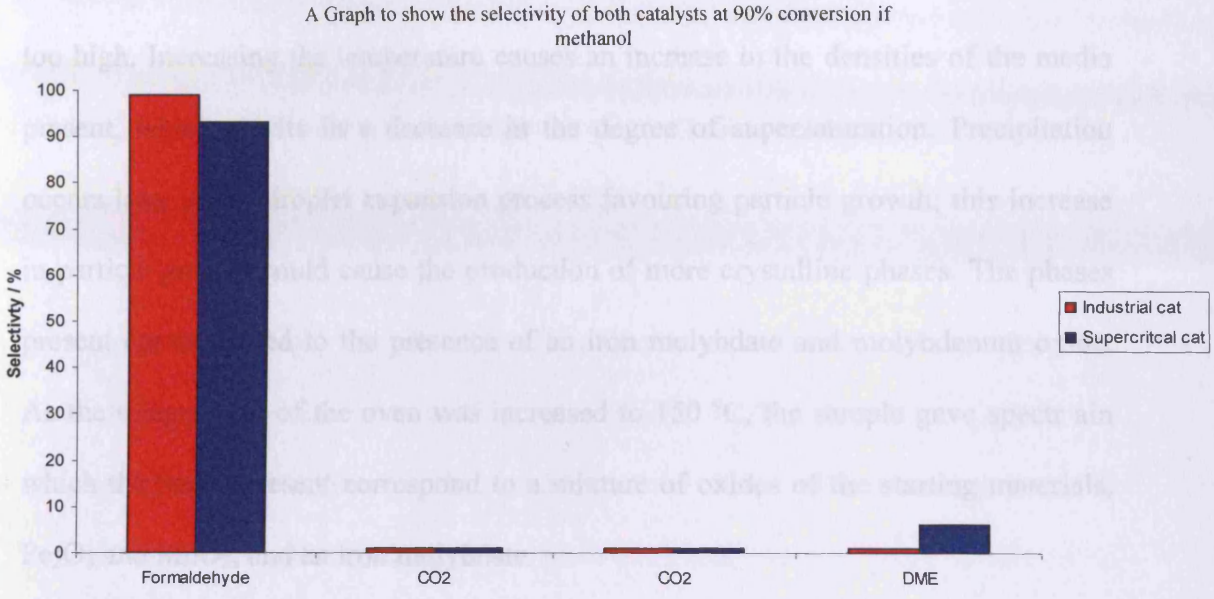

Figure 4.29 – Comparison of the iron molybdate prepared supercritically by bubbling air through the starting solution and a commercially available iron molybdate. The comparison was made at 90% conversion of methanol

4.4 Conclusions

Supercritical antisolvent precipitation has been utilised successfully to produce active iron molybdate catalysts for the selective oxidation of methanol to formaldehyde. The catalysts have been found to exhibit reasonable activity with high selectivity for formaldehyde. From the literature, this appears to be the first time a mixed oxide catalyst has been successfully prepared using the SAS process.

In view of the previous work done by other research groups [4-7], as well as our own [13] performed in this thesis, the initial preparation of an iron molybdate catalyst was performed using pure DMSO as the solvent. The iron molybdate precursors produced from the supercritical process were amorphous at low reaction temperatures. As the temperature of the process was increased the precursors produced become much more crystalline. This was suggested to be due to the fact that the reaction temperature was

too high. Increasing the temperature causes an increase in the densities of the media present, which results in a decrease in the degree of supersaturation. Precipitation occurs later in the droplet expansion process favouring particle growth; this increase in particle growth could cause the production of more crystalline phases. The phases present corresponded to the presence of an iron molybdate and molybdenum oxide. As the temperature of the oven was increased to 150 °C, the sample gave spectr ain which the bands present correspond to a mixture of oxides of the starting materials, Fe_2O_3 and MoO_3, and an iron molybdate.

Post calcined the iron molybdate catalysts were crystalline, even under different process conditions. The phases present in the diffraction patterns obtained for the catalysts corresponded to an iron molybdate and molybdenum oxide. Calcination of the precursors resulted in an increase in the surface area of the catalysts. The increase in surface area of the calcined material was attributed to the fact that this was a true measurement of the surface area, compared to surface area measurements performed on the precursor. The material was light and mobile and could have potentially been drawn into the machine when under vacuum.

The activity of the catalyst for the selective oxidation of methanol was determined using a continuous flow reactor. From the results obtained the production of an iron molybdate using the SAS process was a success. Generally, increasing the reaction temperature resulted in an increase in the conversion of methanol, reaching a maximum of 56 % conversion at 280 °C. The selectivity of the reaction to formaldehyde increased with increasing reaction temperature reaching a maximum of 90 % selectivity at 220 °C.

Hydrogen peroxide was added to the starting solution before processing in the supercritical reactor. This was done in varying concentrations, 0.25 and 0.5 vol %, to observe the effect this has on the precursor obtained from the reaction. The addition of hydrogen peroxide had no effect on the structure of the precursor; precipitation yielded an amorphous precursor. This was attributed to the fact that the addition of hydrogen peroxide did not affect the solubility of the solvent with regards to the SCF, and the saturation and droplet expansion processes that occurred were similar in all cases. At 0.5 vol%, hydrogen peroxide, there appeared to be Fe_2O_3 present in the precursor. The presence of this phase as indicated in the Raman spectra suggested that the starting material, iron (II) acetate, had been oxidised to Fe_2O_3. From the results, it appeared that adding hydrogen peroxide to the starting solution is detrimental to the surface area of the obtained precursor.

After calcination the catalysts appeared to be very similar, the only difference being that the 0.5 vol. % H_2O_2 was found to contain Fe_2O_3. The presence of Fe_2O_3 suggested that the starting material, iron (II) acetate, has been oxidised to Fe_2O_3.

From the results obtained the addition of hydrogen peroxide to the starting solution caused a decrease in the activity of the catalyst. The conversion of methanol decreased from 56 % at 280 °C in the absence of H_2O_2 decreasing to 33 % when 0.25 vol. % H_2O_2 was added. By adding more hydrogen peroxide to the starting solution, the catalyst produced displayed a conversion of methanol that decreased further to 7% at 280 °C. The decrease in activity could be due to the fact that the addition of hydrogen peroxide oxidised some of the starting material present in the starting

solution. The oxidation of the starting material caused an increase in production of single oxides such as Fe_2O_3 and MoO_3. Fe_2O_3 is detrimental to the activity of iron molybdate and this could cause the decrease in the activity of the catalyst.

The use of hydrogen peroxide as an oxidant had detrimental effects to the surface area and the overall catalytic activity of the iron molybdate catalysts obtained from the supercritical process. Air was used as an alternative oxidant, and was bubbled through the starting solution prior to processing in the supercritical reactor

Passing air through the solution had no effect on the structure of the precursor. Amorphously structured precursors were obtained regardless if air was passed through the starting solution or not. In comparison to the precursors obtained when hydrogen peroxide was used, there was no evidence in the Raman spectra for Fe_2O_3. The absence of this phase suggested that passing air through the starting material does not react with individual components of the starting material

Upon calcination the phases present correspond to $Fe_2(MoO_3)_4$ and MoO_3. Passing air through the starting material, according to the XRD patterns obtained, had very little effect on the overall structure of the catalyst. The Raman spectra for both the precursor and catalyst were very similar. Therefore successful preoxidation had taken place. The phases detected by Raman in both the precursor and the catalyst corresponded to the presence of $Fe_2(MoO_3)_4$ and MoO_3..

The activity of the catalyst was much higher than the iron molybdates previously tested. The conversion of methanol increased with increasing reaction temperature,

reaching a maximum of 90 % conversion at 280 °C. The selectivity of the reaction to formaldehyde increased with increasing reaction temperature reaching a maximum of 92 % selectivity at 220 °C. By passing air through the starting solution, the catalyst obtained showed an overall improved activity. The main difference between this catalyst and the catalysts prepared previously was that the Raman spectra for the as-precipitated precursor and the catalyst were very similar. This implies that the phases present in the precursor are present in the final catalyst. Calcination has not dramatically changed the structure of the catalyst. The active phase $Fe_2(MoO_3)_4$ has been maintained to the final catalyst, which has resulted in an increase in activity. The surface area also increased upon calcination of the as-precipitated precursor. The increase in catalytic activity could be attributed to the increase in surface area. There is no evidence for the presence of Fe_2O_3, which is detrimental to the activity of the catalyst.

4.5 References

[1] P.F. Kerr, A.W. Thomas and A.M. Langer, *The Amer. Minerol.*, 1963, **48**, 14

[2] W.E. Farneth, C.J. Machiels, W.H. Cheng, U. Chowdhry, F. Hong, E.M. Mc Carron and A.W. Sleight, *Appl. Catal.*, 1986, **25**, 249

[3] G.D. Kolovertnov, G.K. Boreskov, V.A. Dzisko, B.I. Popov, D.V. Tarasova and G.C. Belugina, *J.. Catal.*, 1996, **6**, 343

[4] J. A. Darr and M. Poliakoff, *Chem. Rev.* 1999, **99** 495

[5] E. Reverchon, *J. Supercrit. Fluids*, 1999, **15**, 1

[6] E. Reverchon, G.D. Porta, S. Pace, A. Di Trolio, *Ind. Eng. Chem. Res*, 1998, **37** 952

[7] E. Reverchon, C. Celano, G.D. Porta, A. Di Trolio, and S. Pace, *Ital. Patent*,1997 No. SA 97A/10

[8] A.P.V. Soares, M.F. Portela and A. Kienneman, *Catal. Rev.*, 2005, **47**, 125

[9] M.R. Sun-Kou, S. Mendioroz, J.L.G. Fierro, J.M. Placios and A. Guerrero-Ruiz, *J. Mater. Sci.,* 1995, **30**, 496

[10] J. Arruano and S. Wanke, *J. Chem. Eng.*, 1975, **53**, 301

[11] F. Trifirò, S. Notarbartolo, and I. Pasquon, *J. Catal*, 1971, **22**, 324

[12] M. Bowker, R. Holroyd, A. Elliot, P. Morrall, A. Alouche, C. Entwistle and A. Toerncrona, *Catal. Lett.* 2002, **83**, 165

[13] Z.Tang, J.K. Edwards, J.K. Bartley, S.H. Taylor, A.F. Carley, A.A. Herzing, C.J. Kiely, G.J. Hutchings, *J. Catal.*, 2007, **249**, 208

5 Results and Discussion

Copper Manganese Oxides Prepared Using Supercritical Antisolvent Precipitation

5.2 Catalyst Preparation

The synthesis of the copper manganese catalysts was performed using the apparatus shown schematically in Chapter 3; the second supercritical reactor was used. A mixed solution of copper (II) acetate and manganese (II) acetate (1:2 ratio) in solvent (dimethylsulfoxide) was prepared.

A detailed description of the supercritical process can be found in chapter 3. The precipitate obtained from the reaction was collected by a Soxhlet thimble contained within the vessel, and then calcined at 300 ^{o}C in air for 2 h.

To investigate the influence of various reaction conditions on the structure and activity of the prepared catalysts, various solvents, pressures and temperatures were

explored. All of these as-prepared catalysts were characterised by the analysis with XRD, BET, FT-IR and in some cases SEM.

5.2.1 Materials

All of the materials were used as supplied. Table 1 lists the details on all these materials including solvents, metal salts and CO_2 gas.

Table 1 – Materials used during for the production of copper manganese oxides supercritically

Materials	Grade	Company
CO_2	SFC, 99.99%	BOC
Copper (II) acetate	ACS reagent, ≥ 98%	Sigma-Aldrich
Manganese (II) acetate	ACS reagent, ≥ 98%	Aldrich
Dimethylsulfoxide, DMSO	ACS reagent, ≥ 98%	Aldrich
Dimethylformamide, DMF	ACS reagent, ≥ 98%	Aldrich
Methanol	ACS reagent, ≥ 98%	Aldrich
Ethanol	ACS reagent, ≥ 98%	Aldrich

5.3 Results and Discussion

5.3.1 Using pure DMSO as solvent

As mentioned previously DMSO is a clean, low toxic and dipolar aprotic solvent. Many metal salts are soluble in DMSO, and DMSO is completely miscible with supercritical CO_2. DMSO has successfully been used by several research groups to

produce metal oxides [3-5]. The results showed well-defined nanoparticles of metal oxide precursors, obtained with high yield due to the excellent miscibility between DMSO and supercritical CO_2 as well as the good solubility with regard to metal acetates in DMSO.

In view of the previous work done by other research groups [3-5], as well as our own [2,5], the initial synthesis of copper manganese oxides was performed using pure DMSO as a solvent. Experiments were conducted for about 2 hours, which results in the synthesis of approximately 1.0 g of solid; the density of this solid was very low and extreme care needed to be taken when collecting it from the precipitation vessel. The yield was calculated to be approximately 65-70 % based on the starting materials of copper (II) acetate and manganese (II) acetate.

5.3.1.1 Characterisation of the Precursor

The precursor obtained from supercritical antisolvent process was characterised by the analysis with XRD, BET, TEM and STEM.

The XRD pattern of the as-prepared precursor is shown in figure 5.1. The copper manganese precursor produced from the supercritical process is clearly amorphous. This agrees with results found in recent literature, in which amorphous [6-8] materials were produced when using the supercritical antisolvent process when using pure DMSO as a solvent. Due to the prompt precipitation induced by the rapid mix between $scCO_2$ and DMSO in supercritical process, it is easy to understand that the amorphous precursor can be obtained using this method.

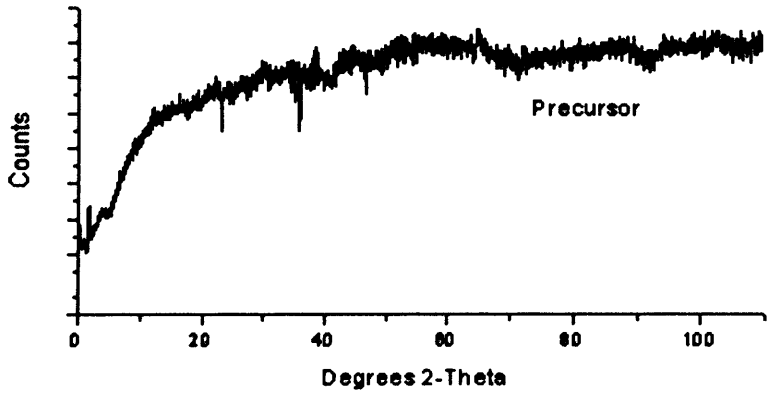

Figure 5.1 – Powder XRD diffraction pattern of the copper manganese oxide precursor obtained using DMSO as the solvent

The BET measurements are shown in Table 5.2. The surface areas of the as-precipitated precursors correspond to values found in the literature [2]. The notable difference between the as-precipitated precursor obtained from the supercritical process and from the coprecipitation reaction was their density; the density of the supercritical precursor was much lower. This was clearly seen upon opening of the lid to the precipitation vessel. Appropriate equipment had to be used as the precursor became extremely mobile under any movement e.g. removing the Soxhlet thimble

Table 5.2 – Surface area measurements of the copper manganese oxide catlsyst prepared using DMSO as the solvent

Sample	Surface Area / m^2g^{-1}	
	Initial Preparation Process	Repeat of Preparation Process
$CuMnO_x$ Precursor	114	117
$CuMnO_x$ cal 300 °C	46	60

5.3.1.2 Characterisation and Catalytic Activity of the as-calcined catalyst

The XRD pattern of the catalyst after calcination at 300 °C for 2 hours in air is shown in Figure 5.2. It can be seen that the as-calcined catalyst is not completely amorphous and there are some crystalline phases present that have developed upon calcination. The phases present in the diffraction pattern correspond to MnO_x. The diffraction pattern shows that there are no typical $CuMn_2O_4$ phases and only some MnO_x is observed.

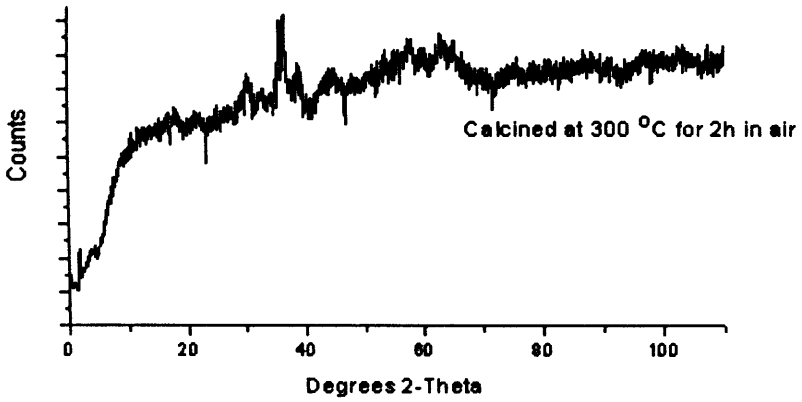

Figure 5.2 – Powder XRD pattern of the as-calcined copper manganese oxide prepared using DMSO as the solvent

The catalyst was tested for CO oxidation using a fixed–bed laboratory microreactor. CO was fed to the reactor at a controlled rate, 22.5 ml min^{-1}, and passed over 25 mg of catalyst at 25 °C. The products were analysed using on-line gas chromatography. The results obtained for the as-calcined catalysts are shown in Figure 5.3.

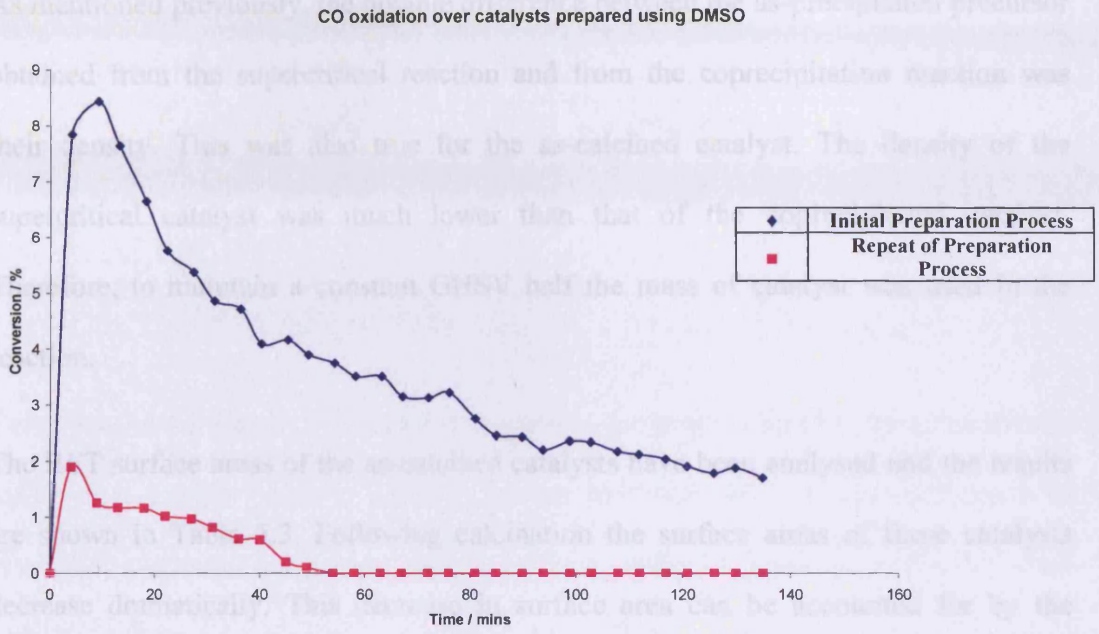

Figure 5.3 – Conversion of carbon monoxide over as-calcined copper manganese oxides prepared using DMSO as the solvent.

Using the conventionally prepared coprecipitation method for the preparation of copper manganese oxides, the expected conversion of CO to CO_2 is approximately 60 %. The activity of the catalyst then decreases with time online, to approximately 20 %. The supercritically prepared catalyst displays some activity for the oxidation of CO. However, the conversion for the supercritically prepared catalyst is significantly lower than that expected for copper manganese oxides. The catalyst obtained from the repeat of the process exhibited much lower catalytic activity for the conversion of CO. During this preparation there were issues with maintaining the pressure at 110 bar and blockages in the solution nozzle. The further decrease in activity of the catalyst obtained from the reaction could be attributed to the interruption to the supercritical conditions during the precipitation process.

As mentioned previously, the notable difference between the as-precipitated precursor obtained from the supercritical reaction and from the coprecipitation reaction was their density. This was also true for the as-calcined catalyst. The density of the supercritical catalyst was much lower than that of the coprecipitated catalyst. Therefore, to maintain a constant GHSV half the mass of catalyst was used in the reaction.

The BET surface areas of the as-calcined catalysts have been analysed and the results are shown in Table 5.3. Following calcination the surface areas of these catalysts decrease dramatically. This decrease in surface area can be accounted for by the formation of particles with high levels of aggregation that occur during the process of calcination at elevated temperatures. As a comparison, the surface areas of two other copper manganese oxides are listed in table 5.4; one is a commercial catalyst, the other is a copper manganese oxide prepared by conventional coprecipitation from a mixed solution of copper and manganese nitrate using sodium carbonate as the precipitating agent. Both these catalysts exhibit much higher surface areas than that of the catalyst produced from the supercritical process.

Table 5.3 – Surface area measurements of the as-precipitated and as-calcined supercritical copper manganese oxide

Sample	Surface Area / m^2g^{-1}	
	Initial Preparation Process	**Repeat of Preparation Process**
$CuMnO_x$ Precursor	40	117
$CuMnO_x$ cal 300 °C	46	60

Table 5.4 – Comparison of surface area measurements of the as-calcined supercritical copper manganese oxide, coprecipitated copper manganese oxide and the commercial copper manganese oxide

Sample	Surface Area / m^2g^{-1}
$scCuMnO_x$ cal 300 °C	46
Coprecipitated $CuMnO_x$	117
Commercial $CuMnO_x$	164

Using the second supercritical reactor resulted in the production of copper manganese oxides that exhibit catalytic activity for the oxidation of CO. The difference in density, could potentially mean that a catalyst could be produced with the same activity as that of a coprecipitated catalyst, yet half the amount of catalyst is required to reach said activity; the focus of this research is to produce a catalyst, where the overall activity compares to or is greater than that of a coprecipitated/commercially prepared hopcalite. Optimisation of the reaction would give an insight into the parameters that greatly affect the activity and those that do not. The subsequent research has been performed to optimise the reaction/reactor setup.

5.3.2 Varying Reaction Parameters

5.3.2.1 Catalysts prepared varying Temperature

The effect of temperature on the catalytic activity has been determined by keeping all other parameters, apart from temperature constant; the pressure of the system was maintained at 110 bar, the flow rates were 0.5 ml min^{-1}, and 15 l min^{-1} respectively for the solution flow rate and the CO_2 flow rate and the nozzle diameter used was 0.030".

The surface area measurements of the as-calcined catalysts are shown in table 5.

Table 5.5 – Surface area measurements of the as-calcined copper manganese oxides prepared by varying the temperature

Sample	Surface Area / m^2g^{-1}
$CuMnO_x$ cal 300 °C prepared at 35 °C	42
$CuMnO_x$ cal 300 °C prepared at 40 °C	48
$CuMnO_x$ cal 300 °C prepared at 50 °C	36
$CuMnO_x$ cal 300 °C prepared at 60 °C	29

The precursors were calcined at 300 °C for 2 h in air. The surface areas obtained for each of the catalysts are shown in Table 5.5. Generally, with increasing process temperature, there was a decrease in the surface area of the as-calcined catalysts. Therefore, increasing the process temperature had a detrimental effect on the surface area of the final catalyst.

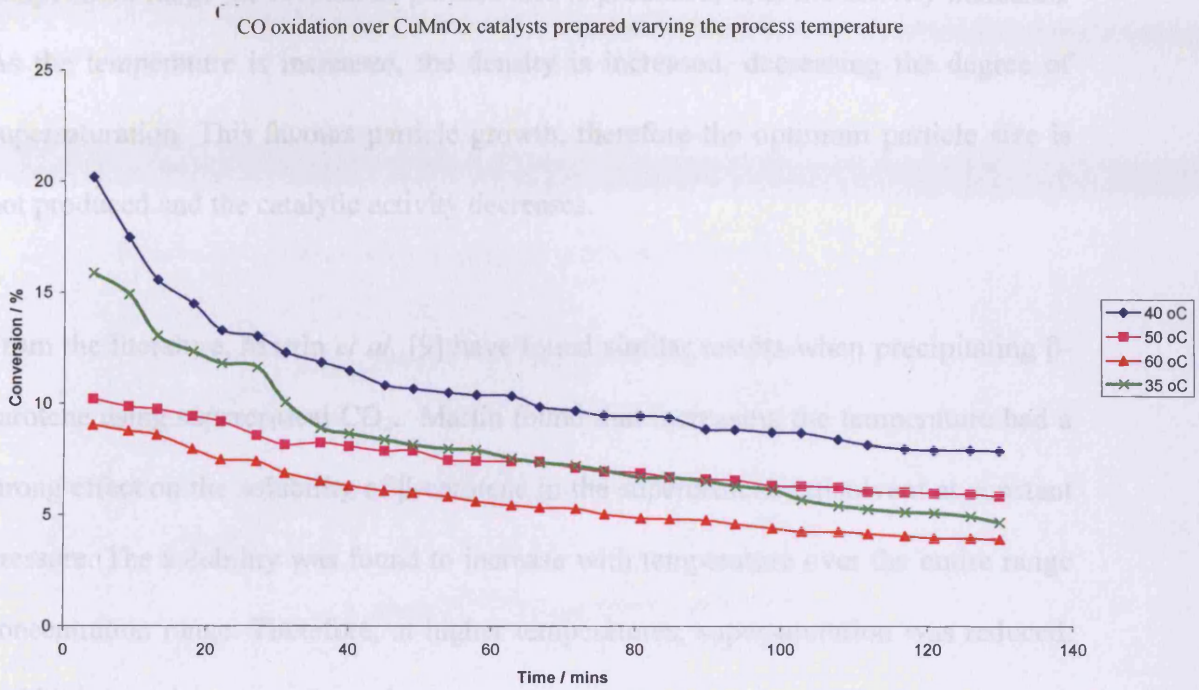

Figure 5.4 – CO oxidation over as-calcined copper manganese oxides prepared by varying temperature

The catalytic activity of the as-calcined catalysts is shown in figure 5.4. It was found that, generally, increasing process temperature lead to a decrease in activity. For the sample prepared at 40 °C there was 20 % conversion, whereas, increasing the process temperature to 60 °C caused the conversion to decrease to 9 % after 130 minutes time-on-line. However at 35 °C the conversion of the catalyst was 16 % initially, falling to 6 % after 130 minutes time-on-line. Therefore, between the process temperature range of 35 and 40 °C there is an increase in activity.

Perhaps this can be explained in terms of particle size; increasing particle size could result in a change in the surface area or alter the surface structure of the catalyst which in turn causes the activity of the catalyst to change. For the reaction there must be an optimum particle size which results in enhanced catalytic activity. Within this

temperature range the favourable particle size is produced, thus the activity increases. As the temperature is increased, the density is increased, decreasing the degree of supersaturation. This favours particle growth, therefore the optimum particle size is not produced and the catalytic activity decreases.

From the literature, Martin *et al.* [9] have found similar results when precipitating β-carotene using supercritical CO_2. Martin found that increasing the temperature had a strong effect on the solubility of β-carotene in the supercritical antisolvent at constant pressure. The solubility was found to increase with temperature over the entire range concentration range. Therefore, at higher temperatures, supersaturation was reduced, and bigger particles were formed.

5.3.2.2 Catalysts prepared varying Solvent

A number of different solvents were investigated to determine the effect solvent has on the activity of the catalyst. By changing the solvent used in the starting solution, this in turn changed the viscosity of the starting solution. The solvents used are listed below in table 5.6, with their respective viscosities:

Table 5.6 – Viscosities of Solvents Used

Solvent	Viscosity / cP
DMSO	1.996
DMF	0.92
Methanol	0.544

The preparation process was performed at 50 °C and 110 bar. The flow rates were 0.5 ml min^{-1}, and 15 l min^{-1} respectively for the solution flow rate and the CO_2 flow rate. The powder XRD patterns of the as-precipitated precursors are shown in figure 5.5.

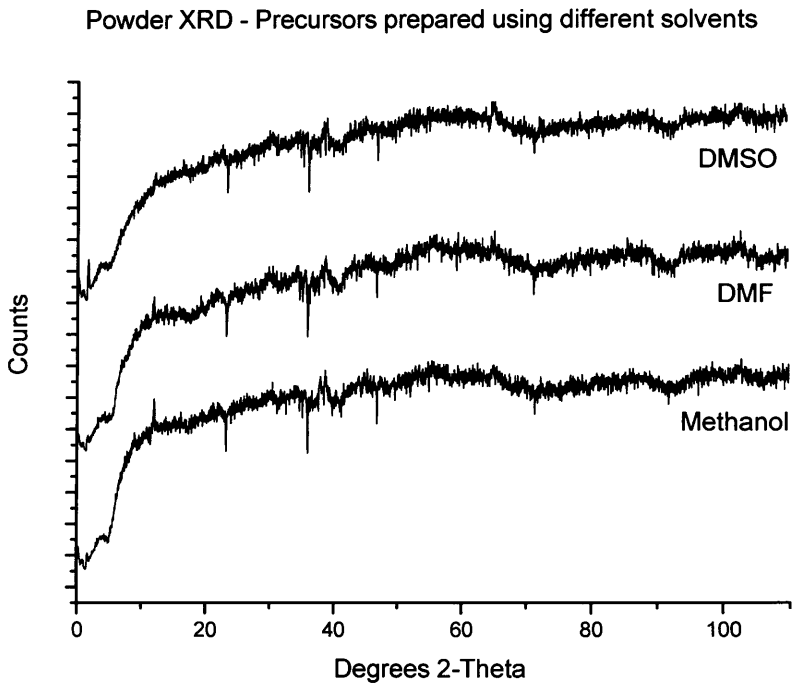

Figure 5.5 – Powder XRD patterns of the as-prepared precursors using different solvents

The XRD patterns obtained were very similar to one another; therefore, changing the solvent had very little effect on the structure of the precursor. The amorphous nature of the precursor was maintained independent of the solvent used. Surface area measurements were not performed on the precursors because they were light and mobile, and could have potentially been drawn into the instrument.

The precursors were calcined at 300 °C for 2 h in air. The surface areas obtained for each of the catalysts are shown in Table 5.7. From the results, the surface areas were

very similar. Therefore, changing the solution had no beneficial effect on the surface area of the final catalyst.

Table 5.7 – Surface area measurements of the as-calcined catalysts prepared using different solvents

Sample (all calcined at 300 °C for 2 h in air)	Surface Area / m^2g^{-1}
$CuMnO_x$ – DMSO	46
$CuMnO_x$ - DMF	38
$CuMnO_x$ – Methanol	42

Figure 5.6 shows the XRD patterns of the as-calcined catalysts. As with the as-precipitated precursors, there appears to be very little difference in the patterns obtained for the different solvents. From the characterisation data, changing the solvent and therefore, changing the viscosity of the solvent resulted in as-calcined catalysts with similar structural compositions. This suggests that the viscosity does not appear to be an important parameter in producing catalysts that are structurally different.

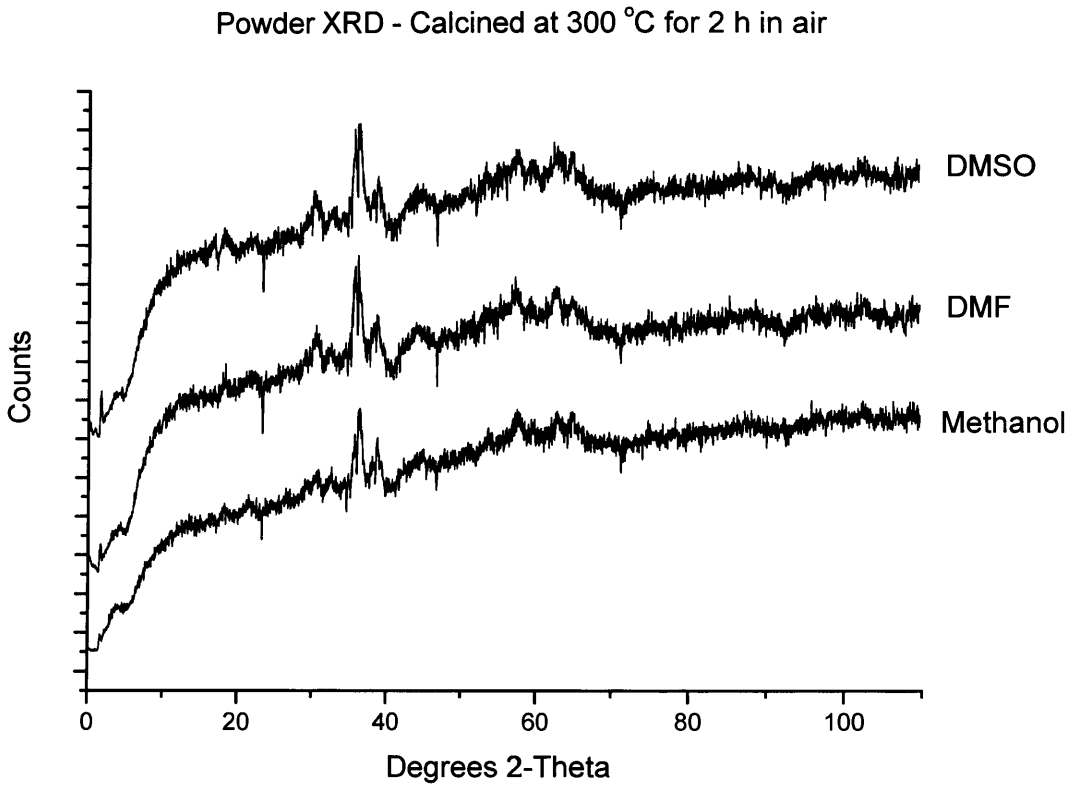

Figure 5.6 –Powder XRD patterns of the as-calcined catalysts prepared using different solvents

The catalytic data of the as-calcined catalysts are shown in Figure 5.7. For all catalysts tested, the general trend appears to be a high initial conversion of CO which decreases with time on line. The DMSO prepared catalyst exhibited the highest conversion of approximately 9 % decreasing to 2 % with time on line. However, the methanol prepared catalyst exhibited the lowest activity under reaction conditions; the initial conversion was 6 % decreasing to approximately 0.5 %.

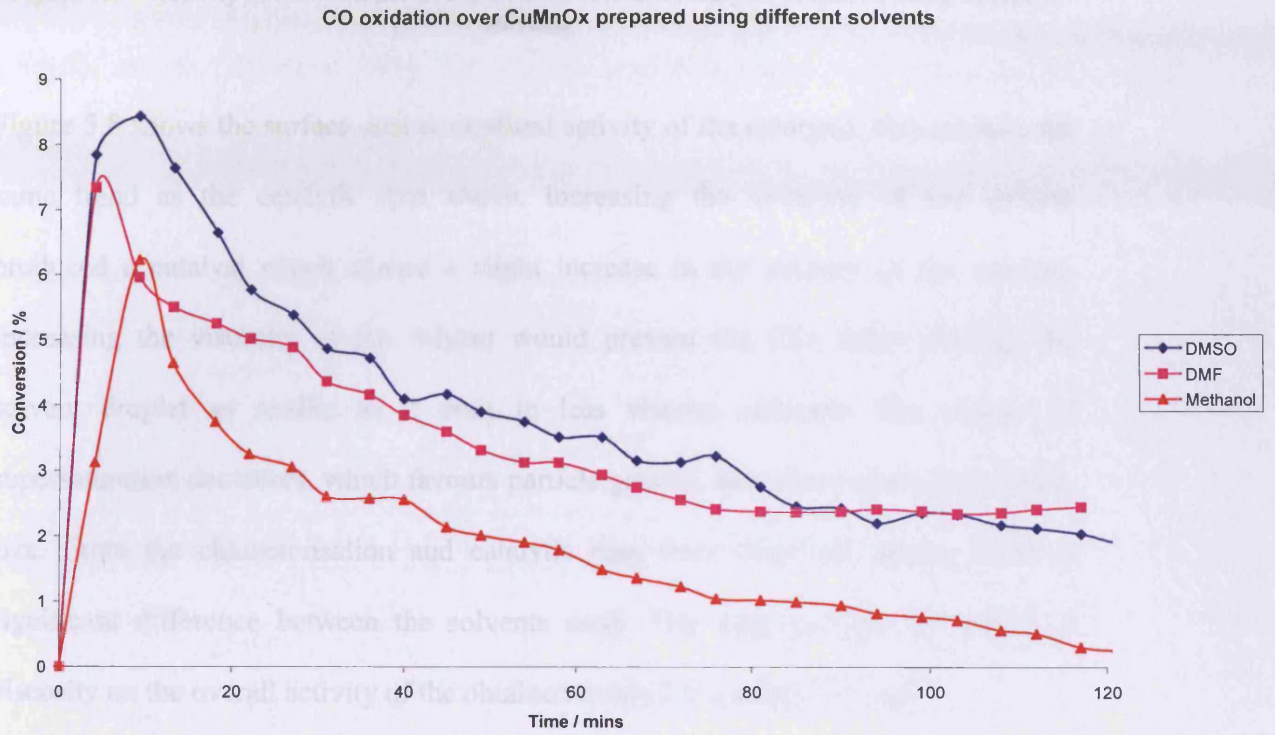

Figure 5.7 – CO conversion over as-calcined copper manganese oxides prepared using different solvents

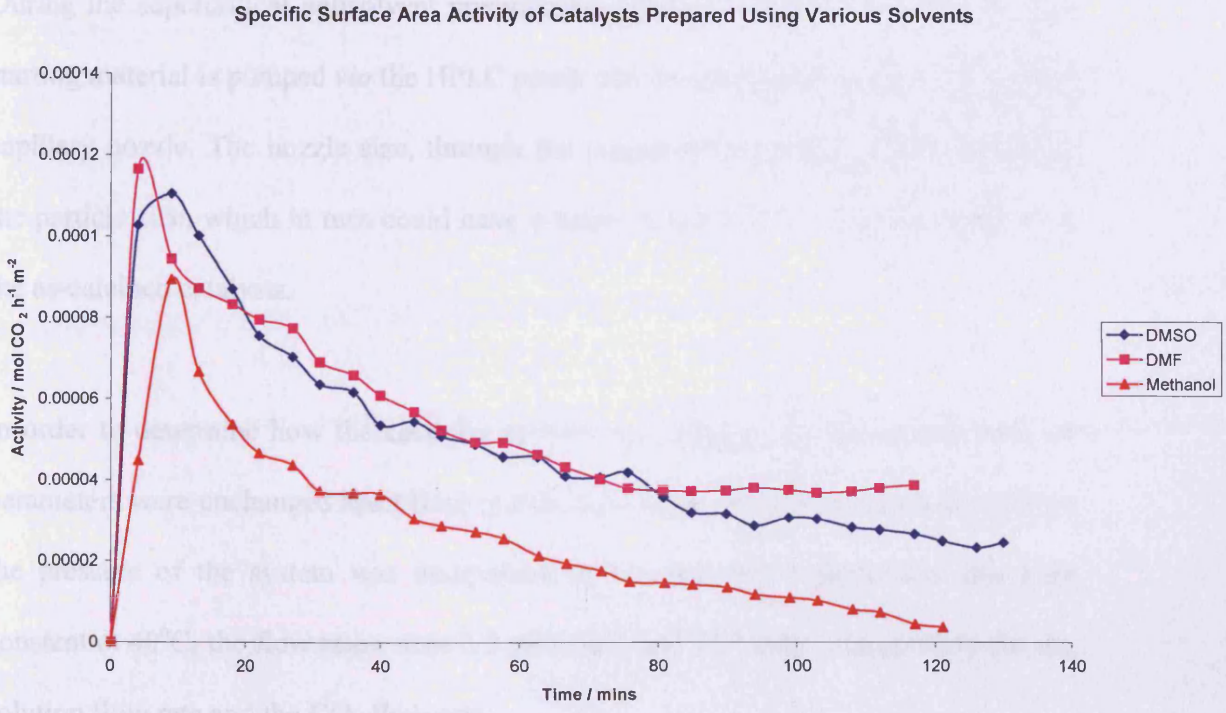

Figure 5.8 – Activity normalised per unit area of as-calcined catalysts prepared using different solvents

Figure 5.8 shows the surface area normalised activity of the catalysts, this exhibits the same trend as the catalytic data above. Increasing the viscosity of the solvent produced a catalyst which caused a slight increase in the activity of the catalyst. Increasing the viscosity of the solvent would prevent the CO_2 from entering the solvent droplet as readily as it does in less viscous solvents. The degree of supersaturation decreases, which favours particle growth, therefore increasing particle size. From the characterisation and catalytic data there does not appear to be a significant difference between the solvents used. This suggests that the affect of viscosity on the overall activity of the obtained catalyst is a negligible one.

5.3.2.3 Catalysts prepared varying Nozzle Size

During the supercritical antisolvent precipitation process, the solvent containing the starting material is pumped *via* the HPLC pump into the precipitation vessel through a capillary nozzle. The nozzle size, through the precipitation process, could influence the particle size, which in turn could have a major impact on the catalytic activity of the as-calcined catalysts.

In order to determine how the catalytic activity was affected by the nozzle size, all parameters were unchanged apart from nozzle size during the precipitation procedure; the pressure of the system was maintained at 110 bar, the temperature was kept constant at 40°C, the flow rates were 0.5 ml min^{-1}, and 15 l min^{-1} respectively for the solution flow rate and the CO_2 flow rate.

The surface area measurements for the as-calcined catalyst obtained from the different preparations are shown in table 5.8. As the nozzle diameter was increased the resulting samples show a decrease in surface area. The smallest nozzle size gave rise to the largest surface area

Table 5.8 – Surface area measurements of the as-calcined catalysts obtained by varying the nozzle size

Nozzle Size	Surface Area / m^2g^{-1}
0.005"	36
0.010"	32
0.030"	10
0.040"	5

The powder XRD patterns obtained on the as-calcined catalyst are shown in figure 9. From the patterns obtained it appears that changing the nozzle size does not affect the overall structure of the catalysts obtained.

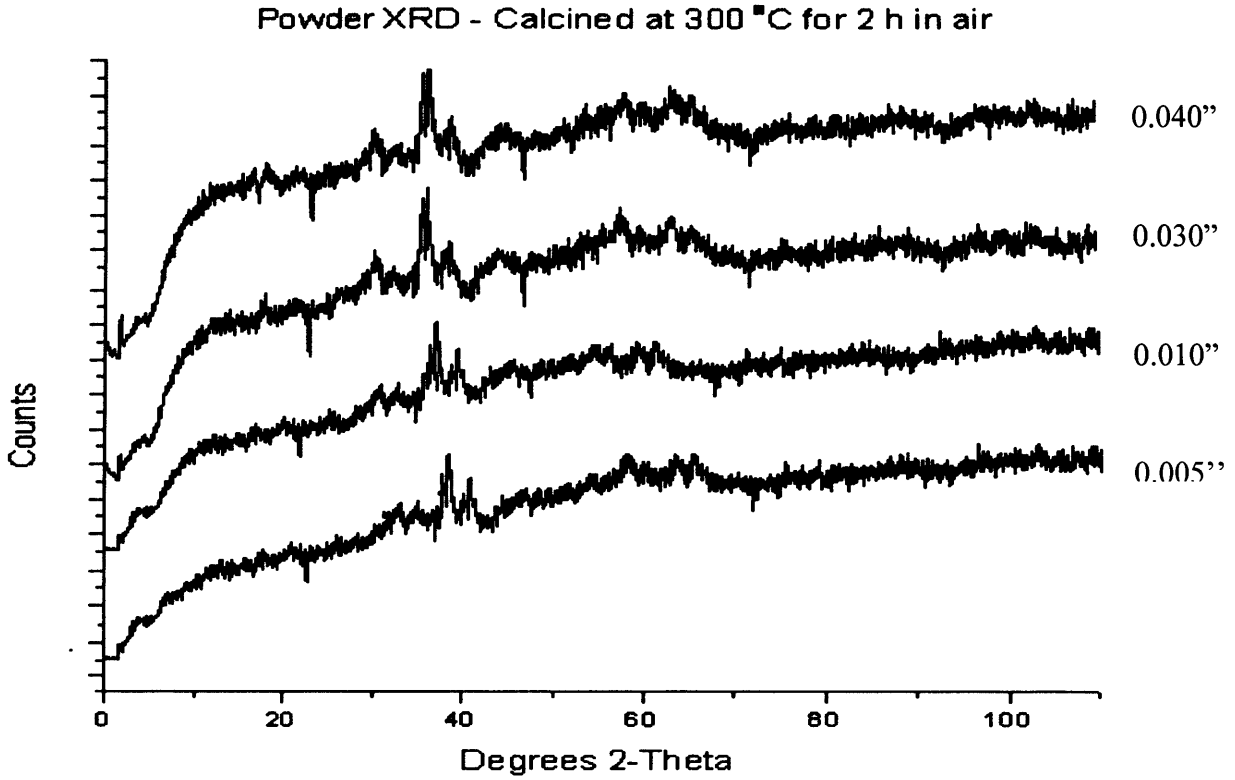

Figure 5.9 –Powder XRD patterns of the as-calcined catalysts prepared using different nozzle sizes

The catalytic data obtained is shown in Figure 5.11. The general trend observed was similar to that of the surface area; with increasing nozzle diameter the catalytic activity increased. However, there appears to be an optimum nozzle size for higher catalytic activity, as increasing the nozzle past 0.03" resulted in a decrease in the activity, from 20% to 13%. The initial conversion of each of the nozzle sizes are shown in Figure 5.10. In terms of process optimisation, the nozzle size could influence the particle formation, which in turn affects the overall catalytic activity.

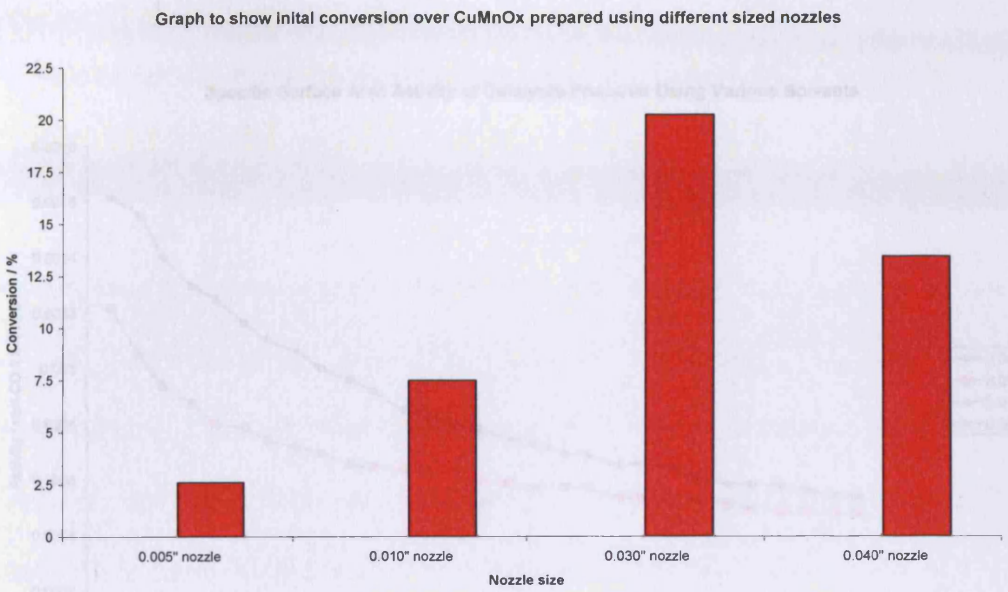

Figure 5.10 – Initial conversion over copper manganese oxide preared using different nozzle sizes

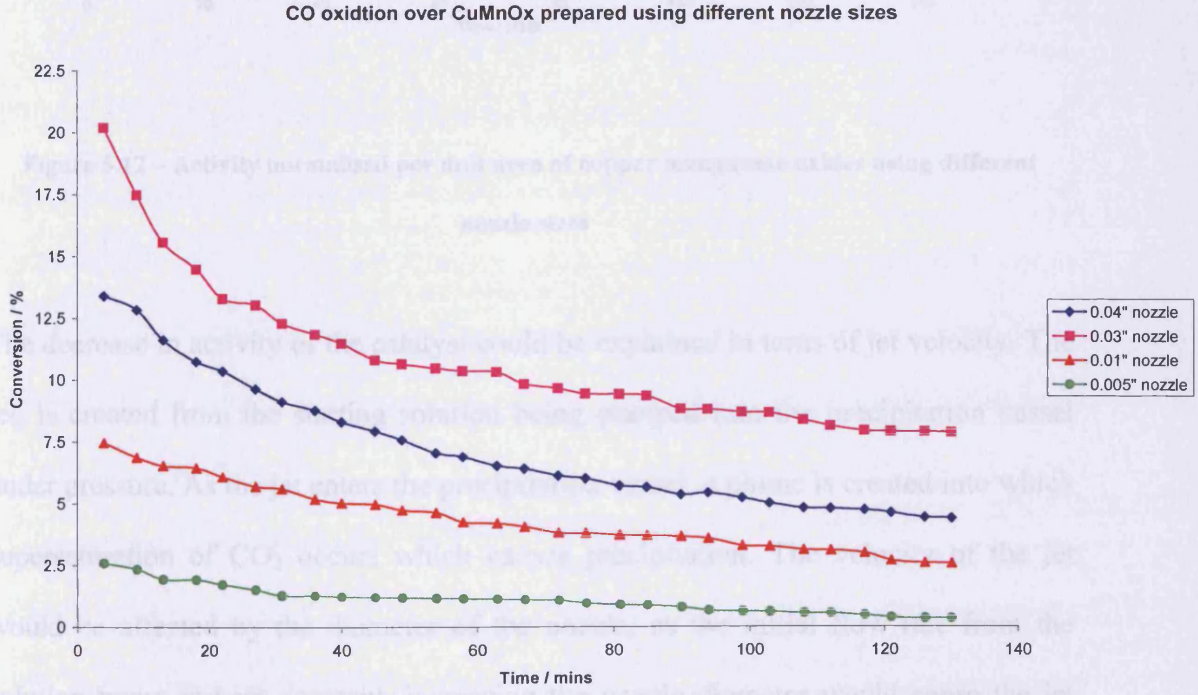

Figure 5.11 – CO oxidation over copper manganese oxide prepared using different nozzle sizes

The activity normalised per unit area of the catalysts is shown in figure 5.12. Correcting for the surface area shows the same trend as mentioned previously; decreasing nozzle diameter is detrimental to the initial activity of the catalyst.

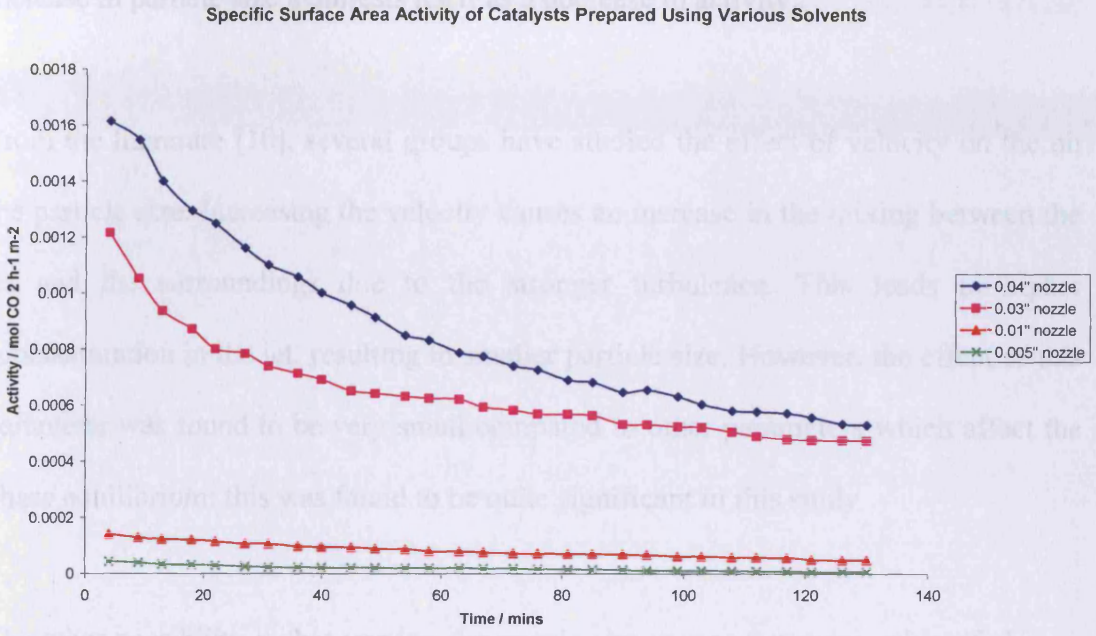

Figure 5.12 – Activity normalised per unit area of copper manganese oxides using different nozzle sizes

The decrease in activity of the catalyst could be explained in terns of jet velocity. The jet, is created from the starting solution being pumped into the precipitation vessel under pressure. As the jet enters the precipitation vessel, a plume is created into which supersaturation of CO_2 occurs which causes precipitation. The velocity of the jet would be affected by the diameter of the nozzle, as the initial flow rate from the solution pump is kept constant, increasing the nozzle diameter would cause the jet velocity to decrease. The same volume of solution is being pumped through a larger hole. The decrease in velocity means a decrease in turbulent mixing that occurs between the solvent and the SCF. The supercritical antisolvent process relies heavily on the fact that it is a rapid process which produces very small particles, therefore, if

the process is slow, particle growth is favoured and the particle size increases. An increase in particle size manifests itself as a decrease in activity.

From the literature [10], several groups have studied the effect of velocity on the on the particle size. Increasing the velocity causes an increase in the mixing between the jet and the surroundings due to the stronger turbulence. This leads to higher supersaturation in the jet, resulting in smaller particle size. However, the effect of this parameter was found to be very small compared to other parameters which affect the phase equilibrium; this was found to be quite significant in this study

The other possibility is that varying the nozzle size causes the segregation of phases, which in turn causes a decrease in the activity of the catalyst. Decreasing the nozzle size would cause an increase in the velocity of the jet, which would cause supersaturation of the droplet to become much quicker, causing the particle size to decrease. This may allow individual components of the starting mixture to precipitate preferentially and phase separation to occur; single oxide phases are produced instead of a mixed oxide phase.

TEM images of the as-calcined catalysts have been obtained for the different nozzle sizes. These were performed by Liverpool University using a scanning transmission electron microscope (STEM).

Figure 5.13 shows the STEM image obtained from the 0.03" nozzle the sample. It appears to be composed of an interlinking branch like material, where the branching seems to be made up of rod and sphere-type crystals.

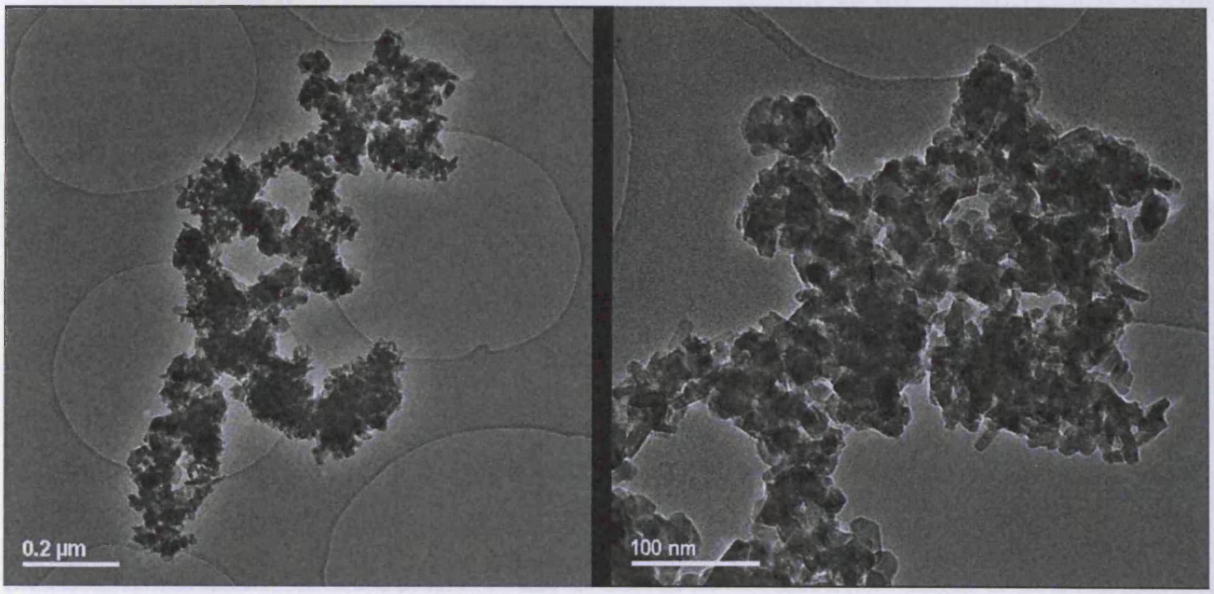

Figure 5.13– STEM Image of the as-calcined catalyst using the 0.030" nozzle

STEM mapping was used to determine the copper and manganese distribution of the catalyst. The images below show that the copper is not homogeneously dispersed throughout the catalyst, compared to the manganese regions, as shown below in figure 5.14. (The colouring of the maps are by intensity of the element, blue being low, green being middle and red being high).

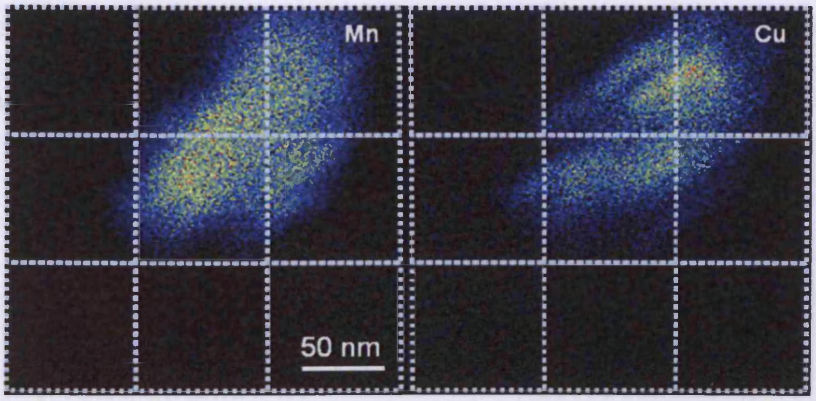

Figure 5.14 – STEM mapping of the as-calcined copper manganese oxide prepared using the 0.030" nozzle

Despite some of the maps showing Cu rich and Mn rich areas, the majority of the maps obtained from the catalyst showed uniform dispersion of copper and manganese regions throughout the catalyst; this is shown in figure 5.15.

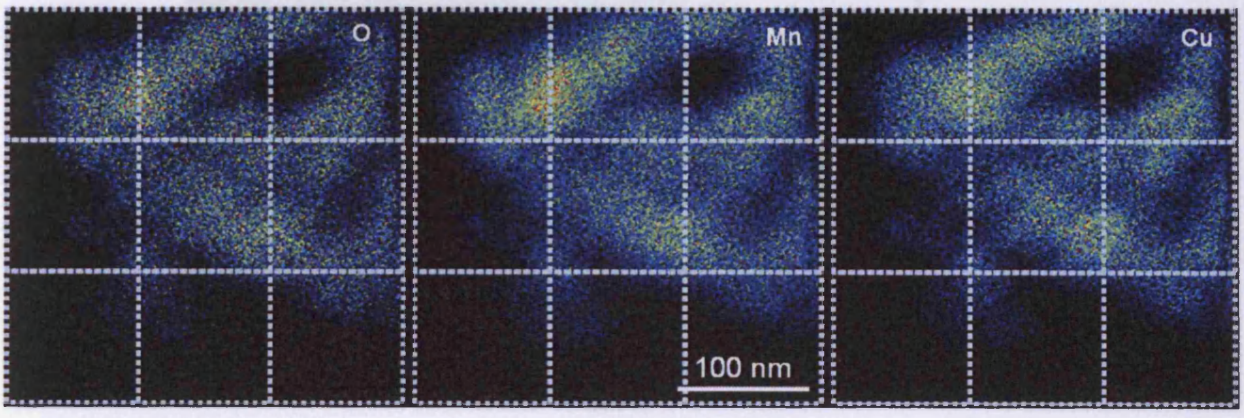

Figure 5.15 – Further STEM mapping of the as-calcined copper manganese oxide prepared using the 0.030" nozzle

Figure 5.16 shows elemental mapped images of the as-calcined catalysts. The images show that each element is well dispersed throughout the catalyst. However, from the images it appears that there are some dense regions of copper in the catalyst. Using the 0.03" nozzle resulted in the production of a catalyst that exhibited the highest catalytic activity. This could be due to the fact that there are two types of copper on the surface of the catalyst; copper well dispersed throughout the structure of the catalyst, and dense, island like regions of copper.

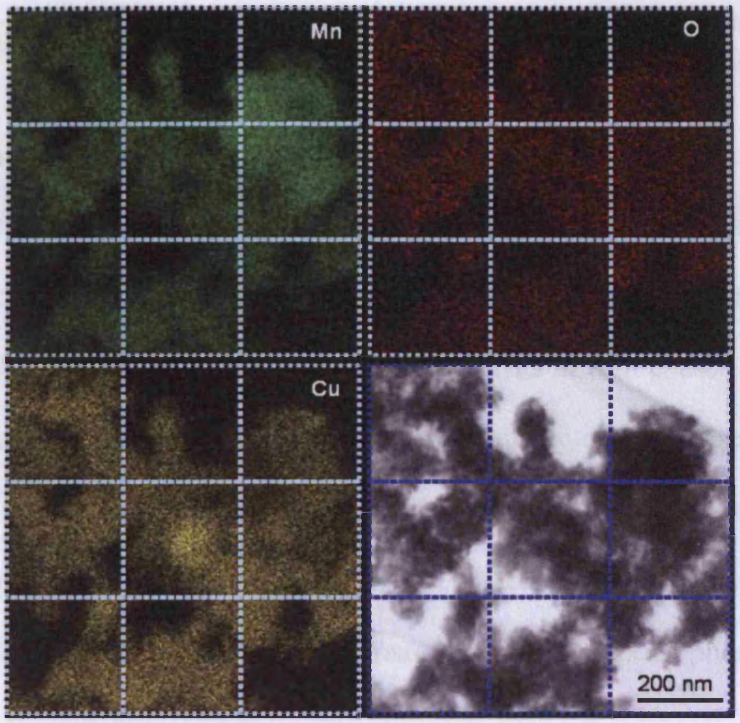

Figure 5.16– Elemental mapping of the as-calcined copper manganese oxide prepared using the 0.030" nozzle

As can be seen from the catalytic data in figure 5.11, the smaller nozzle leads to the production of a catalyst with decreased catalytic activity. For the 0.01" nozzle the morphology is similar to the as-cal;cined catalyst obtained from different nozzle sizes. The structure is still composed of rod and sphere-type crystals. The degree of separation between the copper and manganese areas becomes more prevalent; this is shown in figure 5.17. The two spectra show the difference in the manganese rich and copper rich areas.

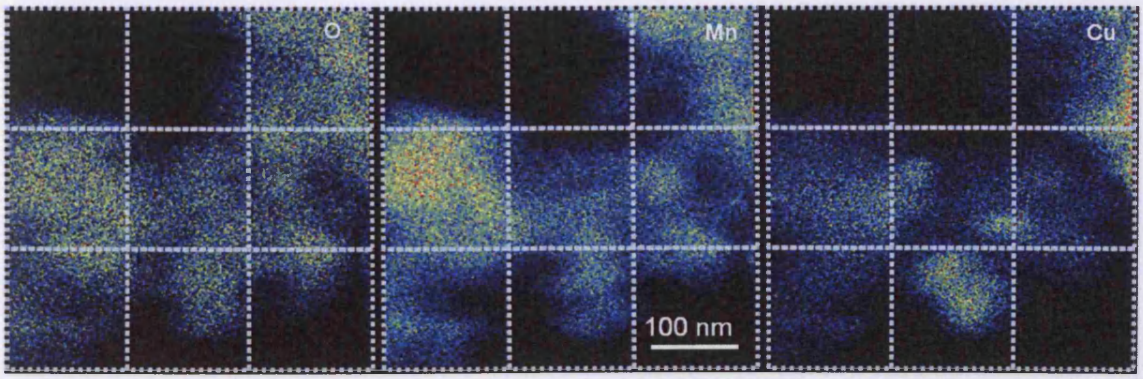

Figure 5.17 – STEM mapping of the as-calcined copper manganese oxide prepared using the 0.010" nozzle

Using the smaller nozzle size has caused a decrease in the activity of the catalyst obtained, with the STEM images showing that there is a greater degree of separation between the copper and manganese. In terms of the process, the smaller the nozzle size, the smaller the droplet that is formed from it. This in turn causes an increase in the rate of supersaturation of CO_2 into the droplet causing and increase in the rate of precipitation, causing the particle size to decrease. This may allow individual components of the starting mixture to precipitate preferentially and phase separation to occur; single oxide phases are produced instead of a mixed oxide phase.

When the nozzle was changed to 0.04'' diameter, there were uniform areas of copper and manganese as well as Cu rich and Mn rich areas. The images are shown in figure 5.18. The general trend observed for the activity of the catalysts was with increasing nozzle size there was an increase in activity. This was true for all nozzle sizes apart from the 0.04" nozzle.

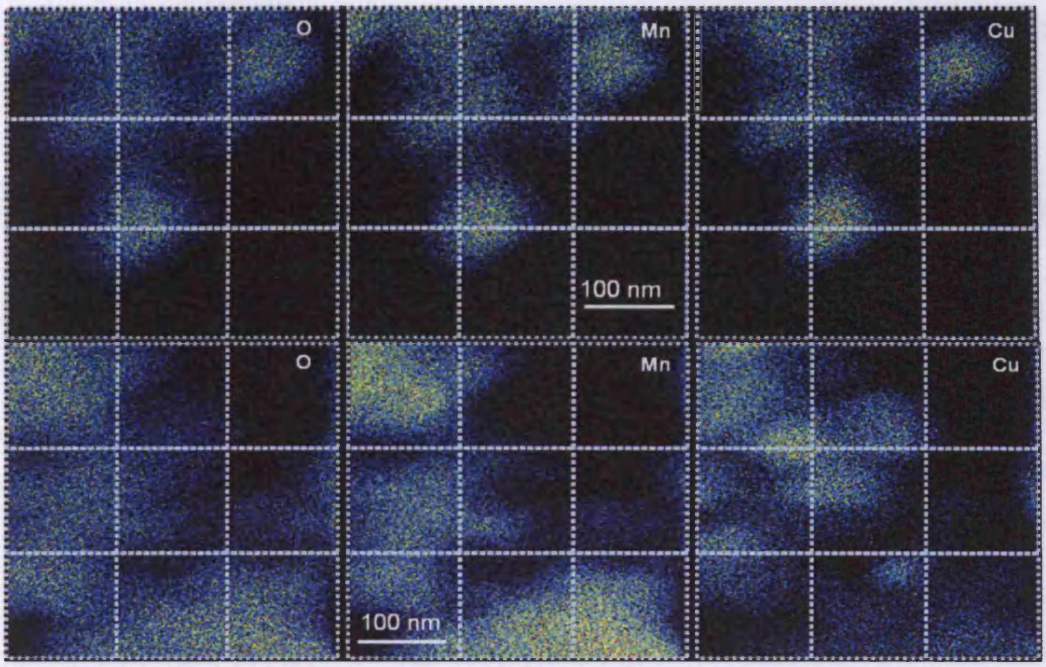

Figure 5.18 – STEM mapping of the as-calcined copper manganese oxide prepared using the 0.040" nozzle

The decrease in catalytic activity could be due to the fact that the nozzle size is too large. The resulting droplet formed is larger which could cause the rate of supersaturation to decrease. This would result in a decrease in the rate of precipitation causing the particle size to increase; which in turn could prevent interaction resulting in cluster formation.

However, normalising for surface area, as shown in figure 5.12, exhibits the general trend of increasing the nozzle size leads to an increase the specific surface area activity of the catalyst. As can be seen from the surface area measurements, increasing nozzle size leads to a decrease in the surface area. Therefore, from the results obtained there appears to be an optimum nozzle size, which allows the production of the

optimum particle size, resulting in favourable surface area of the catalyst leading to enhanced catalytic properties.

5.3.2.4 Catalysts prepared varying the solution flow rate

During the supercritical antisolvent precipitation process, the solvent containing the starting material is pumped *via* the HPLC pump into the precipitation vessel through a capillary nozzle. The flow rate of the solution through the nozzle could influence the particle size, which in turn could have a major impact on the catalytic activity of the as-calcined catalysts.

In order to determine how the catalytic activity was affected by the solution flow rate, all parameters were unchanged apart from the flow rate during the precipitation procedure; the pressure of the system was maintained at 110 bar, the temperature was kept constant at 40 °C, and the 0.03" nozzle was used. The CO_2 flow rate was maintained at 15 l min^{-1}

The surface areas of the as-calcined catalysts are shown in table 5.9. The general trend observed is that with increasing flow rate, resulted in an increase in surface area of the catalyst obtained. This was true for all solution flow rates measured.

Table 5.9 – Surface area measurements of the as-calcined catalysts obtained by varying the nozzle size

Solution flow rate	Surface Area / m^2g^{-1}
0.5 ml min^{-1}	10
1.0 ml min^{-1}	25
2.0 ml min^{-1}	39

The powder XRD patterns obtained on the as-calcined catalyst are shown in figure 5.19. The patterns obtained for the samples obtained by varying the flow rate all appear very similar. Therefore, changing the solution flow rate does not seem to affect the final structure of the catalyst obtained.

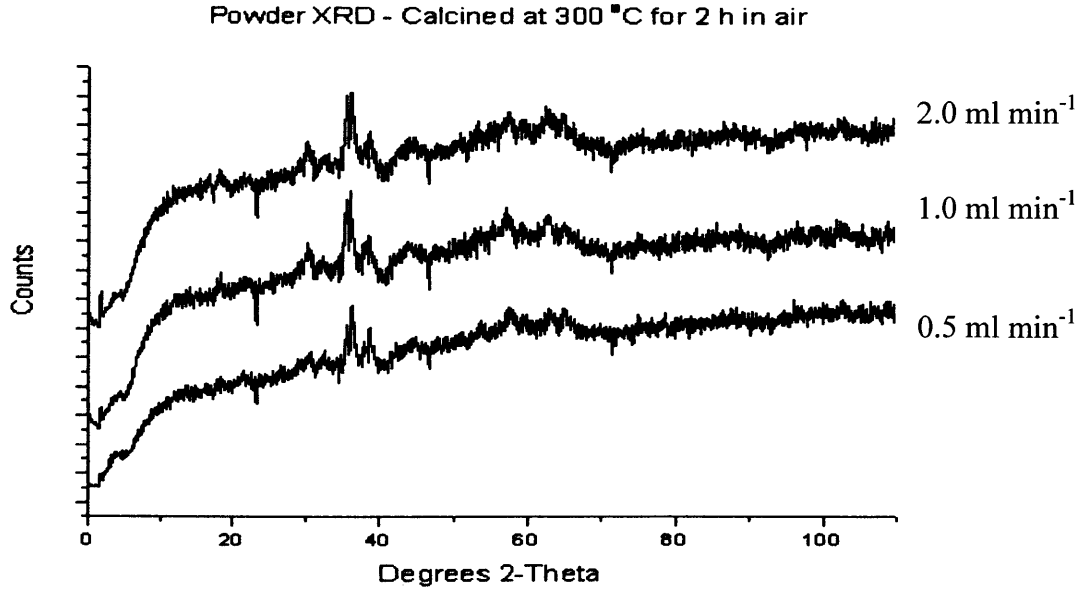

Figure 5.19 –Powder XRD patterns of the as-calcined catalysts prepared using different flow rates

The catalytic activity of the as-calcined catalysts is shown in figure 5.20. The conversion was a maximum of 20% initially with the 0.5 ml min^{-1} compared to 14% for the 2.0 ml min^{-1} flow rate whioch decreased with time on-line.

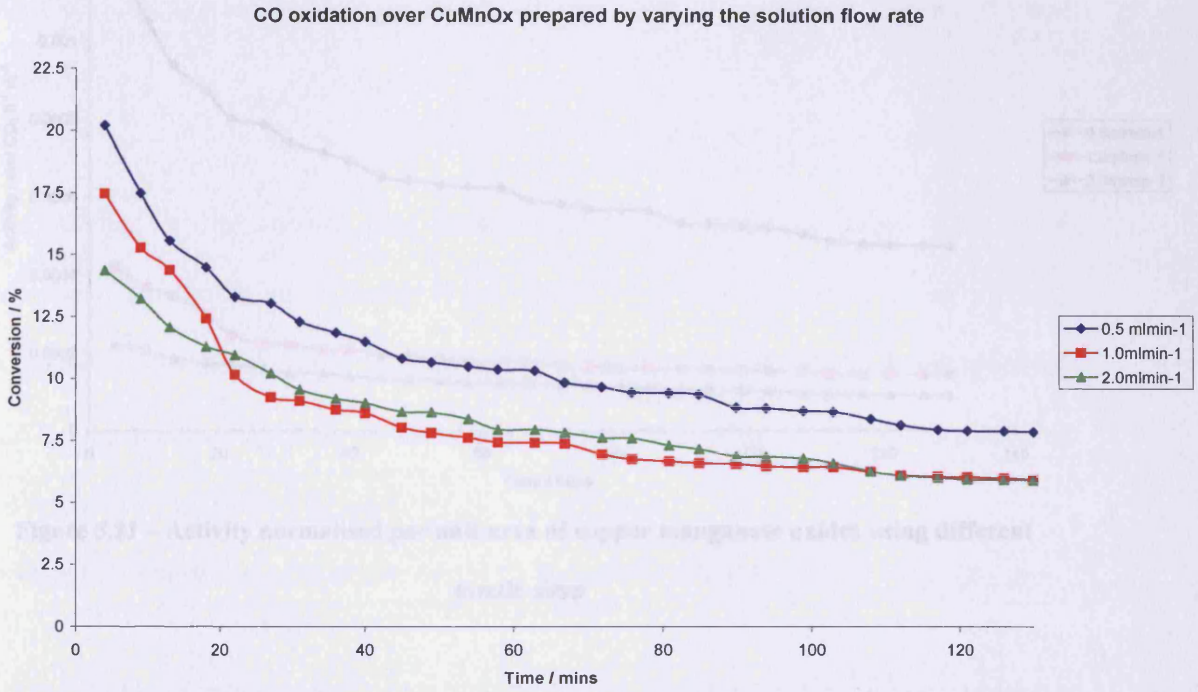

Figure 5.20 – CO oxidation over copper manganese oxide prepared varying the solution flow rate

The activity normalised per unit area is shown in figure 5.21. Increasing the solution flow rate had a detrimental effect on the activity of the catalyst. With increasing flow rate, the velocity of the solution through the nozzle increases, therefore the jet velocity increases. As the jet enters the precipitation vessel, the supersaturation is rapid causing precipitation. As the velocity of the jet has increased, the resulting precipitation would produce smaller particles. The decrease in activity could be the result in the production of smaller particles where the efficiency of the production of the active phase has decreased.

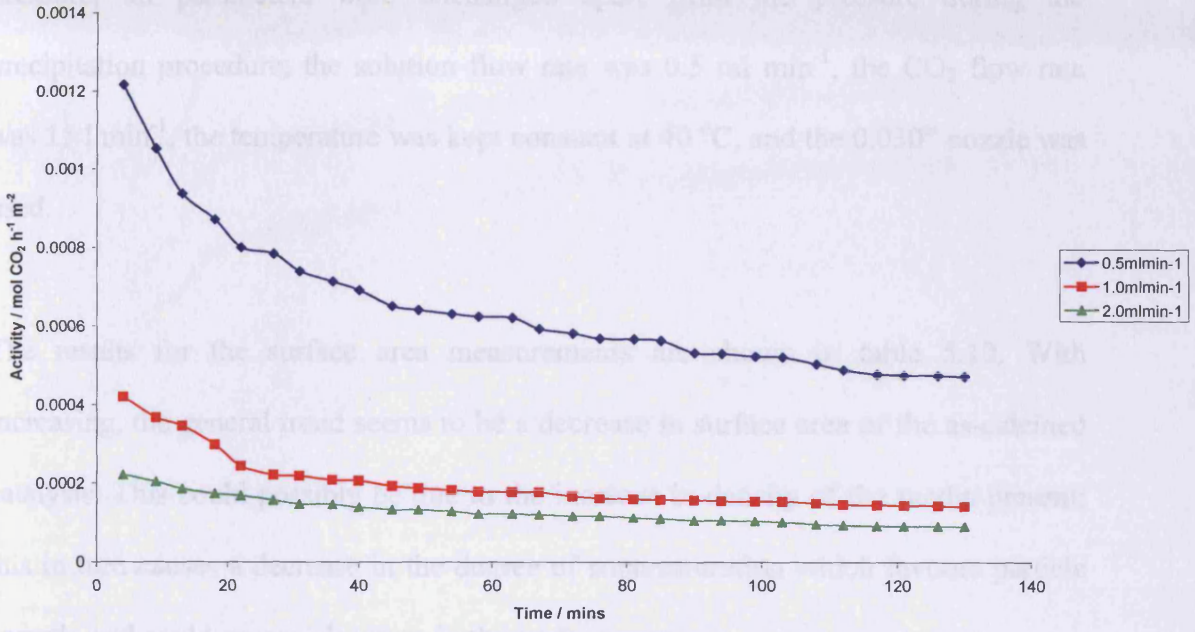

Figure 5.21 – Activity normalised per unit area of copper manganese oxides using different nozzle sizes

From the literature, [10] the effect of increasing the solution flow rate had no noticeable effect on the size and yield of the crystals obtained. Increasing the solution flow increases the mixing between the jet and the surroundings due to the stronger turbulence. This leads to higher supersaturation in the jet. However, the effect of this parameter was found to be very small compared to other parameters. It was concluded that the solution flow rate does not have a significant effect on the yield or the particle size.

5.3.2.5 Catalysts prepared varying the pressure

To determine how the activity of the obtained catalyst was affected by the process pressure, all parameters were unchanged apart from the pressure during the precipitation procedure; the solution flow rate was 0.5 ml min^{-1}, the CO_2 flow rate was 15 l min^{-1}, the temperature was kept constant at 40 °C, and the 0.030" nozzle was used.

The results for the surface area measurements are shown in table 5.10. With increasing, the general trend seems to be a decrease in surface area of the as-calcined catalysts. This could possibly be due to the increase in density of the media present; this in turn causes a decrease in the degree of supersaturation which favours particle growth, and could cause a decrease in the surface area.

Table 5.10 – Surface area measurements of the as-calcined catalysts obtained by varying the process pressure

Pressure / bar	Surface Area / m^2g^{-1}
90	38
110	32
130	29

The powder XRD patterns obtained on the as-calcined catalyst are shown in figure 5.22. The patterns obtained for the samples obtained by varying the pressure all appear very similar. Therefore, changing the pressure did not seem to have a major effect on the final structure obtained.

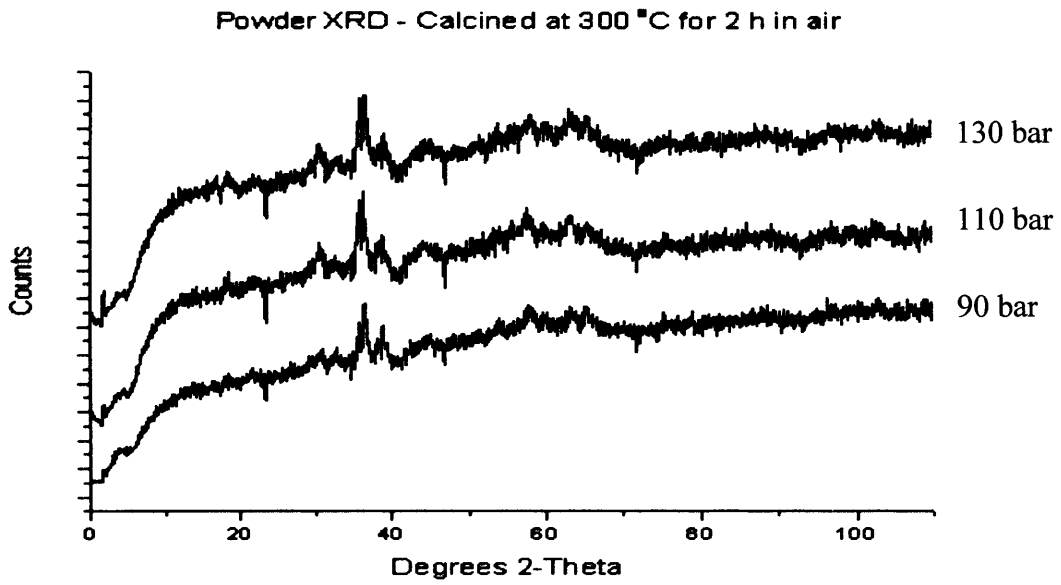

Figure 5.22 –Powder XRD patterns of the as-calcined catalysts prepared varying the process pressure

The catalytic data of the as-calcined catalysts are shown in figure 5.23. With increasing pressure during preparation the catalytic activity of the obtained catalyst increases. Increasing the pressure of the system during preparation, causes an increase in the densities of the media presents. This in turn decreases the degree of supersaturation, which in turn favours particle growth. However, the pressure range and solvent system used needs to be considered in detail, as different solvent systems expand in CO_2 over different pressure ranges; if the solvent expands in the pressure range, degree of supersaturation increases, favouring nucleation, resulting in smaller particles. More research is required to elucidate the effect of solvent system and pressure range on particle size and activity; this was not performed during this research but is any area of work that requires more investigation.

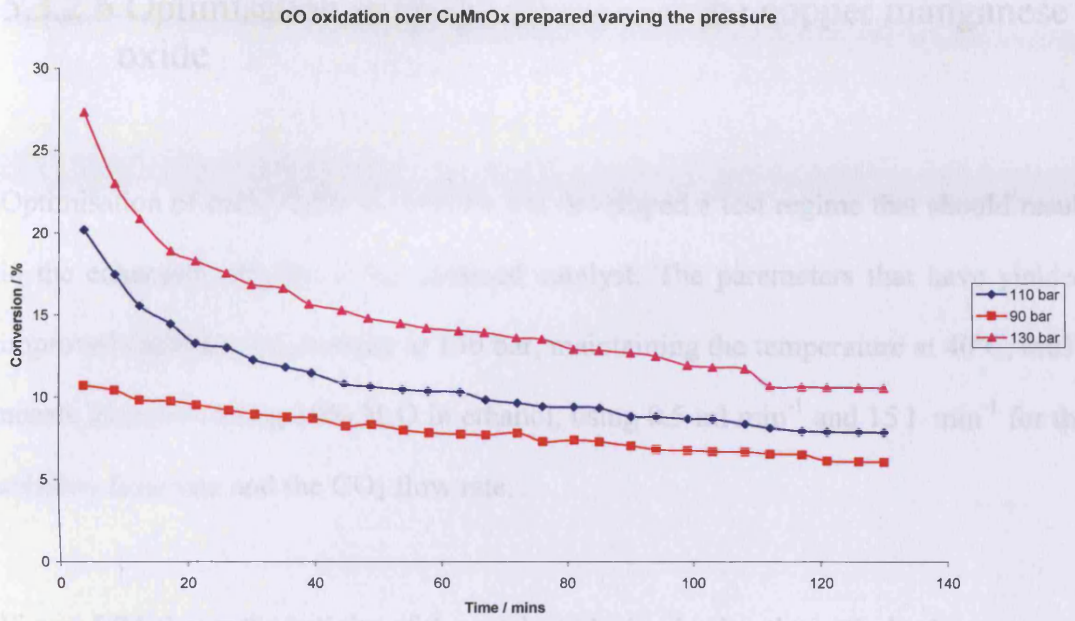

Figure 5.23 – CO oxidation over copper manganese oxide prepared varying the pressure

During the liquid batch processing the rate of pressure increase is the most relevant parameter in controlling particles size and morphology [11]. However, for gas batch and continuous operation contradictory results have been obtained by several authors [12-20]. From the results found within this research increasing the pressure resulted in an increased activity of the catalyst produced from the SAS process. From the literature, it appears that the effect of pressure on the particle size is complex, and contradictory results have been found. The effect of pressure is dependent on the solvent system used and the pressure range the reactions are performed in. Further research is required to elucidate this problem fully.

5.3.2.6 Optimisation in the production of the copper manganese oxide

Optimisation of each of the parameters has developed a test regime that should result in the enhanced activity of the obtained catalyst. The parameters that have yielded improved catalysts are pressure at 130 bar, maintaining the temperature at 40°C, 0.03" nozzle diameter, using 10% H_2O in ethanol, using 0.5 ml min^{-1} and 15 l min^{-1} for the solution flow rate and the CO_2 flow rate.

Figure 5.24 shows the activity of the catalyst obtained using the optimised parameters. The conversion of the catalyst increased from a maximum of 20% in the previous processes to 42% conversion. This shows that it is possible to produce a highly active hopcalite catalyst using the supercritical antisolvent process. There is much scope for the production of highly active mixed oxide catalysts, this result shows that through process optimisation it is possible to adjust the properties to enhance catalytic activity.

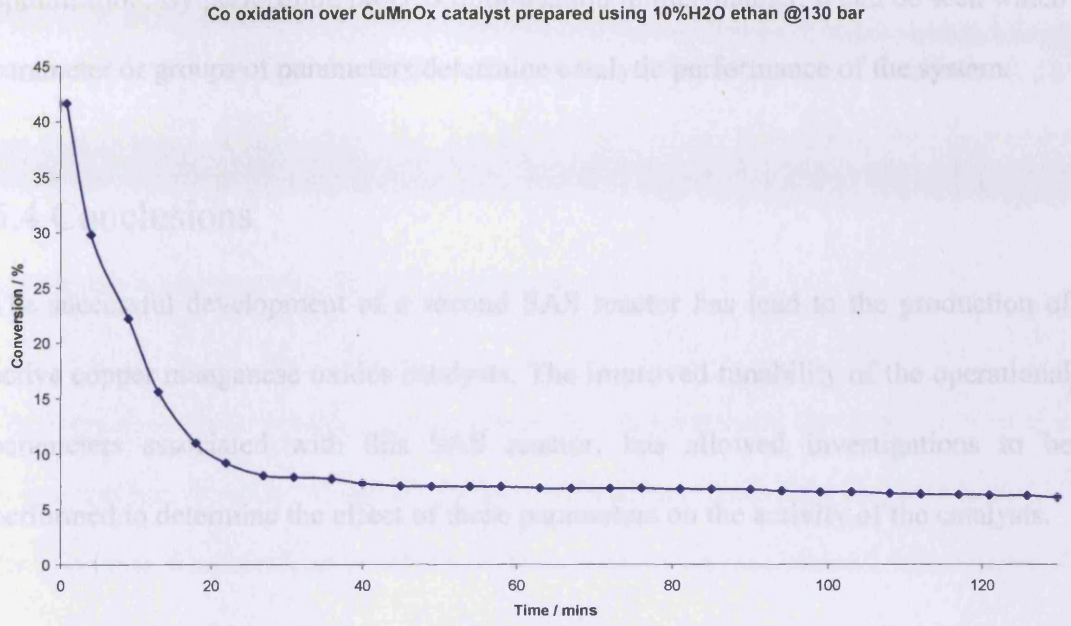

Figure 5.24 – CO oxidation over the optimised copper manganese oxide

Optimisation of the process parameters, as performed in this research, was performed in a holistic manner. The parameter under investigation was varied, the resulting catalyst was tested, and the change in CO conversion was noted. By selecting the parameters which resulted in improved conversion of the catalysts produced, the process parameters were tuned to produce a catalyst with much higher performance, from 20% to 42% conversion. This is a time consuming approach to determine the optimum process parameters for the required catalyst. This process would have to be repeated for each catalyst prepared on the supercritical reactor.

An alternative approach to this is to develop matrices, where several parameters are changed from preparation to preparation. This is a much quicker approach to process

optimisation. By performing process optimisation in this manner, it can be seen which parameter or groups of parameters determine catalytic performance of the system.

5.4 Conclusions

The successful development of a second SAS reactor has lead to the production of active copper manganese oxides catalysts. The improved tunability of the operational parameters associated with this SAS reactor, has allowed investigations to be performed to determine the effect of these parameters on the activity of the catalysts.

In view of the previous work done by other research groups, as well as our own, the initial synthesis of copper manganese oxides was performed using pure DMSO as the solvent. The precursors obtained initially were amorphous in nature which became more crystalline upon calcination. The surface areas were found to decrease upon calcination, which was attributed to the formation of particles with high levels of aggregation that occur during the heat treatment at elevated temperatures. The catalyst obtained exhibited some catalytic activity for the oxidation of CO; approximately 9% conversion initially, decreasing with time on-line. The main reason for performing this reaction was to check the reactor was functioning correctly and safely, but also to see if an active catalyst was produced when performing the process; because of the nature of the catalysts obtained, the construction of the reactor was deemed a success.

To determine the effect of the operational parameters on activity of the catalyst a series of experiments were performed. Increasing the process temperature was found to causes a decrease in activity. This was attributed to a change in particle size;

increasing particle size could result in a change in the surface area or alter the surface structure of the catalyst which in turn causes the activity of the catalyst to change. As the temperature is increased, the density is increased, decreasing the degree of supersaturation. This favours particle growth, therefore the optimum particle size is not produced and the catalytic activity decreases.

Changing the solvent resulted in the preparation of precursors that were very similar to one another; therefore, changing the solvent had very little effect on the structure of the precursor. The amorphous nature of the precursor was maintained independent of the solvent used. Upon calcination, the catalysts were again very similar, however in terms of catalytic activity increasing the viscosity of the solvent resulted in an increase in the activity of the catalyst. It was suggested that increasing the viscosity of the solvent would prevent the CO_2 from entering the solvent droplet as readily as it does in less viscous solvents. The degree of supersaturation decreases, favouring particle growth; therefore increasing particle size. From the characterisation and catalytic data there was not a significant difference between the solvents used. This suggested that the affect of viscosity on the overall activity is negligible.

Increasing the nozzle diameter had a detrimental effect on the surface areas of the catalysts obtained; the smallest nozzle size gave rise to the largest surface area. The general trend observed was increasing nozzle diameter resulted in an increase in the catalytic activity. Decreasing the diameter causes an increase in the velocity of the jet. This in turn increases the mixing between the jet and the surroundings due to the stronger turbulence. This leads to higher supersaturation in the jet, resulting in smaller

particle size. The other possibility was that varying the nozzle size causes the segregation of phases, which in turn causes a decrease in the activity of the catalyst. Decreasing the nozzle size would cause an increase in the velocity of the jet, which would cause supersaturation of the droplet to become much quicker, causing the particle size to decrease. This may allow individual components of the starting mixture to precipitate preferentially and phase separation to occur; single oxide phases are produced instead of a mixed oxide phase.

The effect of changing the solution flow rate on catalytic activity of resulting catalysts was also investigated. The general trend observed was that with increasing flow rate there was an increase in surface area. This was true for all solution flow rates measured. Increasing the flow rate was detrimental to the nature of catalyst obtained in terms of initial activity of the catalysts. Increasing the flow rate causes an increase in the velocity of the jet. This in turn increases the mixing between the jet and the surroundings due to the stronger turbulence, favouring nucleation, resulting in the production of smaller particles. The decrease in activity could be attributed to the production of smaller particles.

With increasing pressure the catalytic activity of the samples prepared was found to increase. Increasing the pressure of the system, causes an increase in the densities of the media presents. This in turn decreases the degree of supersaturation, which in turn favours particle growth. However, the pressure range and solvent system used needs to be considered in detail, as different solvent systems expand in CO_2 over different pressure ranges; if the solvent expands in the pressure range, degree of supersaturation

increases, favouring nucleation, resulting in smaller particles. Further research is required to elucidate this problem fully.

By utilising the information gathered in the above tests, the overall process was optimised and a test regime developed to obtain a catalyst with enhanced catalytic activity. The conversion of the catalyst increased from a maximum of 20% in the previous processes to 42% conversion. This shows that it is possible to produce a highly active hopcalite catalyst using the supercritical antisolvent process. This result shows that through process optimisation it is possible to adjust the properties to enhance catalytic activity.

5.5 References

[1] P. Porta, G. Moretti, M. Musicani and A. Nardella, *Catal. Today*, 1991, **9**, 211

[2] A.A. Mirzaei, H.R. Shaterian, R.W. Joyner, M Stockenhuber, S.H. Taylor and G.J. Hutchings, *Cat. Comm.*, 2003, **4**, 17

[3] E. Reverchon, G.D. Porta, D. Sannino, L. Lisi and P. Ciambelli, *Stud. Surf. Sci. Catal.* 1998, **118**, 349

[4] E. Reverchon, G.D. Porta, D. Sannino, and P. Ciambelli, *Powder Technol.*, 1999, **102**, 127

[5] Z.Tang, J.K. Edwards, J.K. Bartley, S.H. Taylor, A.F. Carley, A.A. Herzing, C.J. Kiely, G.J. Hutchings, *J. Catal.*, 2007, **249**, 208

[6] E. Reverchon, I. De Marco and G.D. Porta, *J. Supercrit. Fluids*, 2002, **23**, 81

[7] E. Alonso, I. Montequi, S. Lucas and M.J. Cocero, *J. Supercrit. Fluids*, 2007, **39**, 453

[8] E. Reverchon, *J. Supercrit. Fluids*, 1999, **15**, 1

[9] A. Martin and M.J. Cocero, *J. Supercrit. Fluids*, 2004, **32**, 203

[10] P. Subra, C.G. Laudani, A.Vega-Gonzalez and E. Reverchon, *J. Supercrit. Fluids*, 2005, **35**, 95

[11] E. Reverchon, *J. Supercrit. Fluids*, 1999, **15**, 1

[12] P.M. Gallagher, V.J. Krukonis and G.D. Botsaris, *AIChE. Symp. Series*, 1991, **284**, 96

[13] S.-S. Yeo, G.-B. Lim, P.G. Debenedetti and H. Bernstein, *Bioengng*, 1993, **41**, 341

[14] T.W. Randolph, A.D. Randolph, M. Mebes and S. Yeung, *Biotechnol. Progess*, 1993, **9**, 429

[15] D.J. Dixon, K.P. Johnston and R.A. Bodmeier, *AIChE J.*, 1993, **39**, 127

[16] J. Robertson, M.B. King, J.P.K. Seville, D.R. Merrifield and P.C. Buxton, *4th International Symp. Supercrit Fluids*, 1997, 47

[17] W.J. Scmidt, M.C. Salada, G.G. Shook and S.M. Speaker, *AIChe J.*, 1995, **41**, 2476

[18] R. Bodmeier, H. Wang, D.J. Dixon, S. Mawson and K.P. Johnston, *J. Pharm. Res.*, 1995, **13**, 1211

[19] E. Reverchon, G.D. Porta, D. Sannino and P. Ciambelli, *Powder Technol.*, 1999, **102**, 127

[20] F. Miguel, A. Martin, T. Gamse and M.J. Cocero, *J. Supercrit. Fluids*, 2006, **36**, 225

6 Summary and Future work

Utilising the SAS process has resulted in the production of active mixed oxides. Both the iron molybdates and copper manganese oxides prepared have shown high catalytic activity when prepared in this manner. The successful development of a second SAS reactor has lead to improved tunability of the operational parameters and has allowed investigations to be performed to determine the effect of these parameters on the nature of catalysts produced which may then be reflected in terms of activity.

Iron molybdates were initially prepared using pure DMSO as the solvent. Amorphous precursors were obtained which become more crystalline upon calcination. Increasing the process temperature was found to decrease both the activity of the catalysts and the selectivity to formaldehyde. This was attributed to increased density of the media present, which in turn decreased the degree of supersaturation. Precipitation occurred later in the droplet expansion process favouring particle growth. Therefore, the optimum particle size was not produced and the catalytic activity decreased.

The preoxidation of the starting solution was investigated to determine whether it was capable of producing the final catalyst without the need for a calcination step. Hydrogen peroxide was initially tested. Adding hydrogen peroxide to the starting solution was found to cause a decrease in the activity of the catalysts produced. As the volume of hydrogen peroxide was increased it was apparent from the characterisation data that there was oxidation of the components of the starting solution. The presence of Fe_2O_3, as indicated by the characterisation, was detrimental to the activity of the catalyst and this was shown by the decrease in the conversion of methanol. The use of hydrogen peroxide as an oxidant also had detrimental effects to the surface area and the overall catalytic activity of the iron molybdate catalysts obtained from the supercritical process.

Air was used as an alternative oxidant, and was bubbled through the starting solution prior to processing in the supercritical reactor. Passing air through the solution had no effect on the structure of the precursor. Amorphously structured precursors were obtained regardless if air was passed through the starting solution or not. Upon calcination the phases present correspond to $Fe_2(MoO_3)_4$ and MoO_3. The Raman spectra for both the precursor and catalyst were very similar, therefore, successful preoxidation had taken place. The activity of the catalyst was much higher than the iron molybdates previously tested. By passing air through the starting solution, the resulting catalyst was more active. This was suggested to be due to the fact that calcination had not dramatically changed the structure of the catalyst, the active phase $Fe_2(MoO_3)_4$ had been maintained to the final catalyst, resulting in an increase in

activity. The surface area also increased upon calcination of the as-precipitated precursor.

.

To determine the success of the second SAS reactor, copper manganese oxides were prepared to assess their activity for CO oxidation. The precursors obtained initially were amorphous in nature which became more crystalline upon calcination. The catalyst obtained exhibited some catalytic activity for the oxidation of CO. Approximately 9 % conversion was achieved initially, decreasing with time on-line.

To determine the effect of the operational parameters on activity of the catalyst a series of experiments were performed. These included pressure, temperature, solvent, solution flow rate and the nozzle diameter. By varying these processes individually, it produced a change in the catalyst which, in turn, resulted in a change in the activity of the catalyst for CO oxidation.

From the experiments performed and from reports in the literature, it appears that the effect of each parameter on the activity of the catalyst is a complex one. However, from the results obtained it appears that the consideration is how the parameter change affects the density of the SCF and the solubility of the solvent with regards to the SCF. An increase in density of the SCF, result in a decrease in the degree of supersaturation, which favours particle growth and larger particles are formed. A decrease in density, favours nucleation and smaller particles are formed. It is the effect of the change in density on the particle sizes obtained and how this relates to the catalyst and subsequently the activity of the catalyst that is of importance.